

Use of Tailored Blend Morphologies to Obtain Electrically Conductive Composites

by

Daria STRUGOVA

MANUSCRIPT-BASED THESIS PRESENTED TO ÉCOLE DE
TECHNOLOGIE SUPÉRIEURE IN PARTIAL FULFILLEMENT FOR THE
DEGREE OF DOCTOR OF PHILOSOPHY
Ph.D.

MONTREAL, MAY 24, 2023

ÉCOLE DE TECHNOLOGIE SUPÉRIEURE
UNIVERSITÉ DU QUÉBEC



Daria STRUGOVA, 2023



This Creative Commons licence allows readers to download this work and share it with others as long as the author is credited. The content of this work can't be modified in any way or used commercially.

BOARD OF EXAMINERS
THIS THESIS HAS BEEN EVALUATED
BY THE FOLLOWING BOARD OF EXAMINERS

Mrs. Nicole R. Demarquette, Thesis Supervisor
Department of Mechanical Engineering, École de Technologie Supérieure

Mr. Éric David, Thesis Co-supervisor
Department of Mechanical Engineering, École de Technologie Supérieure

Mr. Sylvain G. Cloutier, President of the Board of Examiners
Department of Electrical Engineering, École de Technologie Supérieure

Mr. Ricardo J. Zednik, Member of the jury
Department of Mechanical Engineering, École de Technologie Supérieure

Mr. Patrick C. Lee, External Evaluator
Department of Mechanical and Industrial Engineering, Toronto University, Canada

THIS THESIS WAS PRESENTED AND DEFENDED
IN THE PRESENCE OF A BOARD OF EXAMINERS AND PUBLIC
ON MAY 4, 2023
AT ÉCOLE DE TECHNOLOGIE SUPÉRIEURE

ACKNOWLEDGMENT

I would like to deeply thank everyone who helped me in this journey.

I would like to express my sincere gratitude to my PhD thesis directors, Prof. Nicole Demarquette and Prof. Eric David, for their unwavering guidance, support, and encouragement throughout my research journey. Their invaluable insights and expertise have been instrumental in shaping the direction of my work and helping me achieve my academic goals.

I also thank the members of the jury Prof. Sylvain Cloutier and Prof. Ricardo Zednik from École de Technologie Supérieure, and Prof. Patrick Lee from Toronto University for agreeing to evaluate this work during defense.

Thank you to the researchers, research staff, and technicians at the École de Technologie Supérieure. A special thank goes to Mazen Samara for his invaluable assistance in reviewing my articles and thesis. I would also like to extend my gratitude to Nabil, Radu, Simon, and all the staff in the Mechanical Engineering Department for their practical support whenever it was needed.

Thanks go also to my friends and colleagues who have been an integral part of my journey through my PhD. I am deeply grateful to Maria, Jose and Camila, Nourin, Etienne, Alena, Manon, Julie, Andre, Marwa, Emna, Scheyla, Rafael, and Iman for your invaluable support and encouragement throughout my research. Your insights, feedback, and discussions have been instrumental in shaping my ideas and improving my work. I wish all of you the best of luck on your future plans.

I would like to give a special thanks to Andrey, Mitasha, and Chloe, with whom I started this journey in 2017. Your friendship and support were invaluable and helped me greatly,

especially at the beginning of my PhD. I will always cherish the memories we shared and the experiences we had together. Thank you for being such amazing friends and colleagues.

I would like to express my heartfelt gratitude to my parents and my brother, who have always been there to support and encourage me, no matter what my dreams and ambitions were. Their unwavering love and belief in me have been a constant source of strength and inspiration throughout my PhD journey. I am deeply grateful for their guidance, patience, and sacrifices, which have enabled me to pursue my goals and achieve my dreams.

Utilisation de morphologies de mélange sur mesure pour obtenir des composites électriquement conducteurs

Daria STRUGOVA

RESUME

Cette thèse visait à concevoir des nanocomposites à base de polymères électriquement conducteurs avec une concentration seuil de percolation exceptionnellement basse grâce au contrôle de leur morphologie, et à évaluer comment cette morphologie, donc les propriétés électriques, seraient stables lors du post-traitement. Pour ce faire, les relations entre les propriétés morphologiques, électriques et rhéologiques du mélange polypropylène/polystyrène auquel des nanotubes de carbone multiparois (PP/PS/MWCNT) furent ajoutés, préparés par un procédé conventionnel de mélange à l'état fondu ont été étudiées.

Des composites avec une concentration seuil de percolation (PTC) de 0,3 % en poids de MWCNT ont été obtenus en raison de l'effet de double percolation obtenu en utilisant la morphologie co-continue de la matrice PP/PS. Le PTC a encore été réduit à 0,06% en poids de MWCNT lors de l'utilisation d'un traitement thermique basé sur l'effet d'exclusion de volume des cristaux de PP. Une conductivité électrique de 10^{-5} S.m^{-1} a alors été atteinte. Ceci représente une augmentation de la conductivité électrique de plus de 10 ordres de grandeur si on compare à celle du mélange sans MWCNT. De plus, ce traitement thermique n'a pas affecté la morphologie co-continue du mélange PP/PS et donc ces propriétés furent conservées.

Un modèle pour caractériser la morphologie co-continue des composites PP/PS/MWCNT en utilisant leur caractérisation rhéologique a été développé. La quantification de la morphologie effectuée par le modèle corrobore celle observée par microscopie électronique à balayage. Ce modèle a été utilisé pour évaluer la morphologie des composites soumis à un recuit thermique, utilisé pour améliorer les propriétés électriques. Le modèle a également été utilisé pour sonder l'évolution de la morphologie des composites PP/PS/MWCNT. Les résultats ont montré une légère diminution de la taille du domaine caractéristique pour les composites avec différentes concentrations de MWCNT, conduisant à une morphologie co-continue plus fine, en ligne avec les propriétés électriques mesurées. Plus précisément, le PTC a été réduit de 0,28 % en poids à 0,06 % en poids de MWCNT.

Enfin, les propriétés électriques et morphologiques des composites co-continus PP/PS/MWCNT soumis à des déformations contrôlées ont été évaluées. Un équilibre délicat entre la concentration de MWCNT, la déformation de cisaillement et les taux de cisaillement (les paramètres d'écoulement), qui a affecté la morphologie et les propriétés électriques des composites, a été observé. La stabilisation de la morphologie et de la conductivité électrique ont été obtenus à des niveaux critiques de concentration de MWCNT.

VIII

Mots-clés: concentration seuil de percolation électrique, effet de double percolation, conductivité électrique, composites thermoplastiques, mélange de polymères, morphologie co-continue

Use of tailored blend morphologies to obtain electrically conductive composites

Daria STRUGOVA

ABSTRACT

This thesis aimed at designing electrically conductive polymer-based nanocomposites with an exceptionally low percolation threshold concentration through control of their morphology, and to evaluate how this morphology, hence the electrical properties, would be stable during post-processing. The relationships between morphological, electrical, and rheological properties of polypropylene/polystyrene filled with multiwall carbon nanotubes (PP/PS/MWCNT) composites prepared by conventional melt-mixing process were investigated.

Composites with a percolation threshold concentration (PTC) of 0.3 wt.% MWCNT were obtained owing to the double percolation effect achieved by using co-continuous morphology of PP/PS matrix. The PTC was further decreased to 0.06 wt.% MWCNT upon using a thermal treatment based on the volume exclusion effect of PP crystals. An electrical conductivity of 10^{-5} S.m^{-1} was reached, for composites with 0.06 wt.% MWCNT, representing an increase of over 10 orders of magnitude compared to that of the PP/PS matrix alone. The co-continuous morphology of the PP/PS blend was not affected by the thermal treatment, indicating that other properties of the composite were not impacted.

Furthermore, a model to characterize the co-continuous morphology of PP/PS/MWCNT composites using their rheological characterization was developed. The quantification of the morphology carried on by the model corroborated the one observed by scanning electron microscopy. The model was used to assess the morphology of composites subjected to thermal annealing, employed to enhance the electrical properties. The model was also used to probe the morphology evolution of PP/PS/MWCNT composites. The results showed a slight decrease in the characteristic domain size for composites with different MWCNT concentration, leading to a more refined co-continuous morphology, in line with the measured electrical properties. Specifically, the PTC was reduced from 0.28 wt.% to 0.06 wt.% MWCNT.

Finally, the electrical and morphological properties of co-continuous PP/PS/MWCNT composites under deformation flow were evaluated. A delicate balance between MWCNT concentration, shear strain, and shear rates (the parameters of the deformation flow), which affected the morphology and electrical properties of the composites, was observed. The stabilization of morphology and electrical conductivity was achieved at critical levels of MWCNT concentration, and recovery was possible. The PTC and electrical conductivity were reduced during deformation but recovered after recovery step, even increasing by one order of magnitude.

Keywords: electrical percolation threshold concentration, double percolation effect, electrical conductivity, thermoplastic composites, polymer blend, co-continuous morphology

TABLE OF CONTENTS

	Page
INTRODUCTION	1
0.1 Context of the research	1
0.2 Objectives and research steps	2
0.3 Approach and methodology	3
0.1 Organization of the PhD thesis	4
CHAPTER 1 ELECTRICALLY CONDUCTIVE COMPOSITES WITH TAILORED BLEND MORPHOLOGIES	7
1.1 Electrical properties of polymer-based composites	7
1.1.1 Percolation threshold mechanism in electrically conductive polymer composites	7
1.1.2 Double percolation effect – generalities	12
1.1.3 Prediction of filler location inside polymer blend matrix	16
1.1.4 Conclusion remarks	17
1.2 Linear shear rheology	18
1.2.1 Co-continuous morphology modelling	19
1.2.2 Two-phase model and the elasticity of the filler network	24
1.2.3 Design of experiments	26
CHAPTER 2 ULTRA-LOW PERCOLATION THRESHOLD INDUCED BY THERMAL TREATMENTS IN CO-CONTINUOUS BLEND-BASED PP/PS/MWCNTS NANOCOMPOSITES	31
2.1 Introduction	32
2.2 Materials and Methods	34
2.2.1 Materials	34
2.2.2 Processing	34
2.2.3 Characterization	37
2.3 Results	41
2.3.1 Effect of the Treatments on Electrical Conductivity and Morphology of PP/PS/MWCNTs Composites	41
2.3.2 Crystallization Behavior and Electrical Conductivity of PP/MWCNTs and PP/PS/MWCNTs Nanocomposites	46
2.4 Discussion	53
2.5 Conclusions	56
CHAPTER 3 LINEAR VISCOELASTICITY OF PP/PS/MWCNT COMPOSITES WITH CO-CONTINUOUS MORPHOLOGY	59
3.1 Introduction	59
3.2 Materials and Methods	65

3.2.1	Materials	65
3.2.2	Composites' preparation	65
3.2.3	Characterizations.....	66
3.3	Results and Discussion	68
3.3.1	PP/PS/MWCNT composites' morphology and the YZZ model fitting....	69
3.3.2	Effect of thermal annealing on electrical conductivity and characteristic domain size of co-continuous morphology of PP/PS/MWCNT composites	74
3.4	Conclusion	80
CHAPTER 4 EFFECT OF STEADY SHEAR DEFORMATION ON ELECTRICALLY CONDUCTIVE PP/PS/MWCNT COMPOSITES		
4.1	Introduction.....	83
4.2	Materials and Methods.....	87
4.2.1	Materials	87
4.2.2	Composites preparation	88
4.2.3	Characterizations.....	88
4.3	Results.....	92
4.4	Discussion.....	108
4.5	Conclusion	113
CONCLUSION		
RECOMMENDATIONS.....		
ANNEX I	SUPPORTING ELECTRONIC INFORMATION FOR ARTICLE 1.....	113
ANNEX II	SUPPORTING ELECTRONIC INFORMATION FOR ARTICLE 2.....	117
ANNEX III	SUPPORTING ELECTRONIC INFORMATION FOR ARTICLE 3.....	120
APPENDIX VITA		
LIST OF BIBLIOGRAPHICAL REFERENCES.....		

LIST OF TABLES

		Page
Table 2.1	Percolation threshold and fitting values of experimental data according to Equation (2.6) for PP/PS/MWCNTs composites after each treatment	42
Table 2.2	Ultra-low PT values of CNT-thermoplastic systems achieved by different modifications and treatments.	54
Table 3.1	Properties of the polymers	65
Table 3.2	Fitting parameters for Equations (3.12) and (3.15).....	77
Table 4.1	Properties of the polymers	88
Table 4.2	Experimental data for PP/PS blend with different weight concentration of components.....	91
Table 4.3	Parameters of the experimental protocol presented in Figure 4.1	91
Table 4.4	p_c and fitted coefficients for PP/PS/MWCNT composites before and after 250% of shear strain applied at different steady shear rates.....	97
Table 4.5	Morphology of neat PP/PS, 50/50 wt.% blend and PP/PS/MWCNT composites, containing 0.5 wt.% and 2 wt.% of MWCNT wt.% before any deformation and after 250% of shear strain at different steady shear rates	100
Table 4.6	Critical shear strain for composites sheared at 0.05 s^{-1} and 1 s^{-1} of steady shear rates	103
Table 4.7	Maximum surface coverage of PP/PS/MWCNT 50/50/x wt.% composite interface by MWCNT mesh	109

LIST OF FIGURES

		Page
Figure 0.1	Main steps of the PhD project.....	4
Figure 1.1	Schematic illustration of percolation mechanism.....	8
Figure 1.2	Summary of methods for PTC reduction.....	12
Figure 1.3	Schematic illustration of double percolation effect.....	13
Figure 1.4	Schematic of useful morphologies of polymer blends [83].....	14
Figure 1.5	Schematics of an ideal co-continuous morphology for (a) the components contribution, (b) the interfacial contribution and (c) deformation of interfaces.....	20
Figure 1.6	Storage modulus of PS/POE co-continuous blends as a function of frequency. (a) PS/POE 40/60; (b) PS/POE 50/50; (c) PS/POE 60/40. Insets are the corresponding SEM pictures.....	23
Figure 1.7	SAOS tests performed at 160 °C for LLDPE/EVA/GN composites.....	24
Figure 1.8	Schematic representation of the origin of viscoelasticity in polymer nanocomposites above the percolation threshold.....	25
Figure 1.9	Shear protocols to a) investigate the effect of shear rate and b) investigate induced droplets coalescence process.....	27
Figure 1.10	Cac as a function of p in rotational and irrotational shears together with illustrations of droplets break-up and coalescence (adapted from Grace [110]).....	29
Figure 2.1	Temperature vs. time for fast-cooling treatment, isothermal treatment, and slow-cooling treatment.....	37
Figure 2.2	Effect of treatments on the electrical conductivity of PP/PS/MWCNTs composites as a function of MWCNTs concentration.....	41
Figure 2.3	Morphology evolution of selected PP/PS/MWCNTs composites after fast-cooling treatment for: (a) 0 wt.% of MWCNTs; (b) 0.1 wt.% of MWCNTs; and (c) 0.5 wt.% of MWCNTs.....	44

Figure 2.4	Characteristic domain size of PP/PS/MWCNTs composites after fast cooling as a function of MWCNTs concentration44
Figure 2.5	Morphology of the selected PP/PS/MWCNTs composites with 0.3 wt.% of MWCNTs for (a) fast-cooling treatment; (b) isothermal treatment; and (c) slow-cooling treatment45
Figure 2.6	Characteristic domain size of ζ vs. MWCNTs concentration for different treatments for PP/PS/MWCNTs composites46
Figure 2.7	Typical non-isothermal crystallization of PP and PP/MWCNTs curves with different MWCNTs wt.%47
Figure 2.8	Effect of MWCNTs on non-isothermal crystallization of PP for both PP/MWCNTs and PP/PS/MWCNTs composites: (a) influence of MWCNTs concentration on crystallization temperature (peak); and (b) the effect of MWCNTs amount on degree of crystallinity during non-isothermal cooling from 200 °C to 50 °C at 10 °C/min48
Figure 2.9	(a) Heat flow as a function of time for PP/MWCNTs composites with different MWCNTs wt.% at 135 °C; (b) relative crystallinity of PP/MWCNTs composites with different MWCNTs wt.% at 135 °C.....49
Figure 2.10	(a) Crystallization half time and (b) induction time for PP/MWCNTs and PP/PS/MWCNTs composites at 135 °C.....50
Figure 2.11	Microscopic observations of PP pure and PP/MWCNTs with 0.1 wt.% of MWCNTs for fast-cooling treatment (a-b); isothermal treatment (c-d); and slow-cooling treatment (e-f).....51
Figure 2.12	Electrical conductivity as a function of time for PP/PS/MWCNTs composite with different concentrations of MWCNTs measured every 10 s at 1 Hz of frequency and 135 °C for: (a) 0–0.1 wt.% of MWCNTs; and (b) 0.3–1 wt.% of MWCNTs.....52
Figure 2.13	Time for complete crystallization of PP (Time 2) and time when electrical conductivity levels off (Time 1) as a function of MWCNTs concentration for PP/PS/MWCNTs composites56
Figure 3.1	A schematic of an ideal co-continuous morphology (redrawn from refs. [89,95]).....62
Figure 3.2	Experimental protocol.....67

Figure 3.3	Storage modulus as a function of frequency for PP/PS/MWCNT composites with different concentrations of MWCNT at 200 °C. PP, PS, and PP/PS blend of 50/50 wt.%	70
Figure 3.4	Storage modulus as a function of frequency for (a) PP, PS, and PP/PS blend with YZZ model fitting data (dashed line) and (b) PP/PS/MWCNT composite with 0.3 wt.% of MWCNT with model data representing the fit of the YZZ model (dashed line) and model data representing the fit of the Equation (3.15) (solid line).....	70
Figure 3.5	Morphology evolution of selected PP/PS/MWCNT composites for (a) 0 wt.% of MWCNT, (b) 0.3 wt.% of MWCNT, and (c) 0.5 wt.% of MWCNT	72
Figure 3.6	Characteristic domain size of PP/PS/MWCNT composites calculated with the help of Equation (3.14) – experimental data and predicted with the YZZ model for PP/PS/MWCNT with 0-0.1 wt.% of MWCNT and Equation (3.15) for PP/PS/MWCNT with 0.3-0.5 wt.% of MWCNT – model data	73
Figure 3.7	(a) Electrical conductivity as a function of time for PP/PS/MWCNT composites with different concentrations of MWCNT measured at 20 Hz of frequency and 200 °C. (b) Time-dependent evolution of storage modulus at 200 °C for PP/PS/MWCNT composites with different MWCNT concentrations	74
Figure 3.8	TEM of the PP/PS/MWCNT composite with 0.5 wt.% of MWCNT for (a) and (b) before treatment and (c) and (d) after thermal annealing. Arrows show the PP/PS interface.....	76
Figure 3.9	Characteristic domain size of PP/PS/MWCNT composites before and after 30 min of annealing calculated with the help of the YZZ model for PP/PS/MWCNT with 0-0.1 wt.% of MWCNT and Equation (3.12) for PP/PS/MWCNT with 0.3-0.5 wt.% of MWCNT	78
Figure 3.10	Network elasticity as a function of reduced filler content related to PP/PS/MWCNT composites (solid squares) and power-law fitting to the experimental data (solid lines) for composites before and after thermal annealing: (a) rheological PT – G_0' versus $(P - P_c)$ plots and (b) electrical PT σ' versus $(P - P_c)$ plots.....	80
Figure 4.1	Experimental protocols	90

Figure 4.2	SEM observations for (a) PP/PS 50/50 wt.% and (b) PP/PS/MWCNT 50/50/0.5 wt.%. TEM of PP/PS/MWCNT 50/50/0.5 wt.% composite with different magnification	93
Figure 4.3	Electrical conductivity and transient shear viscosity vs. applied shear strain for PP/PS/MWCNTs 50/50/x wt.% composites at 200 °C at: (a) and (c) steady shear rate of 0.05 s ⁻¹ ; (b) and (d) steady shear rate of 1 s ⁻¹	95
Figure 4.4	Electrical conductivity vs. MWCNT wt.% for composites before and after 250% of applied shear strain at different steady shear rates.....	97
Figure 4.5	<i>G'</i> versus frequency for PP/PS/MWCNT composites with 0.5 and 2 wt.% of MWCNT after shear strain applied at a steady shear rate of: (a) and (c) 0.05 s ⁻¹ , and (b) and (d) 1 s ⁻¹	99
Figure 4.6	ξ vs. applied shear strain for all composites at a steady shear rate of: (a) 0.05 s ⁻¹ , and (b) 1 s ⁻¹	102
Figure 4.7	(a) Electrical conductivity vs. shear strain at a steady shear step and as a function of time at a stress relaxation step for all composites; (b) Stress vs. shear strain and time for all composites.....	105
Figure 4.8	Electrical conductivity vs. MWCNT wt.% for composites before, after 250% of applied shear strain at 1 s ⁻¹ , and after 250% of applied shear strain at 1 s ⁻¹ plus 30 min of stress relaxation at 0.05 rad/s	106
Figure 4.9	Evolution of characteristic domain size for PP/PS/MWCNT 50/50/0.5 wt.% composite before any deformation, after shear strain applied at a steady shear rate of 1 s ⁻¹ , and after shear strain applied at a steady shear rate of 1 s ⁻¹ plus stress relaxation step of 10 min	107
Figure 4.10	Morphology of PP/PS/MWCNT 50/50/0.5 wt.% composite: (a) before any deformation, (b) after 250% of shear strain at a shear rate of 1 s ⁻¹ , and (c) after 250% of shear strain at a shear rate of 1 s ⁻¹ + 30 min of stress relaxation step.....	108
Figure 4.11	Schematic of a triangular array of MWCNT	110
Figure 4.12	Schematic summary of the results	112

LIST OF ABBREVIATIONS

BDS	Broadband dielectric spectrometer
CB	Carbon black
CNT	Carbon nanotubes
DC	Direct current
DRD	Dielectro-rheological device
DSC	Differential scanning calorimetry
DSST	Dynamic strain sweep test
EMI	Electromagnetic interference shielding
GN	Graphene
GO	Graphene oxide
LVE	Linear viscoelastic
MWCNT	Multi-wall carbon nanotubes
NA	Nucleating agent
PB	Polymer blend
PLA	Poly(lactic acid)
POE	Poly(ethylene-co-1-octene)
PT	Percolation threshold
PTC	Percolation threshold concentration
PP	Polypropylene
PS	Polystyrene
SAOS	Small amplitude oscillatory shear
SC	Stereocomplex crystallization
SEM	Scanning electron microscopy
TEM	Transmission electron microscopy

LIST OF SYMBOLS

ΔH	Heat of fusion
ΔH_m	Heat of fusion of 100% crystalline
Σ	Maximum interface coverage
X_c	% of the crystalline phase
$X(t)$	Relative crystallinity
α	Interfacial tension
γ	Shear strain
γ_c	Critical shear strain
$\gamma_{filler-polymerB}$	Interfacial energy between filler and polymer B
$\gamma_{filler-polymerA}$	Interfacial energy between filler and polymer A
$\gamma_{polymerA-polymerB}$	Interfacial energy between polymer A and polymer B
γ_0	Strain amplitude
γ_1 and γ_2	Surface tensions of component 1 and component 2, respectively
γ_1^d, γ_2^d , and γ_1^p, γ_2^p	Dispersive and polar parts of the surface tensions of component 1 and component 2, respectively
$\dot{\gamma}$	Shear rate
$\dot{\gamma}_c$	Critical shear rate
ϵ_0	Vacuum permittivity
$\epsilon^*(\omega)$	Complex permittivity
$\epsilon'(\omega)$	Real part of the complex permittivity
$\epsilon_p''(\omega)$	Imaginary part of the permittivity due to the polarization phenomena
$\epsilon_{tot}''(\omega)$	Total imaginary part of the permittivity
η_m	Viscosity of the matrix
η_d	Viscosity of the dispersed phase

η_0	Zero-shear viscosity
η_1 and η_2	Viscosity of polymer 1 and polymer 2, respectively
ξ	Characteristic domain size
σ	Electrical conductivity
$\sigma^*(\omega)$	AC complex conductivity
σ'	Real part of electrical conductivity
φ_1 and φ_2	Volume fraction of polymer 1 and polymer 2, respectively
ω	Frequency
ω_a	Wetting coefficient
A	Distance between the plates
A_{MWCNT}	Area covered by all MWCNT
A_{SEM}	Total area of the SEM image
Ca	Capillary number
Ca_c	Critical capillary number
$F_{viscous}$	Viscous force
$F_{interfacial}$	Interfacial force
G'	Storage modulus
$G_A' interface$, $G_B' interface$, and $G_C' interface$	Elastic modulus due to interface deformation of the cylinders type A, type B, and type C, respectively
G'_0	Frequency-independent elastic modulus
$G'_1(\omega)$ and $G'_2(\omega)$	Storage modulus of component 1 and component 2, respectively
$G_{blend}^*(\omega)$	Complex modulus
$G_{components}^*(\omega)$	Components' contribution
$G_{interface}^*(\omega)$	Interface contribution
L_{int}	Interface length between two phases
P	Mass fraction of filler

P_c	Percolation threshold concentration
R_v	Volume average radius of the drops
S_V	Specific area
$S_{Vpromoted}$	Promoted interface area
Z'	Real part of the complex impedance
a and b	Radius and length of cylinder, respectively
a', b'	Edges of square section of parallelepiped shape element
d	Plate area
dH_c	Heat flow required for crystallization for a certain time
k	Scaling factor
k_B and k_C	Constants that relate to a random orientation and possible distortion of a co-continuous element, respectively
l_c	Characteristic length of cylinder shape elements for model co-continuous morphology
l'_c	Length of parallelepiped shape elements for model co-continuous morphology
p	Viscosity ratio of fluid 1 over fluid 2
t	Fitted exponent
v	Fitted exponent
w	Filler weight fraction

INTRODUCTION

01. Context of the research

Electrically conductive polymer-based composites hold great promise in various industrial applications due to their advantages, which include the ability to adjust electrical conductivity over a wide range, processability into complex geometries, flexibility, lightweight, and corrosion resistance. They can be used for various applications, including sensors, intelligent medical devices, energy harvesting, actuators, flexible electronics, robotics, static dissipation, and EMI shielding [1-12].

These composites are normally obtained by dispersing electrically conductive particles such as carbon black (CB) [13-23], carbon nanotubes (CNTs) [2-8,24-28], and graphene [12,29-37] within thermoplastics. Once a certain concentration of electrically conductive particles, known as percolation threshold concentration (PTC), is added to the thermoplastic matrix, the later will start conducting electricity. Obviously, this PTC should be kept as low as possible in order to reduce material costs and minimize any negative effects on other material properties. However, reaching a very low PTC by dispersing of conductive fillers within the polymer matrix can be challenging with conventional polymer processing methods, which contributed to an extensive search of methods to reduce PTC in such composites.

One of the most effective methods for reducing the PTC is to tailor the location of the conductive nanoparticles in a polymer blend matrix. This matrix consists of two immiscible polymers forming a co-continuous morphology where one polymer percolates through the matrix of the other polymer. By controlling the interfacial tension between the conductive filler and the polymers in the blend, it is possible to tailor the location of the filler. This can be achieved either within one continuous phase or at the interface between the two continuous phases. Through this process, known as double percolation theory, it is possible to lower the concentration of the conductive filler [1-9,24-28,38-58].

Although many methods to decrease the PTC in electrically conductive polymer-based composites have been reported in the literature, there is still room for improvement of the PTC concentration, for these kinds of composites. In particular, it would be interesting to know if through processing, it is possible to decrease this PTC even further.

During the processing of composites, they are subjected to deformation flow that may lead to a disruption of the morphology and destruction of the electrically conductive filler network. This can result in a decrease in electrical conductivity, even when a very low PTC has been achieved during material preparation. Furthermore, post-processing, such as injection molding or thermal treatments, subjects the material to flows and high temperatures, which may further disrupt the morphology and hence, the electrical properties. Rheology which is the study of deformation of mater can be used as a tool to investigate this morphology' evolution during deformation flows. Indeed, constitutive equations can be employed to characterize the morphology of composite materials from rheological measurements performed in the linear viscoelastic regime [24,59-63]. To assess how controlled flow affects the morphology of composites, a series of rheological tests can be conducted. This involves a succession of steps that includes: (1) characterizing the morphology within the linear viscoelastic regime, followed by (2) subjecting the material to controlled flow, and finally (3) characterizing the morphology again within the linear viscoelastic regime. By comparing the results of steps 1 and 3, it is possible to determine how the controlled flow impacts the morphology of the composites. Unfortunately, rheological models to characterize the morphology of blends presenting a co-continuous morphology to which nanoparticles are added did not exist prior to this work.

02. Objectives and research steps

The aim of this research project was to design electrically conductive nanocomposites with an exceptionally low percolation threshold concentration through control of their morphology and to evaluate how this morphology, hence the electrical properties, would remain stable during post-processing.

To achieve this goal, two immiscible polymers, polypropylene, and polystyrene, were selected as a matrix to create a co-continuous morphology and multi-walled carbon nanotubes were chosen as the electrically conductive filler. Once a co-continuous morphology was optimized it was necessary to design a suitable post-treatment that would result in a lower percolation threshold concentration and good electrical conductivity. The results of this study are presented in Chapter 2 of the thesis and were published in the *Nanomaterials* journal. In order to evaluate the stability of the morphology during post-processing, it was necessary to develop a tool that would characterize and quantify it. A rheological model to do that was developed. It is described in Chapter 3 of the thesis and was reported in *Journal of Rheology*. The third step aimed to investigate the evolution and stabilization of the rheological, morphological, and electrical properties of co-continuous PP/PS/MWCNT composites under deformation flow at varying shear rates, the results are reported in Chapter 4 of the thesis and in a manuscript which was submitted to the *Journal of Rheology*.

03. Approach and methodology

This PhD project, based on the primary aim and objectives, was divided in three main parts that are summarized in Figure 0.1.1.

In the first step of this study, co-continuous blends of two immiscible polymers, namely polypropylene (PP) and polystyrene (PS), were selected to create a double-percolated structure that could effectively tailor the location of multiwall carbon nanotubes (MWCNTs) - a highly conductive filler. PP/PS/MWCNTs composites were prepared via melt mixing using a twin-screw extruder, with varying amounts of MWCNTs (ranging from 0 to 5 wt.%). Furthermore, these composites were subjected to the additional thermal treatment aimed at using the volume exclusion effect of PP crystallites on electrical conductivity and PTC of PP/PS/MWCNT composites.

Given the co-continuous morphology of the polymer matrix of filled composites, the second step was to develop a rheological model for characterizing this morphology considering the effect of the filler on the rheological properties. By using this model, the study enabled to quantify the co-continuous morphology and establish a correlation between the morphological properties of PP/PS/MWCNT composites and their electrical properties. Further, the composites were subjected to thermal annealing in order to enhance their electrical properties and to probe the morphology evolution.

In the last step, the PP/PS/MWCNT composites were subjected to steady shear flow (simulating deformation flow) in order to investigate the evolution and stabilization of their rheological, morphological, and electrical properties. Further, PP/PS/MWCNT composites were subjected to a recovery step which followed steady shear flow. It was done in order to investigate the possible recovery of the properties.

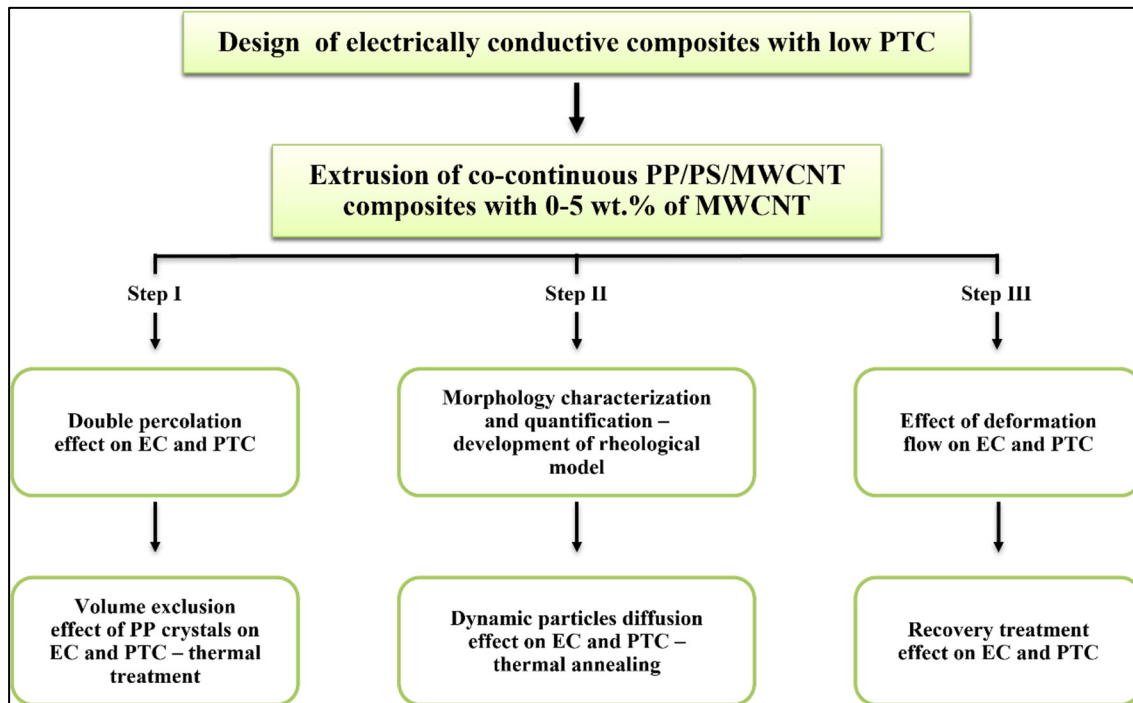


Figure 0.1.1 Main steps of the PhD project

04. Organization of the PhD thesis

This thesis is structured into four main chapters. After this introduction, a brief literature review is presented on electrically conductive composites, based on polymer blends as a matrix and conductive nanoparticles as a filler. In this section, the concept of tailored blend morphologies for achieving better nanoparticle dispersion is also discussed. The subsequent three chapters each focus on an individual article related to a specific step of the project. Finally, following the above three steps, the conclusions drawn from the research, as well as recommendations for future work in this area are presented.

In chapter 2, the paper entitled ‘Ultra-Low Percolation Threshold Induced by Thermal Treatments in Co-Continuous Blend-Based PP/PS/MWCNTs Nanocomposites’ published in *Nanomaterials* is presented. This article focuses on the first stage of the project, which investigates the impact of post-processing treatments on the percolation threshold concentration of electrically conductive composites. Specifically, the article examines the use of these treatments to achieve a lower percolation threshold. The article also emphasizes the influence of polymer crystallization on the electrical properties of the composites, which are based on a polymer blend matrix containing at least one semi-crystalline polymer.

Chapter 3 presents the paper ‘Linear viscoelasticity of PP/PS/MWCNT composites with co-continuous morphology’ published in *Journal of Rheology*. This article is related to the second step of the project and focuses on the development of a rheological model for characterizing the rheological and morphological properties of filled polymer composites presenting co-continuous morphology of the matrix, in order to establish a correlation between the morphological and electrical properties.

In chapter 4, the paper entitled ‘Effect of steady shear deformation on rheological, morphological and electrical properties of PP/PS/MWCNT composites with co-continuous morphology’ submitted to *Journal of Rheology* is presented. This article is related to the third

step of the project and aimed to shed light on the effect of shear deformation on the evolution of rheological, morphological, and electrical properties and their possible stabilization, of electrically conductive polymer composite, presenting co-continuous morphology.

In the conclusion chapter, the conclusions of the whole project are given. This section summarizes the research findings and provides a final perspective on the significance of the work together with the research limitations and suggestions, and on how these limitations can be addressed in future studies.

In addition to the main chapters, three annexes are also included at the end of the thesis. They provide supplementary information regarding the articles reported in chapters 2, 3 and 4, respectively.

CHAPTER 1

ELECTRICALLY CONDUCTIVE COMPOSITES WITH TAILORED BLEND MORPHOLOGIES

This literature review provides an overview of electrically conductive polymer composites, including their matrix morphology and the types of electrically conductive particles that can be used as a filler to achieve a low percolation threshold. The review also examines methods to reduce the percolation threshold, such as the use of immiscible polymer blends with a co-continuous morphology to achieve a double percolation effect, as well as post-processing treatments. Further, the review explores the use of linear viscoelastic rheology to assess the evolution of rheological, morphological, and electrical properties, and to identify possible properties stabilization methods.

1.1 Electrical properties of polymer-based composites

To develop a comprehensive understanding of the mechanisms involved in achieving high electrical conductivity and low percolation threshold concentration in electrically conductive polymer-based composites, this study explores several theories and concepts. Section 1.1 and its subsection cover the percolation threshold mechanism theory, as well as various methods for reducing the percolation threshold concentration. Section 1.2 and its subsections provide an overview of the double percolation effect and the morphology of immiscible polymer blends, specifically the co-continuous morphology, which was chosen as the matrix to achieve a double percolation effect. The wetting coefficient theory is presented in Section 1.2.2 to explain how the location of the filler inside the polymer matrix can be predicted. Finally, Section 1.3 presents the concluding remarks for Section 1.

1.1.1 Percolation threshold mechanism in electrically conductive polymer composites

The percolation theory is the most often used theory for describing transport processes in anisotropic systems. It is used to predict the probability of cluster formation from particles connecting each other, as well as the magnitude of percolation thresholds and composite characteristics (electrical, mechanical, thermal, and so on).

A schematic illustration of the percolation mechanism is shown in Figure 1.1 which presents the electrical conductivity of a composite as a function of electrically conductive filler concentration. Three main regions can be identified in this graph. First, at very low filler concentrations, electrical conductivity is extremely low (almost the same as the conductivity of the polymer matrix). The second region is a region of rapid conductivity increase with a very little increase in the filler concentration. The filler particles begin to interconnect in this area, which helps to create a conductive network throughout the composite's volume. This occurs at a concentration known as percolation threshold concentration – P_c . In the third region, the electrical conductivity reaches a plateau, because the formation of the conducting network is completed, and the conductivity of the composite approaches the conductivity of the filler.

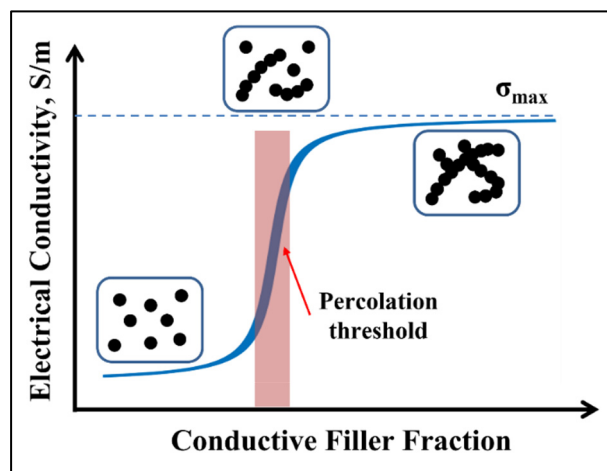


Figure 1.1 Schematic illustration of percolation mechanism

It is known that, above the percolation threshold p_c , a heterogeneous material consisting of a mixture of an insulator and a conductor has a power dependence of electrical conductivity σ on the concentration of conductive fillers [64]. Equation (1.1) can be used to calculate the percolation threshold concentration of composites.

$$\sigma = k \cdot (P - P_c)^t, \text{ with } P > P_c, \quad (1.1)$$

where σ is the electrical conductivity of the composite, P is the mass fraction of MWCNTs, P_c is the percolation threshold concentration, t is a fitted exponent that depends, only, on the dimensionality of the system, and k is a scaling factor. It should be noted that this equation is valid for $P > P_c$.

By definition, the percolation threshold concentration is the minimum concentration of electrically conductive filler particles required to achieve a continuous conductive network in a composite material. In polymer-based composites, as was shown in the introduction, the addition of filler particles such as carbon nanotubes, graphene, or metal nanoparticles can enhance their electrical properties. However, achieving a low percolation threshold concentration in polymer composites can be challenging, as the polymer matrix typically has low electrical conductivity, but it is not impossible, and there are various methods that can be employed to achieve this goal. These methods will be reviewed in detail in the following section.

1.1.1.1 Methods of percolation threshold reduction

Over the years, significant efforts have been devoted to the design of polymer-based composites with a low percolation threshold concentration [7,25,28,42,43,47,65-68]. A low percolation threshold concentration results in a lower quantity of filler within the polymer matrix, which reduces the cost of the final material. Additionally, composites with low filler concentration are easier to process and facilitate shaping of the final product.

One of the effective approaches to achieve a low percolation threshold in polymer composites is to use well-dispersed conductive particles with a high aspect ratio as fillers. This method has been demonstrated, experimentally, to decrease the percolation threshold, in accordance with theory [69,70].

However, each matrix has a solubility limit for the filler, beyond which non-connected agglomerations may form. This limitation is especially problematic when using a single polymer as the matrix, as a high concentration of conductive filler is required to achieve the desired electrical conductivity for these kinds of composites [11,20,21,25,31,38,51].

Numerous alternatives have been reported in the literature to reduce the percolation threshold concentration. One promising approach to achieve a lower percolation threshold is to use a double percolation effect by using immiscible polymer blends with a co-continuous morphology. This approach allows for careful control of the distribution of the conductive filler, thus reducing the percolation threshold concentration [1,4,11,13-22,25,26,29-31,38,51]. To improve the affinity of nanoparticles towards the interface, recent studies have focused on both covalent and noncovalent modifications of either nanoparticles or matrices, in order to increase nanoparticles trapping ability at the interface [6,7,9,11,24-26,28,40,42,43,47,48,52,56]. Optimizing the mixing parameters such as temperature, time, mixing intensity, and flow, can have a significant impact on electrical properties of conductive polymer composites [19,28,42,57,71]. However, controlling processing parameters in order to achieve desirable electrical properties, in electrically conductive filled polymer composites, can be challenging. This is because the electrical properties of these composites are influenced by a complex interplay between various factors, as was explained above, such as the nature and distribution of conductive fillers, polymer matrix, processing conditions, and the interface between the conductive fillers and the polymer matrix.

Further reduction of the PT can be achieved by using different post-mixing thermal treatments. Thermal annealing treatment, which is done above the melting or softening temperature, is a

common method to improve the electrical properties of polymer/filler or PB/filler composites [11,14,18,29-31,35,38,40,68,72-74]. During the annealing process, the polymer matrix softens, and the filler particles diffuse, leading to the formation of a more stable filler network. However, the matrix morphology can evolve and affect the filler network formation.

It is important to consider the parameters for post-processing treatments of polymer composites. Typically, these treatments involve maintaining quiescent conditions at high temperatures, such as polymers melting or softening temperatures, for a specified period of time. However, another crucial factor to consider is the nature of the matrix. If the matrix is composed of at least one semi-crystalline polymer, then the post-processing treatment can be optimized based on the crystallization kinetics of the semi-crystalline polymer. Despite the importance of understanding the effect of crystallization on the electrical percolation threshold of polymer/filler conductive composites, there are still limited studies that have conducted a comprehensive evaluation of this relationship [75-82]. This highlights the need for further research in this area to deepen our understanding of the impact of crystallization on the electrical properties of these types of composites.

Figure 1.2 provides an overview of all approaches employed for the reduction of the percolation threshold concentration. This research project primarily focuses on two methods: the matrix effect and the post-processing effect. The former involves the use of a polymer blend with co-continuous morphology to achieve a double percolation effect.

In order to consider all factors associated with the matrix's impact (double percolation effect in polymer blends with co-continuous morphology) it is essential to investigate the fundamental principles of polymer blend morphology, and the underlying mechanisms that govern the distribution of a conductive filler within the blend.

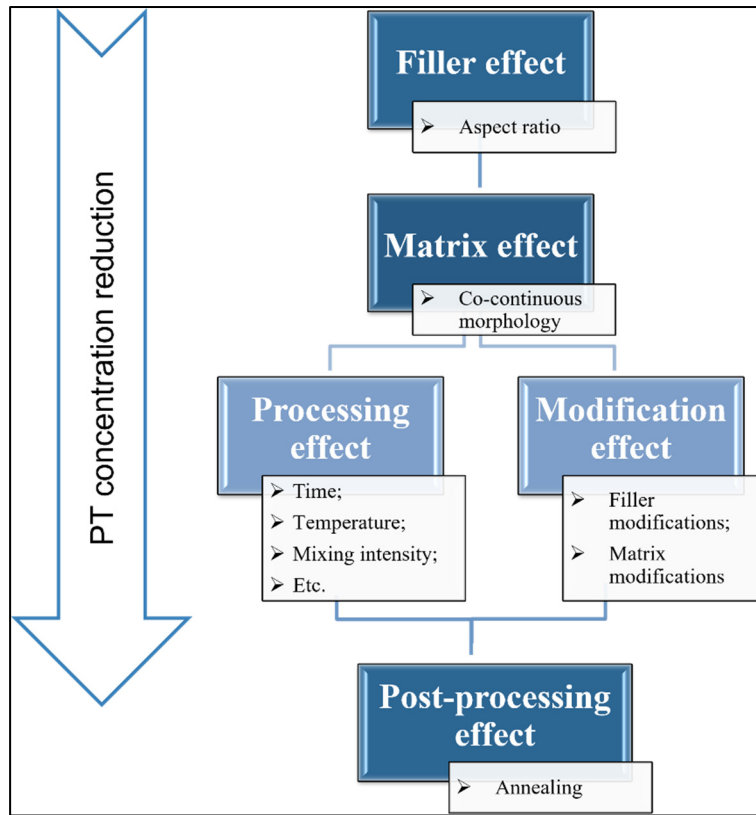


Figure 1.2 Summary of methods for PTC reduction

1.1.2 Double percolation effect – generalities

It has been extensively reported that by using the immiscible polymer blends with a co-continuous morphology, it is possible to tailor the location of the electrically conductive filler inside the matrix, which can lead to the double percolation effect. This is achieved by controlling the interfacial tension between the filler and the polymers forming the blend [1,4,11,13-22,25,26,29-31,38,51]. This concept is illustrated in Figure 1.3, where two immiscible polymers are mixed together, with one of them being pre-mixed with the conductive filler. In two cases the filler location can lead to reaching the double percolation effect. In the first case, the polymer premixed with the conductive filler will percolate into the other polymer, resulting in the filler being uniformly distributed within one phase, creating an electrically conductive network within this phase. In the second case, the filler will diffuse to

the interface of the two polymers and create the conductive network at the interface. In this scenario, significantly low electrical PT can be achieved.

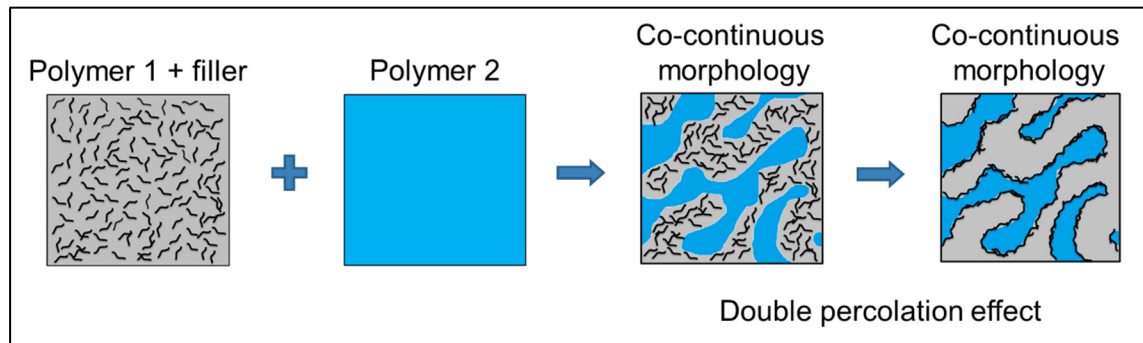


Figure 1.3 Schematic illustration of double percolation effect

The co-continuous morphology of immiscible polymer blends, as well as tailoring the location of the conductive filler play a crucial role in the reduction of PT concentration. In the upcoming sections, we will discuss the methods used to achieve this morphology and ways of prediction of filler location.

1.1.2.1 Morphology of immiscible polymer blends

The study of immiscible polymer blends is of significant interest due to their ability to exhibit unique properties that a combination of those of the individual polymers, resulting in potential applications in a wide range of fields. The mixing of immiscible polymer blends leads to the formation of a two-phase system, where each phase consists of a separate polymer. This two-phase system can be used to obtain electrically conductive nanocomposites by tailoring the location of the conductive particles, because particles can be selectively distributed within the blend.

The final properties of polymer blends are influenced by a variety of factors, with morphology being a critical component. The morphology of polymer blends is influenced by interfacial tension between the polymers, the rheological properties of the polymers, the composition of

the blend, and the processing parameters. By altering these parameters, it is possible to create polymer blends with various morphologies, such as spherical droplets, fibers/rods, lamellae, and co-continuous structures, as shown in Figure 1.4 [83]. These morphologies can be exploited for various applications. For example, the droplet-dispersed morphology can improve toughness, while the rod morphology can enhance strength. The lamellae morphology is useful for barrier properties, and the co-continuous morphology can provide good electrical conductivity.

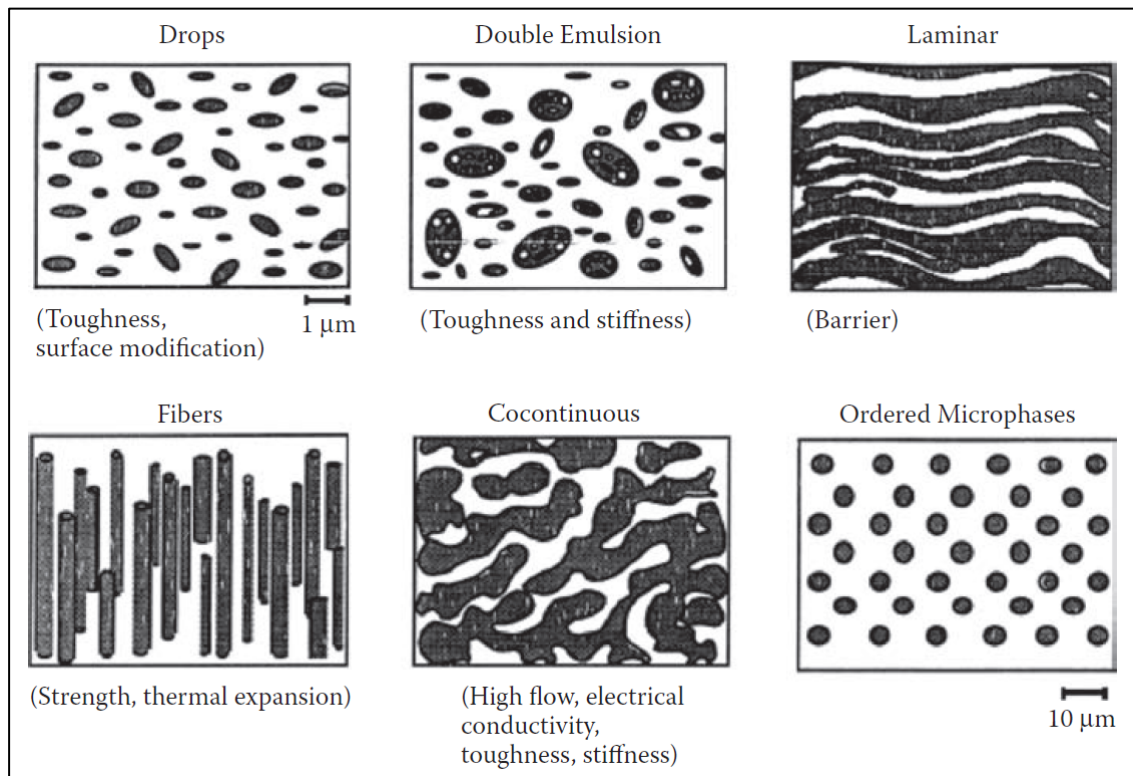


Figure 1.4 Schematic of useful morphologies of polymer blends [83]

1.1.2.2 Co-continuous morphology of immiscible polymer blends

In the context of electrically conductive composites, co-continuous morphology is highly desirable because it can lead to improved electrical conductivity. This morphology is attractive as it not only helps to control the electrical properties by tailoring the location of conductive

fillers and reducing the percolation threshold [11,20,25,26,31,42], but it also offers numerous advantages such as increased stiffness, strength, dimensional stability, and improved heat resistance. These benefits make the co-continuous morphology a highly desirable outcome for those seeking to optimize the properties of electrically conductive polymer blend systems.

Co-continuous morphology is normally achieved when the following relation is fulfilled [84,85]:

$$\frac{\varphi_1}{\varphi_2} \cong \frac{\eta_1}{\eta_2} \quad (1.2)$$

where φ_1 and φ_2 – volume fraction of polymer 1 and polymer 2, respectively; η_1 and η_2 – viscosity of polymer 1 and polymer 2, respectively. It should be noted that it's important to consider the viscosity, used in Equation (1.2), of each individual polymer at the shear rate at which the blend will be processed. Furthermore, the volume fraction should take into account the density of the polymer in the molten state.

1.1.2.3 Characterization of co-continuous morphology of immiscible polymer blends

In order to effectively analyze and understand the co-continuous morphology, as well as be able to correlate morphological properties with electrical one, it is necessary to quantify co-continuous morphology. One approach to quantify the co-continuous morphology is calculating the characteristic domain size ξ of the morphology. This is accomplished by determining the total area of the SEM (scanning electron microscopy) image and dividing it by the total interfacial length between polymer 1 and polymer 2 [30,31]:

$$\xi = \frac{A_{SEM}}{L_{int}} \quad (1.3)$$

where A_{SEM} is the total area of the SEM image and L_{int} is the interface length between the two phases.

While SEM can be a valuable tool for determining the characteristic domain size in co-continuous morphology of polymer blends, this approach has several limitations. These limitations include image resolution, sample preparation, sample orientation, and material contrast. Additionally, statistical analysis is of great importance in obtaining accurate results. It is necessary to measure the characteristic domain size on a statistically significant number of images to ensure accurate measurements.

The other approach for quantification of co-continuous morphology is to use rheology as a tool to probe the morphology. The advantages and limitations of this approach are shown in Section 2.1.

1.1.3 Prediction of filler location inside polymer blend matrix

To accurately predict the distribution of conductive fillers within a co-continuous polymer blend (PB) matrix, one can calculate the wetting coefficient. The calculation of the wetting coefficient can be performed by utilizing thermodynamic models, which are based on determining the most energetically favorable states of the polymer-filler system. Young's equation can be used to estimate the wetting coefficient (ω_a) [26,44,51]:

$$\omega_a = \frac{\gamma_{filler-polymerB} - \gamma_{filler-polymerA}}{\gamma_{polymerA-polymerB}} \quad (1.4)$$

where $\gamma_{filler-polymerB}$ – the interfacial energy between the filler and polymer B; $\gamma_{filler-polymerA}$ – the interfacial energy between the filler and polymer A and $\gamma_{polymerA-polymerB}$ – the interfacial energy between polymer A and polymer B.

In order to determine the wetting coefficient, the interfacial properties of each component should be known. Two methods for determining the interfacial tension from the surface tension of each component [86,87] were developed. The harmonic-mean correlation function (Equation 1.5) and the geometric mean correlation function (Equation 1.6) are both based on the surface tension of the individual components.

$$\gamma_{12} = \gamma_1 + \gamma_2 - 4 \left(\frac{\gamma_1^d \gamma_2^d}{\gamma_1^d + \gamma_2^d} + \frac{\gamma_1^p \gamma_2^p}{\gamma_1^p + \gamma_2^p} \right) \quad (1.5)$$

$$\gamma_{12} = \gamma_1 + \gamma_2 - 2\sqrt{\gamma_1^d \gamma_2^d} - 2\sqrt{\gamma_1^p \gamma_2^p} \quad (1.6)$$

where, γ_1 and γ_2 are the surface tensions of component 1 and component 2, respectively; $\gamma_1^d, \gamma_2^d, \gamma_1^p, \gamma_2^p$ are the dispersive and polar parts of the surface tensions of component 1 and component 2, respectively.

The value of ω_a , calculated by using Equations (1.4-1.6) defines the location of the filler in the blend system. There are three cases of location of the filler in the polymer blend: 1) when $\omega_a > 1$, the filler will have more affinity to polymer A; 2) when $-1 < \omega_a < 1$, the filler will be located at the interface of the two polymers; 3) when $\omega_a < -1$, the filler will have more affinity to polymer B.

1.1.4 Conclusion remarks

After achieving the double percolation effect by controlling the morphology of the polymer blend and the location of the conductive filler, it is important to study the stability of the morphology and the filler network during subsequent processing steps. These may involve greater strains and strain rates, such as, for example, those encountered during injection molding when forming the final product.

To investigate these effects, it is essential to establish appropriate tools monitoring the evolution of morphology and filler network stability. This requires the development of suitable techniques for quantifying the morphology and probing its evolution, which will be discussed in the following sections.

1.2 Linear shear rheology

As shown above, developing electrically conductive polymer-based composites with a low percolation threshold concentration can be achieved using a double percolation effect. For that a polymer blend with a co-continuous morphology as a matrix should be used. The quantification of co-continuous morphology is crucial for its characterization and correlation with electrical properties, and it can be accomplished by two ways, using SEM images in conjunction with Equation (1.3), or using rheology.

Once the desired morphology is obtained, it is vital to ensure its stability during post-processing and deformation. Fortunately, rheological tests in the linear viscoelastic region can provide valuable insights into the microstructural properties of polymer blend composites. These tests can be employed to quantify co-continuous morphology and study its evolution, as well as monitor the development and evolution of the filler network.

In section 2.1, the model used to analyze the rheological behavior of polymer blends with co-continuous morphology is explained. This model is used to quantify the morphology and provide a detailed understanding of the microstructural properties of polymer blends. Section 2.2 presents the model that explains the effect of the filler network on rheological properties of filled polymer composites. In section 2.3, a strategy to study the evolution of morphology is proposed. This strategy involves monitoring the rheological and electrical properties during, as well as after the application of deformation to the composites.

1.2.1 Co-continuous morphology modelling

Several models have been developed to analyze the linear viscoelastic rheological behavior in small amplitude oscillatory shear (SAOS) of polymer blends with dispersed droplets type morphology, whether filled or not. It should be noted that SAOS tests are a common technique in polymer blend rheology, to assess the morphology of polymer blends. The results of SAOS tests, fitted to constitutive equations, are used to determine the rheological properties of the material and its morphology [24,59-63]. Performing SAOS tests on polymer blends, it is possible to characterize the morphology of both pure polymer blends and filled polymer blends with droplet-dispersed morphology.

Examples of models to characterize this morphology include the Palierne model [59], Gramespacher and Meissner model [60], and Bousmina model [61]. However, there is a lack of models available for characterizing more complex morphologies of polymer blends, such as a co-continuous morphology, particularly when fillers are added. To address this issue, researchers have developed several models aimed at predicting the rheological behavior of polymer blends with a co-continuous morphology [29,88-92]. Only a few of these models, however, provide a quantitative analysis of the co-continuous morphology through rheological analysis [29,88,89].

One such model is that developed by Yu et al. [89,93], referred to as the YZZ model. For a polymer blend with co-continuous morphology, there are two components that contribute to the storage modulus of the blend [94]. The basic idea came from Palierne [59], and Gramespacher and Meissner [60] models, for PBs with dispersed droplets type morphology:

$$G'_{blend}(\omega) = G'_{components}(\omega) + G'_{interface}(\omega) \quad (1.7)$$

where $G'_{blend}(\omega)$ is the storage modulus of a PB matrix with co-continuous morphology, $G'_{components}(\omega)$ is the PB components contribution, and $G'_{interface}(\omega)$ is an PB interface contribution.

The contribution from the components was developed by Veenstra et al., where Yu et al. [89] replaced the Young's moduli in the original model by the dynamic moduli [95]:

$$G'_{components} = \frac{a'^2 b' G_1'^2(\omega) + (a'^3 + 2a'b' + b'^3) G_1'(\omega) G_2'(\omega) + a' b'^2 G_2'^2(\omega)}{b' G_1'(\omega) + a' G_2'(\omega)} \quad (1.8)$$

where $G_1'(\omega)$ is the storage modulus of component 1 in PB; $G_2'(\omega)$ is the storage modulus of component 2 in PB, and a' can be found from the volume fraction of phase 1: $\varphi_1 = 3a'^2 - 2a'^3$.

Here, an elementary cell of a co-continuous morphology was assumed to consist of three connected parallelepiped shape elements of length $l'_c = a' + b' = 1$, square section of edge a' , and $b' = 1 - a'$ as shown on Figure 1.5(a) what is 1/8 of the primary microstructure.

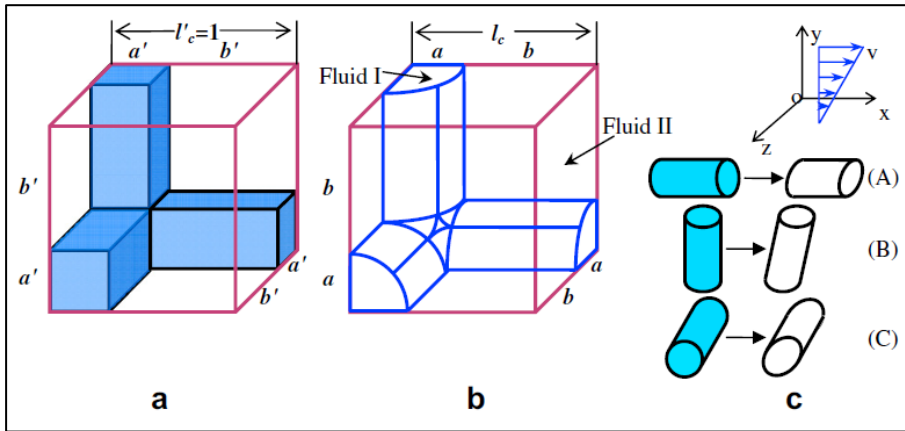


Figure 1.5 Schematics of an ideal co-continuous morphology for (a) the components contribution, (b) the interfacial contribution and (c) deformation of interfaces

Taken from Yu et al. [89]

To take into account the interface contribution, Yu et al. [89] made a modification of the schematic of an ideal co-continuous morphology for the components' contribution proposed by Veenstra et al. [95] (see Figure 1.5(a)) by considering the parallelepiped shape elements to be cylinders instead (see Figure 1.5(b)). It was done in order to consider a critical aspect of blend rheology – the contribution of the interface between two polymers. These cylinders are assumed to have a radius a and a characteristic length l_c with $a' = a/l_c$ and $b' = b/l_c$. Interface contribution of each cylinder can be found from the stress contribution caused by the deformation of each cylinder at the interface (see Figure 1.5(c)). The total interface contribution for the storage modulus can be expressed as:

$$G'_{interface} = G'_A{}_{interface} + G'_B{}_{interface} + G'_C{}_{interface} \quad (1.9)$$

where $G'_A{}_{interface}$, $G'_B{}_{interface}$, $G'_C{}_{interface}$ are the elastic moduli due to interface deformation of the cylinder type A, type B and type C, respectively.

By performing the calculations for the interface contribution of each cylinder, Yu et al. derived an expression for the storage modulus of the interface contribution:

$$G'_{interface} = \frac{k_C}{6} \alpha S_V \left(\frac{k_B}{k_C} + \frac{3}{4} \frac{f_2 \omega^2 \tau^2}{f_1^2 + \omega^2 \tau^2} \right) \quad (1.10)$$

where α is the interfacial tension, ω is the frequency, S_V is the specific area, inversely proportional to the characteristic domain size ξ , given by:

$$S_V = \frac{3\pi ab}{2l_c^3} = \frac{1}{\xi} \quad (1.11)$$

$$\tau = \frac{\eta_m a}{\alpha} \quad (1.12)$$

$$k_C = -\frac{f_2 \omega^2 \tau^2}{f_1^2 + \omega^2 \tau^2} \gamma_0 \quad (1.13)$$

$$k_B = -\frac{f_1 f_2 \omega \tau}{f_1^2 + \omega^2 \tau^2} \gamma_0 \quad (1.14)$$

with

$$f_1 = \frac{40(p+1)}{(2p+3)(19p+16)} \quad (1.15)$$

and

$$f_2 = \frac{5}{2p+3} \quad (1.16)$$

where p is the viscosity ratio of fluid 1 over fluid 2, and γ_0 is the strain amplitude. k_B and k_C are constants that relate to a random orientation and possible distortion of a co-continuous element, respectively, and the ratio $k_B/k_C \leq 1$.

Using Equations (1.7-1.16) the storage modulus of the blend with a co-continuous morphology can be written as:

$$G'_{blend}(\omega) = \frac{\alpha'^2 b' G_1'^2(\omega) + (\alpha'^3 + 2\alpha' b' + b'^3) G_1'(\omega) G_2'(\omega) + \alpha' b'^2 G_2'^2(\omega)}{b' G_1'(\omega) + \alpha' G_2'(\omega)} + \quad (1.17)$$

$$\frac{k_C}{6} \alpha S_V \left(\frac{k_B}{k_C} + \frac{3}{4} \frac{f_2 \omega^2 \tau^2}{f_1^2 + \omega^2 \tau^2} \right)$$

where G'_1 is the storage modulus of component 1; G'_2 is the storage modulus of component 2; More details can be found in Yu et al. [89].

As demonstrated by Yu et al., the developed model effectively fits the experimental data of pure PB with a co-continuous morphology (polystyrene/poly(ethyleneco-1-octene) (PS/POE) co-continuous blends), as illustrated in Figure 1.6. The authors also showed that the model can be used for quantifying the co-continuous morphology of PB by calculating the characteristic length (l_c), which can then be used in Equation (1.11) to determine the characteristic domain size (ξ) of the co-continuous structure.

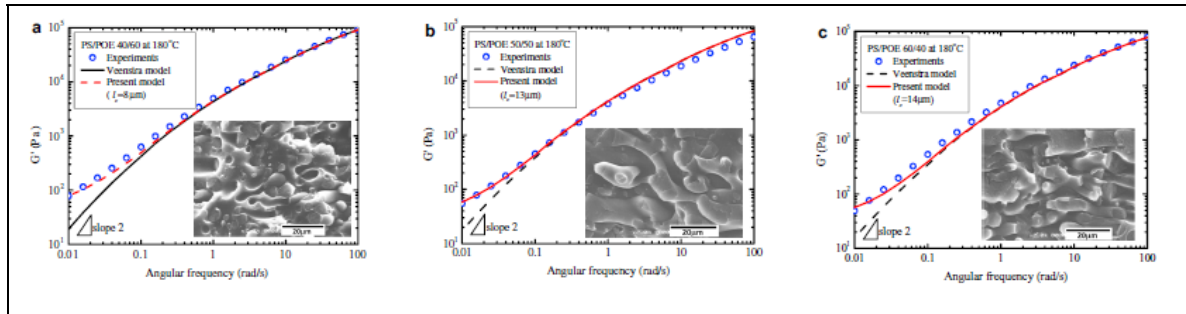


Figure 1.6 Storage modulus of PS/POE co-continuous blends as a function of frequency. (a) PS/POE 40/60; (b) PS/POE 50/50; (c) PS/POE 60/40. Insets are the corresponding SEM

pictures

Taken from Yu et al. [89]

It should be noted that Yu et al. [89,93] rheological model was developed only for unfilled polymer blends with co-continuous morphology. Therefore, it is important to consider the effect of the filler network on rheological properties of the polymer blends with co-continuous morphology.

1.2.2 Two-phase model and the elasticity of the filler network

It is widely accepted that the rigid filler network plays a crucial role in enhancing the elasticity of the matrix, as evidenced by the observed increase in storage modulus for different polymer blend/filler systems [2,29,31]. Figure 1.7 shows a representative illustration of this phenomenon, where the storage modulus is plotted as a function of frequency in SAOS for filled composites of linear low density polyethylene/ethyl vinyl acetate containing graphene (GN) co-continuous composites [31].

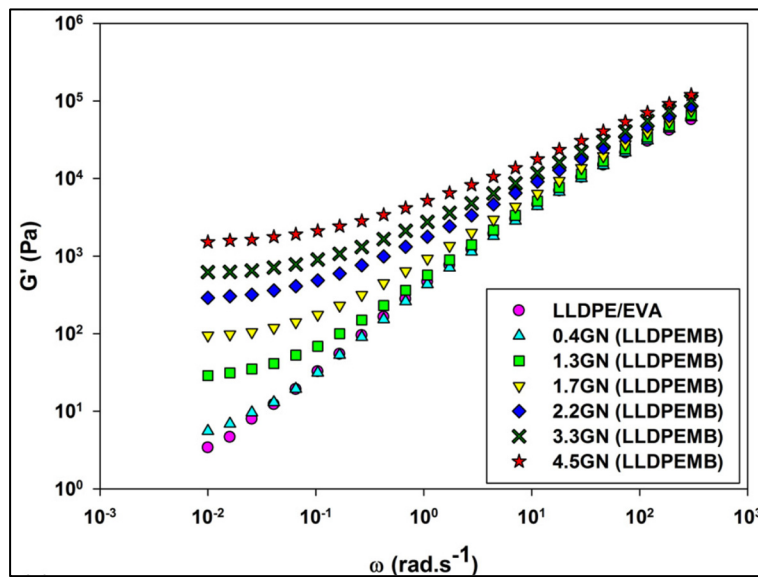


Figure 1.7 SAOS tests performed at 160 °C for LLDPE/EVA/GN composites

Extracted from Helal et al. [31]

The results indicate that the storage modulus increases as the concentration of GN increases, and it eventually reaches a plateau at low frequencies. This increase in G' is a result of the interactions between the filler and the matrix, as well as between particles. The two-phase model, which uses SAOS tests data, has been successfully used to differentiate the elastic response of the filler network from that of the polymer matrix [96,97]. According to this model, the viscous response of the composite is primarily influenced by the polymer matrix at high frequencies, while the elastic response is primarily influenced by the networks formed by

particle clusters at low frequencies (as illustrated in Figure 1.8). To confirm the applicability of this model to a specific polymer nanocomposite system, a master curve is constructed using all the samples with the filler concentration that are above the percolation threshold concentration. The process for building the master curve, and the significance of the scaling parameters are explained in detail elsewhere [96,97]. It is important to note that this model provides an understanding that the elasticity of the filler network dominates that of the matrix at low frequencies. Moreover, the elasticity of the filler network can be studied separately from the matrix and independently of its complexity.

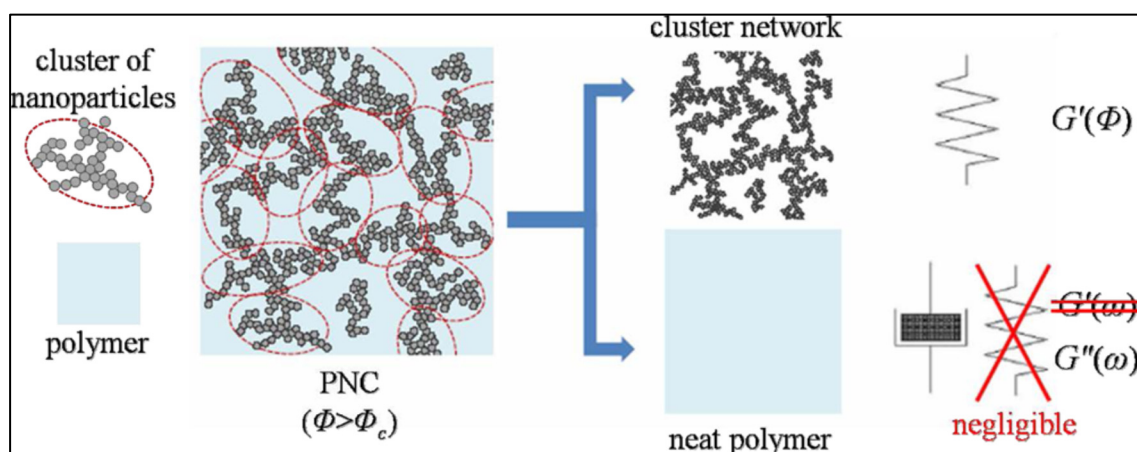


Figure 1.8 Schematic representation of the origin of viscoelasticity in polymer nanocomposites above the percolation threshold

Extracted from [97]

By using the two-phase model, it is possible to predict the rheological percolation threshold. Since the elasticity of the network G'_0 is growing with particles' concentration – p , the rheological percolation threshold can be defined as the minimum particle concentration needed for the formation of a filler network as [97]:

$$G'_0 = k \cdot (P - P_c)^v \quad (1.18)$$

where G'_0 is frequency-independent elastic modulus, P is the mass fraction of MWCNTs, P_c is the percolation threshold, ν is a fitted exponent that depends, only, on the dimensionality of the system, and k is a scaling factor.

1.2.3 Design of experiments

In order to investigate the evolution of the morphology and filler behavior of the composites, it is necessary to subject the material to a deformation flow. In this case, SAOS-deformation-SAOS tests can be used to assess the evolution of the material's properties during deformation, by comparing the results of the first and second SAOS tests [63,98].

Figure 1.9 depicts a typical shear deformation test performed to study the droplet disperse morphology in a polymer blend. The first step involves subjecting the blend to intense shear at a high shear rate, creating a uniform droplet disperse morphology. The subsequent step involves investigating the impact of flow-induced coalescence on the properties of the polymer blend. This method enables the investigation of the behavior of droplets under shear deformation [99].

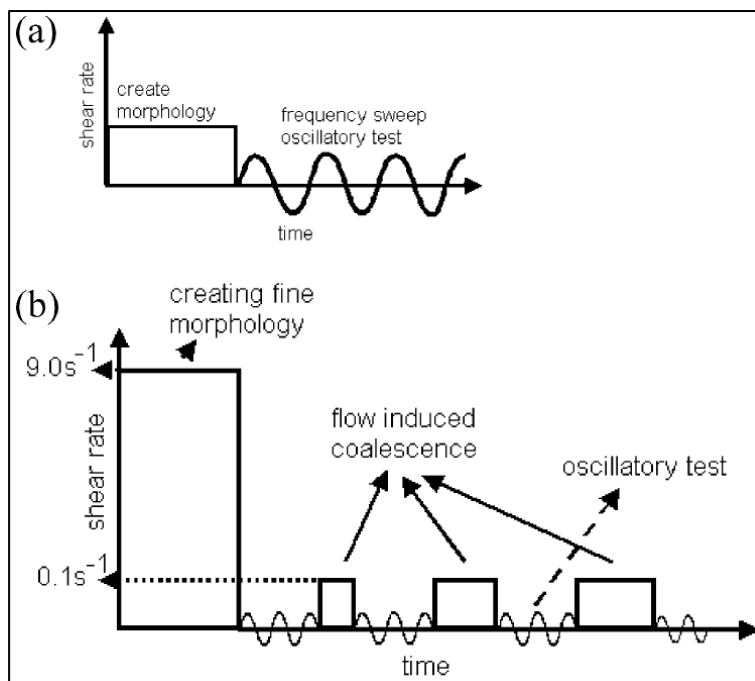


Figure 1.9 Shear protocols to a) investigate the effect of shear rate and b) investigate induced droplets coalescence process

Extracted from [99]

The deformation step in the SAOS-deformation-SAOS sequence is typically carried out at a constant shear rate for a certain period of time or shear strain to induce droplet break-up [100,101] or coalescence [63,98,99,102-108], in both filled and unfilled polymer blends exhibiting droplet disperse morphology.

In the case of electrically conductive composites with a co-continuous morphology, it is crucial to assess the morphology and filler network evolution during shear to investigate its possible stabilization. Shear tests presented in Figure 1.9 can aid in this assessment. This is particularly important because the processing of these composites can significantly impact their resulting properties. High strains and shear rates that are typically associated with melt processing techniques can lead to the destruction of the conductive filler network, which can have a negative impact on the electrical conductivity of the composite. Therefore, understanding the

filler network evolution during shear can help to optimize the processing conditions to maintain the desired electrical properties of the composite.

To replicate coalescence and break-up phenomena during the deformation step, steady shear rates should be selected to induce these phenomena based on established theories. Specifically, Taylor theory [109] and Grace plot [110] were used to determine these values. In the case of droplet disperse morphology, the deformation of a droplet under uniform flow is dependent on the capillary number (Ca) - the ratio of the viscous force ($F_{viscous}$) over the interfacial force ($F_{interfacial}$) (Equation (1.19)) - as well as the viscosity ratio (p) (Equation (1.20)) [109].

$$Ca = \frac{F_{viscous}}{F_{interfacial}} = \frac{\eta_m \dot{\gamma} R_v}{\alpha} \quad (1.19)$$

$$p = \frac{\eta_d}{\eta_m} \quad (1.20)$$

where η_m is the viscosity of the matrix, η_d is the viscosity of the dispersed phase, $\dot{\gamma}$ is the shear rate, R_v is the volume average radius of the drops, α is the interfacial tension.

Droplet break-up and coalescence occur when a flow is applied above or below a certain critical value of the capillary number (Ca_c). Grace [110], experimentally, determined the critical capillary number as a function of the viscosity ratio for both rotational (simple shear) and irrotational (extensional) shear, and this data is presented in Figure 1.10. The critical capillary number can be calculated using Equation (1.21) [111], which is an empirical fit to Grace's data provided by Tucker et al. [111].

$$\log(Ca_c) = -0.506 - 0.0995 \log(p) + 0.124(\log(p))^2 - \frac{0.115}{\log(p) - \log(4.08)} \quad (1.21)$$

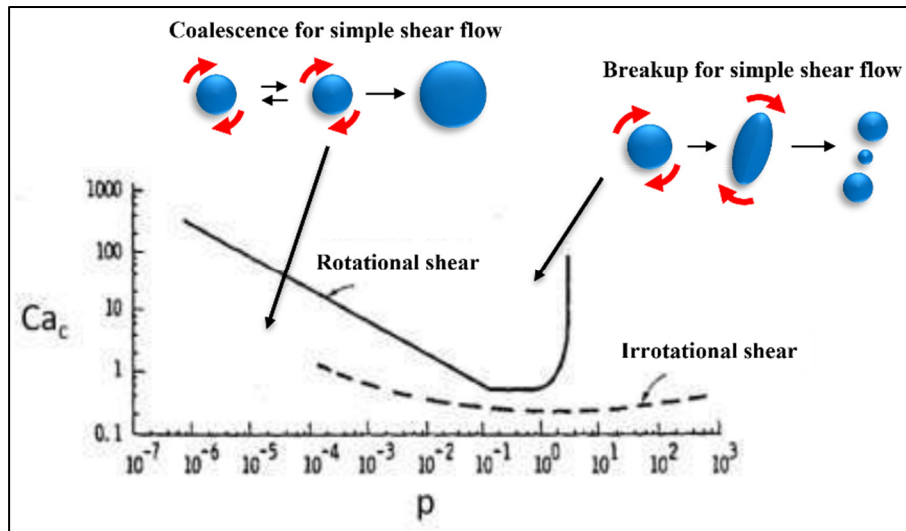


Figure 1.10 Ca_c as a function of p in rotational and irrotational shears together with illustrations of droplets break-up and coalescence (adapted from Grace [110])

Finally, using the Equation (1.21) to obtain the critical capillary number (Ca_c) along with Equation (1.19) it is possible to find the critical shear rate ($\dot{\gamma}_c$), above which break-up happens and below which coalescence takes place. While this theory was originally developed for droplet dispersions, the critical shear rate can also provide an indication of the shear rates required to induce significant changes in composites that exhibit a co-continuous morphology.

CHAPTER 2

ULTRA-LOW PERCOLATION THRESHOLD INDUCED BY THERMAL TREATMENTS IN CO-CONTINUOUS BLEND-BASED PP/PS/MWCNTS NANOCOMPOSITES

Daria Strugova, José Carlos Ferreira Junior, Éric David and Nicole R. Demarquette

Mechanical Engineering Department, École de Technologie Supérieure, Montréal, Québec

Paper published in *Journal of Nanomaterials*, June 2021

DOI: 10.3390/nano11061620

Abstract

The effect of the crystallization of polypropylene (PP) forming an immiscible polymer blend with polystyrene (PS) containing conductive multi-wall carbon nanotubes (MWCNTs) on its electrical conductivity and electrical percolation threshold (PT) was investigated in this work. PP/PS/MWCNTs composites with a co-continuous morphology and a concentration of MWCNTs ranging from 0 to 2 wt.% were obtained. The PT was greatly reduced by a two-step approach. First, a 50% reduction in the PT was achieved by using the effect of double percolation in the blend system compared to PP/MWCNTs. Second, with the additional thermal treatments, referred to as slow-cooling treatment (with the cooling rate 0.5 °C/min), and isothermal treatment (at 135 °C for 15 min), ultra-low PT values were achieved for the PP/PS/MWCNTs system. A 0.06 wt.% of MWCNTs was attained upon the use of the slow-cooling treatment and 0.08 wt.% of MWCNTs upon the isothermal treatment. This reduction is attributed to PP crystals' volume exclusion, with no alteration in the blend morphology.

Keywords: electrical percolation threshold; electrical conductivity; thermoplastic composites; polymer blend; multi-wall carbon nanotubes; polymer crystallization

2.1 Introduction

Conductive thermoplastic composites have gained a lot of attention in different research fields since they are used in a variety of industrial applications. Among their many applications, these materials are used in sensors, intelligent medical devices, energy harvesting, actuators, flexible electronics, robotics, static dissipation and electromagnetic interference (EMI) shielding. The interest in these composite materials stems from their advantages, namely the ability to achieve the electrical conductivity in a wide range, processability into products of complex shapes, as well as flexibility, lightweight, and corrosion resistance [1-12].

Conductive nanocomposites are obtained by dispersing electrically conductive nanoparticles (particles with at least one of their dimensions ranging from 1 to 100 nm) within a matrix. The most used nanoparticles to obtain electrically conductive polymers are carbon black (CB) [13-23], carbon nanotubes (CNTs) [2-8,24-28], and graphene [12,29-37]. Due to the advantages conductive thermoplastic composites present, significant research has been conducted towards achieving certain desired properties at low filler concentrations, primarily by reducing the percolation threshold (PT). The PT is defined as the concentration of particles at which the composite starts to be conductive.

Several methods to reduce the PT concentration have been reported in the literature. One of the simplest methods is to use well-dispersed conductive particles with the highest possible aspect ratio as a filler. This has been experimentally found to lower the PT as was predicted by Bruggeman, V.D., and Böttcher, C. in the 1940s [69,70]. In order to further reduce the PT, more recent studies have dealt with the modification of nanoparticles, whilst others have made use of the controlled matrix morphology to tailor the location of nanoparticles. In particular, the use of immiscible polymer blends (PBs), presenting a co-continuous morphology, has been suggested. By controlling the interfacial tension between the filler and the polymers forming the blend, one can tailor the location of the conductive filler at the interface, thus lowering the

PT. Depending on the used binary blend, the nanoparticles were added alone or with a compatibilizer [6,9,24-26,40,42,47,52]. For example, Chen, J. et al. have shown that introducing 5 wt.% of SEBS-g-MA in PP/PS (70/30 wt.%) co-continuous matrix reduces PT from 1.22 wt.% for PP/PS/MWCNTs to 0.66 wt.% for PP+SEBS-g-MA/PS/MWCNTs [44]. Other additives like graphene, graphene oxide (GO), organoclay, CB, noncovalent and covalent modifiers were also reported in the literature to reduce the PT of PB/CNTs co-continuous systems [9,11,24,28,43,47,48,56].

Furthermore, other researchers suggested that the thermal annealing of polymer/filler or PB/filler composites above the melting or softening temperature could further decrease the PT and improve the electrical conductivity of a system [11,14,18,29-31,35,38,40,68,72-74]. In polymer blend-based composites, this effect is usually accompanied by changes in the blend morphology. First, the morphology coarsens (the domain size becomes larger) and then it is stabilized by increasing the annealing time of the filled composites. This leads to the easier creation of the conductive filler network due to the reduction in the interphase area where the filler is distributed. One of the most dramatic effects was, for example, achieved by Chen, Y. et al. who showed that annealing at 200 °C for 2 h decreased PT from 0.48 wt.% to 0.09 wt.% for a PP/PMMA (30/70 wt.%) co-continuous blend containing MWNTs [68]. All these strategies have been used for polymer pairs containing both amorphous and semi-crystalline polymers. However, the influence of crystallization on PT and electrical conductivity for immiscible polymer blends, containing at least one semi-crystalline polymer, has to date not been adequately evaluated.

To our knowledge, there are few studies that have evaluated the effect of crystallization on the PT of polymer/filler conductive composites [80-82]. Wang, J. et al. have investigated the effect of the cooling rate on the electrical conductivity of PP/MWCNTs composites containing a sorbitol-based external nucleating agent (NA). They showed that the PT was reduced for both PP/MWCNTs and PP/MWCNTs/NA from 0.75 wt.% at a fast-cooling rate of 150 °C/min to 0.36 wt.% at a slow-cooling rate of 1.5 °C/min [80]. Huang, C. et al. have shown the effect of

matrix crystallinity on the PT of PLLA/MWCNTs composites containing 0.15 wt.% of a NA. The PT was reduced from 0.96 wt.% to 0.75 wt.% for the samples which were treated for 0.1 and 6 min, respectively, at 130 °C [82]. Other researchers have reported the effect of stereocomplex (SC) crystallization on the PT and electrical conductivity of miscible PLLA/PDLA blend composites, containing a conductive filler [75-79]. In these cases, the change in PT happens due to the volume exclusion effect of stereocomplex crystals.

The present study aimed to shed light on the effect of the semi-crystalline polymer's crystallization within the PB on the reduction in the percolation threshold. In particular, for this we chose PP and PP/PS blend-based composites containing MWCNTs obtained by the melt-mixing process. It will be shown that two types of treatments aiming to affect PP crystal growth can significantly improve the electrical conductivity and reduce the PT to ultra-low values. These treatments are proposed to achieve lower PTs for other semi-crystalline-based PB co-continuous systems. In addition, it will be shown that the proposed treatments do not significantly change the PB morphology compared to thermal annealing above the melting or softening temperature.

2.2 Materials and Methods

2.2.1 Materials

Commercial polypropylene (PP)—PP4712E1 grade from Exxon Mobile with a density $0.9 \text{ g}\cdot\text{cm}^{-3}$ —and polystyrene (PS)—MC3650 from PolyOne with a density $1.04 \text{ g}\cdot\text{cm}^{-3}$ —were used in this work. Multi-walled carbon nanotubes (MWCNTs) grade NC7000TM from Nanocyl with an average diameter and a length of 9.5 nm and 1.5 μm , respectively (aspect ratio ~ 160), and with a nominal electrical conductivity of $10^6 \text{ S}\cdot\text{m}^{-1}$, were used as the conductive filler in the composites.

2.2.2 Processing

2.2.2.1 Extrusion

The materials were prepared by a melt-mixing process using a Haake Rheomix OS PTW16 twin-screw extruder (Thermo Fisher Scientific Inc., Waltham, MA, USA). The temperature was fixed at 220 °C in all zones, and the screw speed was adjusted to 100 rpm for all compositions. First, a masterbatch of PP with 10 wt.% of MWCNTs was prepared. Second, PP composites with a MWCNTs concentration varying from 0 to 2 wt.%, as well as co-continuous morphology 50/50 PP/PS blends with MWCNTs concentration, also varying from 0 to 2 wt.%, were prepared by dilution of the PP/MWCNTs masterbatch.

To achieve a co-continuous morphology for PP/PS/MWCNTs composites, the calculation of a co-continuous range based on viscosity measurements both PP and PS should be done. The viscosity of both PP and PS was measured using a capillary rheometer at a temperature of 200 °C. For the effective shear rate of 100 s⁻¹ experienced in the twin-screw extruder, both polymers manifested similar viscosities (as can be seen in Figure-A I-1 in the Supplementary Materials) [112,113]. A 50/50 wt.% PP/PS concentration was, therefore, chosen following the analysis of Jordhamo, G. et al. [85].

2.2.2.2 Thermal Treatments

Three thermal treatments were performed by compression molding and were designated here as: (1) fast cooling; (2) slow cooling; and (3) isothermal. Figure 2.1 shows a schematic of the temperature vs. time profile for all thermal treatments.

The three treatments consisted of three steps each, with the first two steps being the same and a third one differing for each treatment. The first step was at a temperature of 200 °C under constant pressure of 0.8 MPa for 10 min. The second one was at a temperature of 200 °C under a pressure of 10 MPa for an additional 10 min.

1. For the fast-cooling treatment, the third step was fast cooling to room temperature, which was performed at a rate of 50 °C/min under a pressure of 10 MPa. The whole treatment, all three steps, took 22 min (Figure 2.1).
2. For the slow-cooling treatment, the third step was fast cooling to 160 °C and a slow cooling from 160 °C to 135°C at a rate of 0.5 °C/min, followed by fast cooling from 135 °C to room temperature under a pressure of 10 MPa. The whole treatment took 1 h 10 min (Figure 2.1). The starting temperature of the treatment (160 °C) was chosen to prevent the so-called annealing effect [11,14,29-31,68] which could involve the coarsening of blend morphology. The temperature of 135 °C at the end of the treatment corresponds to the highest onset temperature of crystallization, evaluated by the DSC analysis.
3. For the isothermal treatment, the third step was fast cooling to 135 °C which was maintained for 15 min. Then, the sample was fast cooled to room temperature under a pressure of 10 MPa. The whole treatment took 36 min (Figure 2.1).

Fast- and slow-cooling treatments were carried out to study how the cooling rate, which has a direct effect on the crystallization kinetics and crystals morphology, affects electrical conductivity due to the volume exclusion effect. Slow cooling was performed at 0.5 °C/min to allow the growth of larger crystals.

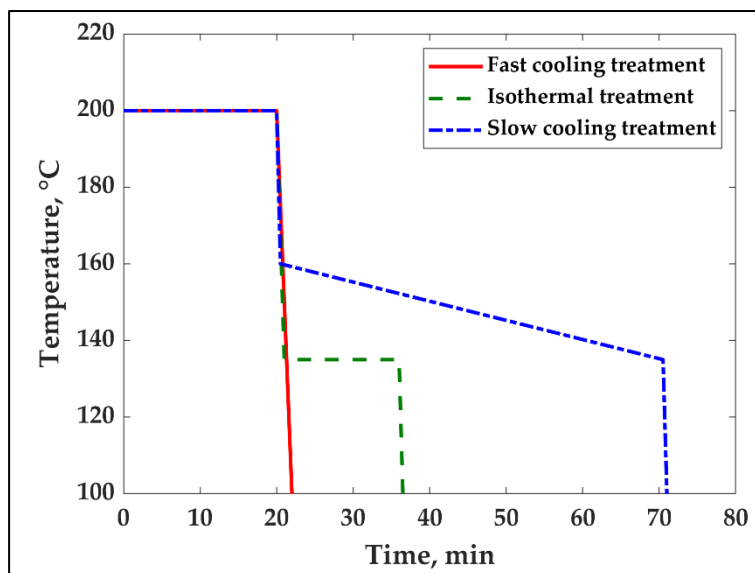


Figure 2.1 Temperature vs. time for fast-cooling treatment, isothermal treatment, and slow-cooling treatment

2.2.3 Characterization

2.2.3.1 Crystallization Studies

Differential scanning calorimetry (DSC) was performed using a Pyris 1 Differential Scanning Calorimeter (PerkinElmer, Waltham, MA, USA). The nitrogen gas flow rate was set to 20 mL/min. The samples were encapsulated in standard aluminum pans and covers. The DSC was calibrated using indium and zinc standards.

Two different cycles were used to determine the crystallinity of the composites as well as the crystallization kinetics.

Non-isothermal crystallization

The samples were heated from 50 °C to 200 °C at 10 °C/min and then cooled down from 200 °C to 50 °C at 10 °C/min under nitrogen atmosphere. This thermal cycle was performed twice for all samples to erase the thermo-mechanical history of the samples. The data from the second heating and cooling cycle were used for calculations. Prior to that, the same thermal cycle was run with empty pans for getting a baseline.

The crystallinity for all compositions was calculated using Equation (2.1):

$$X_c = \frac{\Delta H}{(1 - w)\Delta H_m} \quad (2.1)$$

where X_c is the weight fraction of the crystalline phase, ΔH is the heat of fusion of the sample, ΔH_m is the heat of fusion of 100% crystalline PP (207 J/g) [114], and w is the MWCNTs' weight fraction for PP/MWCNTs composites and (MWCNTs + PS) weight fraction for PP/PS/MWCNTs composites.

Isothermal crystallization

The samples were heated from 50 °C to 200 °C at 50 °C/min and kept at this temperature for 5 min to eliminate any previous thermal history; then, they were cooled to 135 °C at 50 °C/min and kept at 135 °C for 30 min for isothermal crystallization. Again, in this case, prior to testing the sample, the same thermal cycle was run with empty pans to obtain a baseline.

2.2.3.2 Polarized Optical Microscopy

The crystals' growth and their morphology were studied using polarized optical microscopy (POM)—OLYMPUS BX51 microscope (Olympus Co., Tokyo, Japan) equipped with a hot stage. The morphology evolution (crystal growth) at 135 °C was observed. In this case, the heat treatment was performed without any applied pressure. Furthermore, the morphology of

the crystals of pure PP and PP/MWCNTs composites at room temperature obtained by fast-cooling, isothermal, and slow-cooling treatments as described above was also observed.

2.2.3.3 Electrical Conductivity

The electrical properties as a function of frequency for all compositions were evaluated using a broadband dielectric spectrometer (BDS) (Novocontrol Technologies GmbH & Co. KG, Montabaur, Germany) in the frequency range from 10^{-2} to 3×10^5 Hz under an excitation voltage of 3 VRMS applied across the sample.

The electrical conductivity was evaluated from the measurement of the AC complex conductivity as a function of frequency— $\sigma^*(\omega)$, which is related to the complex permittivity by

$$\sigma^*(\omega) = j\omega\varepsilon_0\varepsilon^*(\omega) \quad (2.2)$$

where ω is the frequency, ε_0 is the vacuum permittivity and $\varepsilon^*(\omega)$ is the complex permittivity which includes the contributions of the electrical conductivity and can be expressed as

$$\varepsilon^*(\omega) = \varepsilon'(\omega) - j\varepsilon''_{tot}(\omega) = \varepsilon'(\omega) - j\left(\varepsilon''_p(\omega) + \frac{\sigma}{\omega\varepsilon_0}\right) \quad (2.3)$$

where $\varepsilon'(\omega)$ is the real part of the complex permittivity, $\varepsilon''_{tot}(\omega)$ the total imaginary part, ε''_p represents the imaginary part of the permittivity due to the polarization phenomena, and σ is an electrical conductivity. By combining these two equations, we can obtain:

$$\begin{aligned} \sigma^*(\omega) = j\omega\varepsilon_0\varepsilon^*(\omega) &= j\omega\varepsilon_0 \left(\varepsilon'(\omega) - j \left(\varepsilon''_p(\omega) + \frac{\sigma}{\omega\varepsilon_0} \right) \right) = \\ &\sigma + \omega\varepsilon_0\varepsilon''_p(\omega) + j\omega\varepsilon_0\varepsilon'(\omega) \end{aligned} \quad (2.4)$$

where the real part of the complex conductivity is:

$$\sigma'(\omega) = \sigma + \omega \varepsilon_0 \varepsilon_p''(\omega) \quad (2.5)$$

The equipment measures the total imaginary part— $\varepsilon_{tot}''(\omega)$ since the device cannot distinguish between the two contributions. Accordingly, the electrical conductivity cannot be formally isolated. However, since it does not increase with frequency unlike the contribution from $\varepsilon_p''(\omega)$, the occurrence of a low frequency plateau in the plot of $\sigma'(\omega)$ as a function of frequency indicates that the value of the electrical conductivity dominates the real part of the complex conductivity that then becomes very close to the true DC conductivity at low frequencies. The electrical conductivity values presented in this work refer to the value of $\sigma'(\omega)$ at the lowest frequency (1×10^{-2} Hz). Consequently, this value is always higher than the true conductivity, particularly below the percolation threshold, however, once the percolation threshold is reached, it gives a very good approximation of the conductivity. Disks of 25 mm in diameter and 1 mm in thickness, covered on both sides with 20 nm of gold, were used for the measurements.

2.2.3.4 Scanning Electron Microscopy

The morphology of PP/PS/MWCNTs composites for all treatments was observed by scanning electron microscopy (SEM) using a S3600 Hitachi microscope (Hitachi, Ltd., Tokyo, Japan) in the secondary electrons' mode. The samples were fractured in liquid nitrogen and then polystyrene phase was extracted by using butanone at room temperature, under continuous stirring for two hours. Then, the samples were dried under vacuum at room temperature during 12 h. After drying, the samples were covered with gold by using a gold sputter coater, model K550X. All porous samples after PS extraction were imaged at an accelerating voltage of 5 kV.

2.3 Results

2.3.1 Effect of the Treatments on Electrical Conductivity and Morphology of PP/PS/MWCNTs Composites

Figure 2.2 shows the electrical conductivity as a function of MWCNTs mass fraction for PP/PS/MWCNTs composites after fast-cooling, isothermal, and slow-cooling treatments. Equation (2.6) was used to calculate the percolation threshold of composites that underwent the different thermal treatments:

$$\sigma = k \cdot (P - P_c)^t, \text{ with } P > P_c, \quad (2.6)$$

where σ is the electrical conductivity of the composite, P is the mass fraction of MWCNTs, P_c is the percolation threshold (PT), t is a fitted exponent that depends, only, on the dimensionality of the system, and k is a scaling factor. It should be noted that this equation is valid for $P > P_c$.

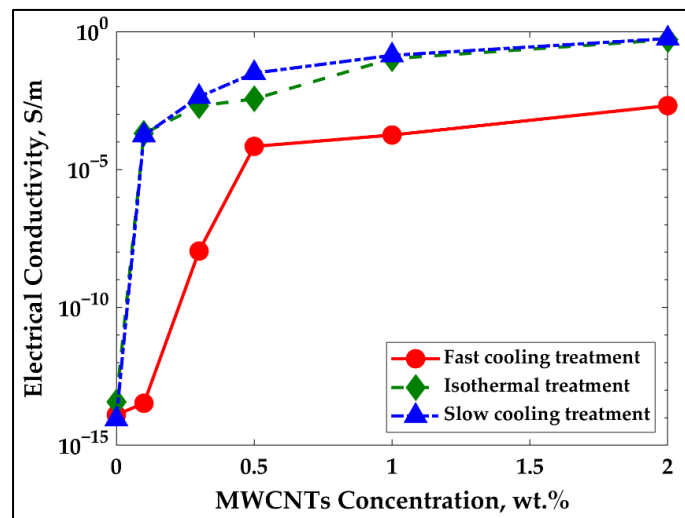


Figure 2.2 Effect of treatments on the electrical conductivity of PP/PS/MWCNTs composites as a function of MWCNTs concentration

A linear regression fit was employed to determine the percolation threshold, $\log(\sigma)$ vs. $\log(P - P_c)$. The results of these fits for each treatment of PP/PS/MWCNTs composites are presented in Table 2.1.

Table 2.1 Percolation threshold and fitting values of experimental data according to Equation (2.6) for PP/PS/MWCNTs composites after each treatment

Parameters	Fast-Cooling Treatment	Isothermal Treatment	Slow-Cooling Treatment
P_c, wt.%	0.28	0.08	0.06
k, S/m	8.5×10^{-4}	0.12	0.15
t	1.60	2.20	2.00
R^2	0.97	0.89	0.99

The results presented in Figure 2.2 and Table 2.1 show that the isothermal and slow-cooling treatments resulted in a much lower percolation threshold. The percolation threshold was drastically reduced from 0.28 wt.% to 0.08 wt.% and 0.06 wt.% of MWCNTs for the isothermal treatment and slow-cooling treatment, respectively, where an increase of 10 orders of magnitude in electrical conductivity was observed. Here, a double effect on reducing the PT of PP/PS/MWCNTs composites was achieved. On the one hand, the PT was reduced due to the effect of the double percolation using the co-continuous morphology of PP/PS/MWCNTs composites. Indeed, the PT was reduced from 0.6 wt.% for PP/MWCNTs composites (as can be seen in Figure-A I-2 and Table-A I-1 in the Supplementary Materials) to 0.28 wt.% for PP/PS/MWCNTs composites for the fast-cooling treatment. On the other hand, the ultra-low PT was achieved for PP/PS/MWCNTs composites after the isothermal and slow-cooling treatments. These results can be explained by the exclusion of the MWCNTs by the PP crystalline structure, as was observed by Wang, J. et al. [80].

PP/PS/MWCNTs composites formed a co-continuous structure, where the quantification of morphology can be done by calculating the characteristic domain size ξ —total area of the SEM

image per total interfacial length between PP and PS phase. The evolution of the morphology of the blends for all composites for different treatments was investigated using SEM images. The characteristic domain size— ξ was studied by averaging at least five different SEM images for the same treatment and the same concentration of MWCNTs by using the following equation [30,31]:

$$\xi = \frac{A_{SEM}}{L_{int}} \quad (2.7)$$

where A_{SEM} is the total area of the SEM image and L_{int} is the interface length between two phases estimated using a homemade image analysis script (as can be seen in Figure-A I-3 in Supplementary Materials, which shows how L_{int} was estimated).

Figure 2.3 and Figure 2.4 show SEM images and the plot of characteristic domain size of PP/PS/MWCNTs composites for which the PS phase was extracted with different filler concentrations after the fast-cooling treatment. It can be seen that upon the addition of MWCNTs the characteristic domain size drastically decreases from 11.3 μm to 1.3 μm for neat PP/PS blend and PP/PS/MWCNTs composite with 0.5 wt.% of MWCNTs, respectively. Indeed, the composites were prepared by adding PP/MWCNTs to PS. PP/MWCNTs presents a higher viscosity than pure PP and transfers, therefore, more stress to the PS phase, and resulting in a finer morphology. Furthermore, the better affinity of MWCNTs to PS favors its migration to the PS phase, preventing its coalescence and coarsening, which is leading to drastic decrease for the characteristic domain size [29,30]. This decrease indicates that MWCNTs refined the morphology and that the number of viable electrical paths is increased, explaining the increase in electrical conductivity shown Figure 2.2.

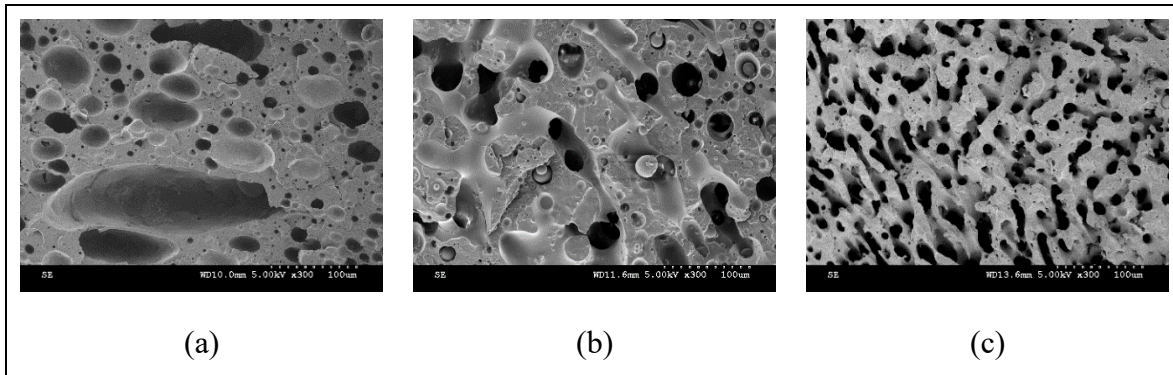


Figure 2.3 Morphology evolution of selected PP/PS/MWCNTs composites after fast-cooling treatment for: (a) 0 wt.% of MWCNTs; (b) 0.1 wt.% of MWCNTs; and (c) 0.5 wt.% of MWCNTs

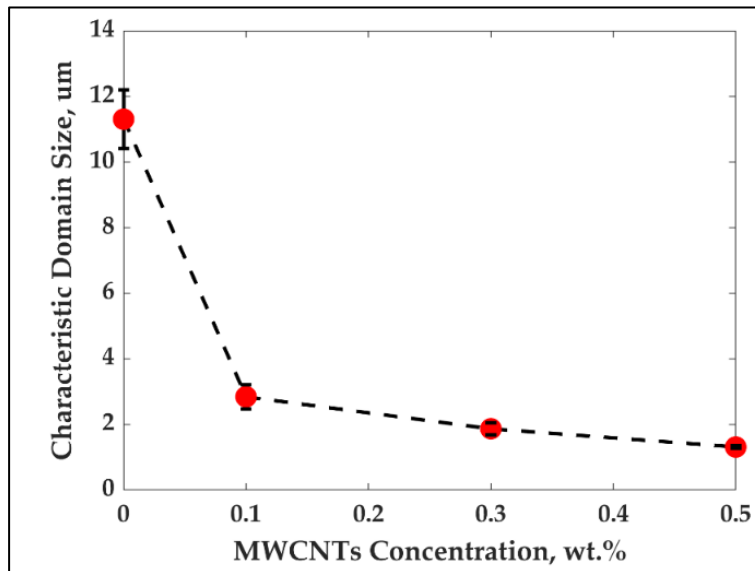


Figure 2.4 Characteristic domain size of PP/PS/MWCNTs composites after fast cooling as a function of MWCNTs concentration

The SEM micrographs for PP/PS/MWCNTs composites with 0.3 wt.% of MWCNTs for each treatment are reported in Figure 2.5(a–c). Figure 2.6 shows the characteristic domain size (ξ) of the PP/PS blends as a function of MWCNTs concentration for different treatments. It can be seen that, for the composites with the same amount of MWCNTs—but for different

treatments—the morphology of the blends did not change, although a larger electrical conductivity was observed upon the slow-cooling and isothermal treatments. For example, the characteristic domain size is $2.8\ \mu\text{m}$, $2.7\ \mu\text{m}$, and $2.7\ \mu\text{m}$ for the PP/PS/MWCNTs composite with 0.1 wt.% of MWCNTs subjected to fast-cooling, isothermal, and slow-cooling treatments, respectively. However, the electrical conductivity is $3.4 \times 10^{-14}\ \text{S/m}$, $2.0 \times 10^{-4}\ \text{S/m}$, and $1.7 \times 10^{-4}\ \text{S/m}$ for the PP/PS/MWCNTs composite with 0.1 wt.% of MWCNTs subjected to fast-cooling, isothermal, and slow-cooling treatments, respectively. These observations indicate that the increase in electrical conductivity upon thermal treatments, in the case of the blends studied here, may not originate from an evolution of the blend morphology as suggested by several researchers [11,14,18,29-31,38,40,72]. Rather, this stems from an evolution of the crystalline morphology of the semi-crystalline polymer. The next section will present an analysis of the crystallization of PP that will help to understand the obtained results.

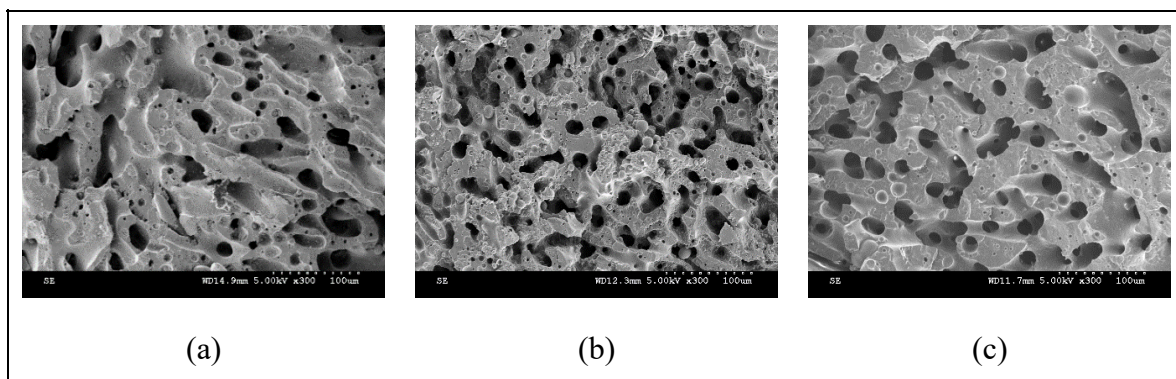


Figure 2.5 Morphology of the selected PP/PS/MWCNTs composites with 0.3 wt.% of MWCNTs for (a) fast-cooling treatment; (b) isothermal treatment; and (c) slow-cooling treatment

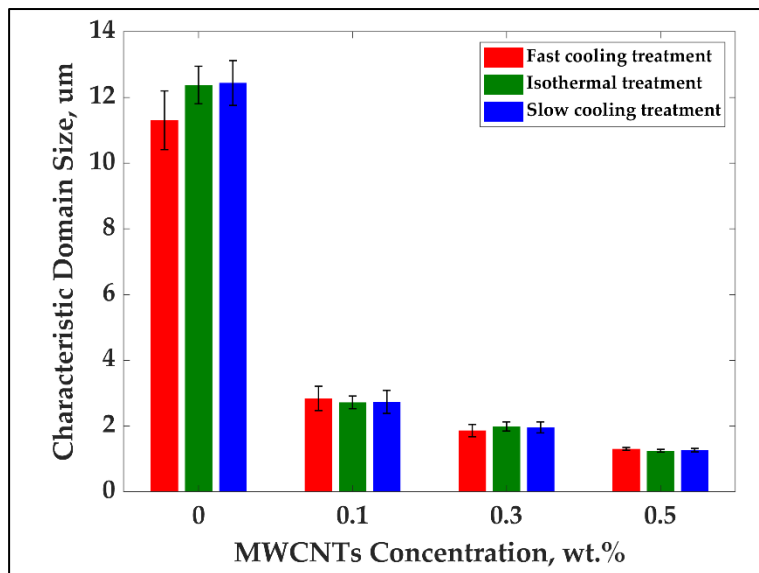


Figure 2.6 Characteristic domain size of ζ vs. MWCNTs concentration for different treatments for PP/PS/MWCNTs composites

2.3.2 Crystallization Behavior and Electrical Conductivity of PP/MWCNTs and PP/PS/MWCNTs Nanocomposites

DSC thermograms of non-isothermal and isothermal crystallization were used to investigate the crystallization state as well as the isothermal crystallization behavior of PP/MWCNTs and PP/PS/MWCNTs nanocomposites.

Figure 2.7 shows typical thermograms obtained by DSC during cooling scans at 10 °C/min for PP and the PP/MWCNTs composite containing 0.1 wt.% of MWCNTs. Similar results were obtained for all composites. These curves were used to infer the peak crystallization temperature, the onset, and end of crystallization, as well as the crystallinity rate for all composites. Melting temperatures for all compositions were also determined by DSC during heating scans at 10 °C/min. The data for peak crystallization temperature (T_c), as well as the degree of crystallinity as a function of MWCNTs concentration for both PP/MWCNTs and PP/PS/MWCNTs, are presented in Figure 2.8(a-b). The data for melting temperatures, the onset, and end of crystallization temperatures can be found in Table-A I-2 in the Supplementary Materials.

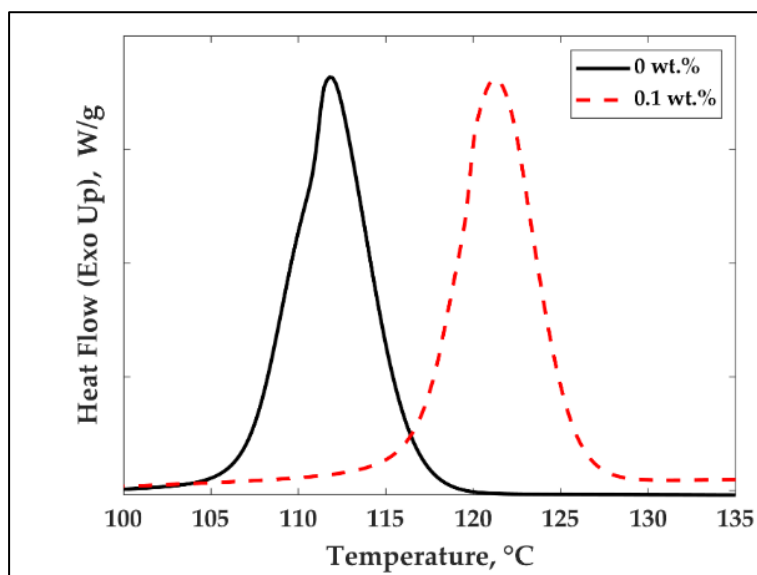


Figure 2.7 Typical non-isothermal crystallization of PP and PP/MWCNTs curves with different MWCNTs wt.%

Figure 2.8(a-b) present the crystallization behavior of PP/MWCNTs and PP/PS/MWCNTs nanocomposites. The peak crystallization temperature (T_c) increases from 112 °C to 126 °C for PP/MWCNTs composites and from 117 to 122 °C for PP/PS/MWCNTs composites as the MWCNTs concentration is increased from 0 to 1 wt.% (Figure 2.8(a)). This increase in crystallization temperature originates from the nucleating effect of the MWCNTs. The effect is more pronounced for PP/MWCNTs composites as opposed to that of PP/PS/MWCNTs composites. This could be due to a favored location of the MWCNTs at the interface between both phases of the blends.

Finally, the addition of MWCNTs and the blending of polymers do not change the degree of crystallinity of PP in the case of PP/MWCNTs composites, as well as in the case of PP/PS/MWCNTs composites (Figure 2.8(b)).

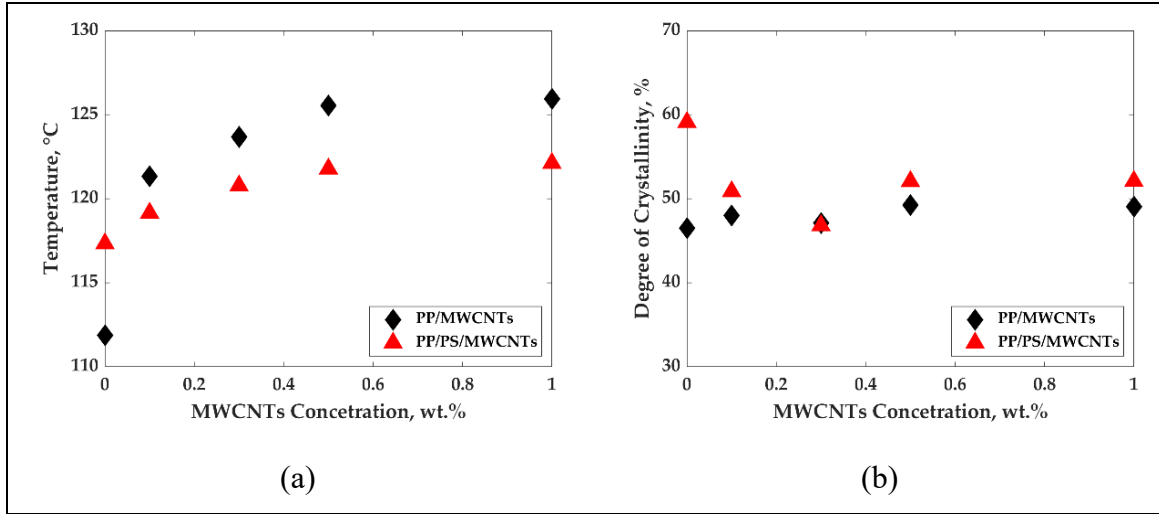


Figure 2.8 Effect of MWCNTs on non-isothermal crystallization of PP for both PP/MWCNTs and PP/PS/MWCNTs composites: (a) influence of MWCNTs concentration on crystallization temperature (peak); and (b) the effect of MWCNTs amount on degree of crystallinity during non-isothermal cooling from 200 °C to 50 °C at 10 °C/min

Figure 2.9(a-b) show typical heat flow curves and the relative crystallinity curves as a function of time during isothermal crystallization tests at a temperature of 135 °C, for the composites studied here to which MWCNTs were added. Similar curves were obtained for all composites. The heat flow curves (Figure 2.9(a)) were used to infer relative crystallinity— $X(t)$ as a function of time, which can be obtained from the area under the exothermic peak up to time t , divided by the total exothermic peak area as expressed in Equation (2.8) [115]:

$$X(t) = \frac{\int_0^t \frac{dH_c}{dt} \times dt}{\int_0^\infty \frac{dH_c}{dt} \times dt} \quad (2.8)$$

dH_c is the heat flow required for crystallization for a certain time dt .

Figure 2.9(b) shows the relative crystallinity curves as a function of time (obtained using Equation (2.8) from Figure 2.9(a) data) for the composites studied here at different MWCNTs

concentrations and at 135 °C. Similar curves were obtained for all composites and were used to infer the crystallization half time ($t_{1/2}$) which is the time required to complete 50% of the crystallization and the induction time which is the time at which the nuclei start to form. The data for $t_{1/2}$ and induction time as a function of MWCNTs concentration are shown in Figure 2.10(a-b).

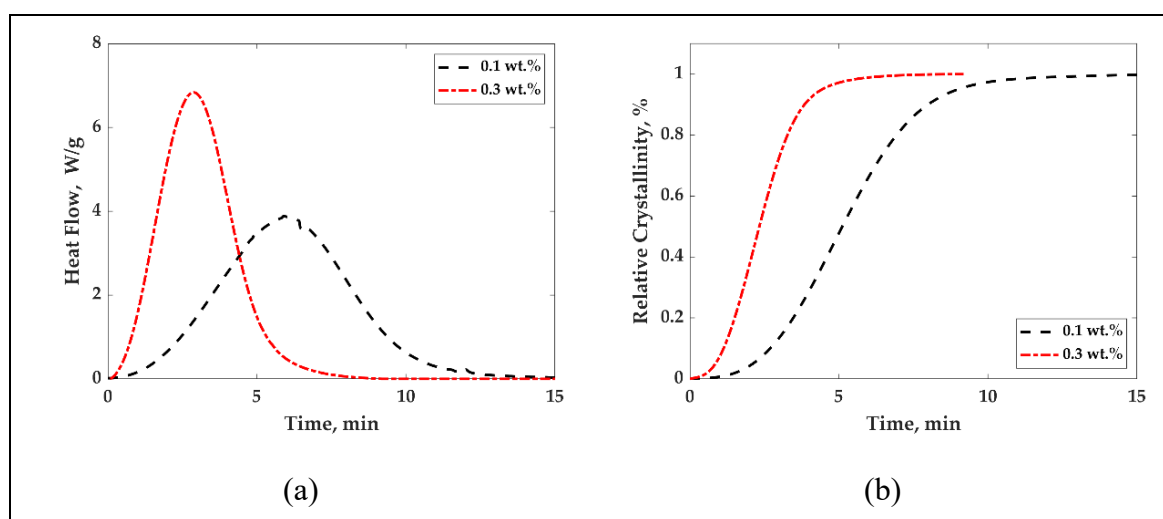


Figure 2.9 (a) Heat flow as a function of time for PP/MWCNTs composites with different MWCNTs wt.% at 135 °C; (b) relative crystallinity of PP/MWCNTs composites with different MWCNTs wt.% at 135 °C

Figure 2.10(a-b) present crystallization half time (a) and induction time (b) for PP/MWCNTs and PP/PS/MWCNTs composites with different MWCNTs concentrations at 135 °C.

The results presented in Figure 2.10(a) show that upon the addition of MWCNTs for PP/MWCNTs composites, the crystallization half time drastically decreases, indicating that MWCNTs act as a nucleating agent. The crystallization half time was found to be equal to 62, 6, 3, and 2.6 min for composites with 0, 0.1, 0.3, and 0.5 wt.%, respectively. For PP/PS/MWCNTs composites, not only the effect of MWCNTs amount on relative crystallinity should be taken into account, but also the matrix composition. The crystallization half time did not significantly change with the increase in the MWCNTs concentration. The crystallization

half time was determined to be 12, 7, and 5 min for composites with 0.1, 0.3, and 0.5 wt.%, respectively, which is approximately two times more than that for PP/MWCNTs composites, with the same MWCNTs amount. This could be caused by the selective localization of MWCNTs at the interface inside the PP/PS matrix, which weakens the nucleation effect since nucleation is not a factor for PS. However, $t_{1/2}$ for the pure PP/PS blend, it is three times smaller than for pure PP. The presence of PS in the mixture could have changed the energy needed for the ultimate crystallization of PP. The same behaviour was observed for the induction time of crystallization for both PP/MWCNTs and PP/PS/MWCNTs (Figure 2.10(b)).

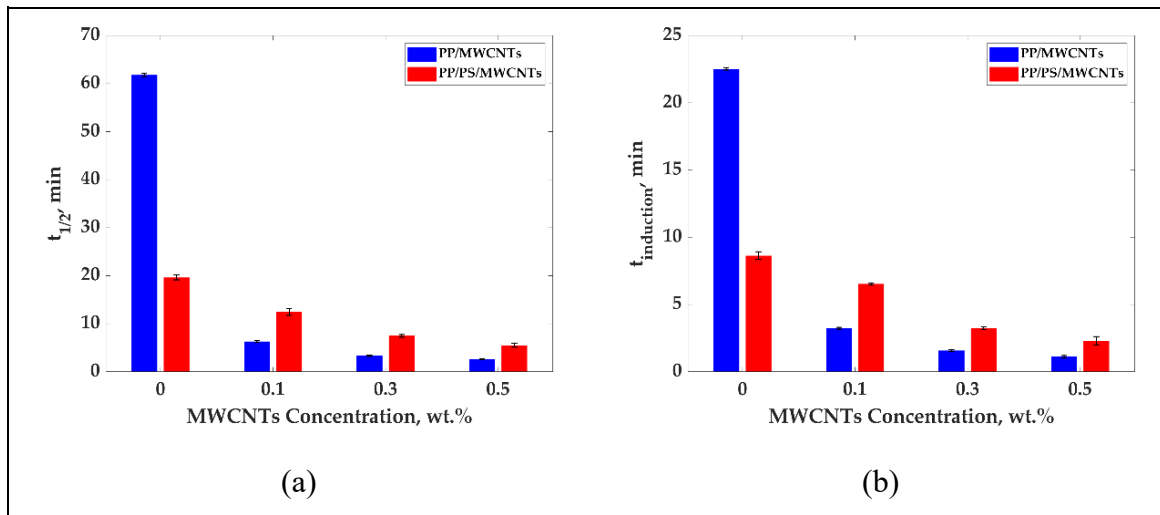


Figure 2.10 (a) Crystallization half time and (b) induction time for PP/MWCNTs and PP/PS/MWCNTs composites at 135 °C

The crystallization of pure PP and PP/MWCNTs with 0.1 wt.% of MWCNTs after the fast-cooling, isothermal, and slow-cooling treatments was investigated by polarized optical microscopy, and the crystal morphology is shown in Figure 2.11(a–f). A concentration of 0.1 wt.% was chosen as it is not possible to visualize by optical microscopy, the spherulites for higher concentrations of MWCNTs. The treatment temperature of 135 °C was chosen for isothermal and slow-cooling treatment to obtain larger crystals as mentioned previously. It can be clearly seen that the cooling rate affects the crystal size when fast cooling is compared to the other two treatments. The crystals of pure PP—which was fast cooled—are so small that

they cannot be easily identified compared to the crystals obtained from isothermal and slow-cooling treatments, where the size is around 100 μm for both treatments. The crystals size for the PP/MWCNTs composite with 0.1 wt.% of MWCNTs decreased compared to neat PP. Nevertheless, there is a big difference in the crystal size for the samples, which were treated by fast-cooling treatment compared to isothermal and slow-cooling treatments, although crystal sizes for composites are difficult to identify by POM.

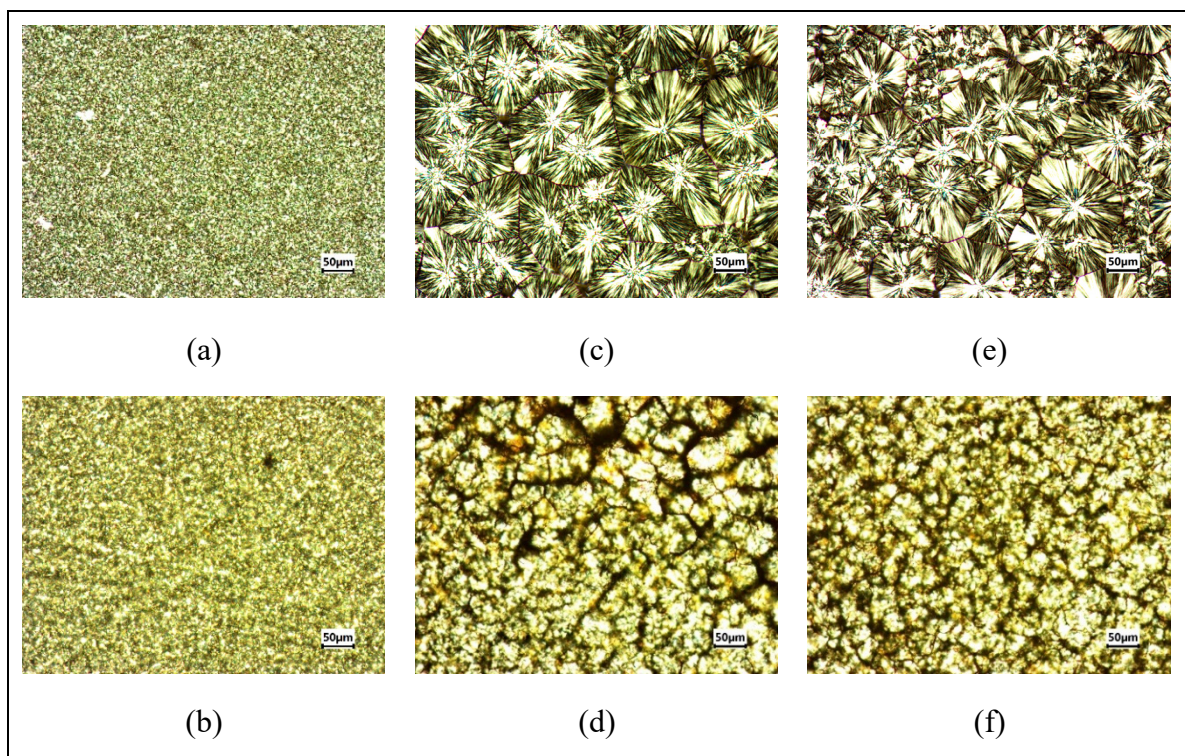


Figure 2.11 Microscopic observations of PP pure and PP/MWCNTs with 0.1 wt.% of MWCNTs for fast-cooling treatment (a-b); isothermal treatment (c-d); and slow-cooling treatment (e-f)

Figure 2.12(a-b) show the dynamic process of filler conductive network formation, which was observed by measuring the electrical conductivity as a function of time for the PP/PS/MWCNTs composite at 135 °C. It can be seen that, at a very low concentration of MWCNTs, the electrical conductivity was constant for around 11.5 min of treatment and then drastically increases by five orders of magnitudes (Figure 2.12(a)). The electrical conductivity

of composites with 0.1 wt.% of MWCNTs is low at the start of the treatment due to the poor connection of nanoparticles inside the polymer matrix, but when the critical point of particle's connections is achieved, they create an electric pathway and the electrical conductivity rapidly increases. Figure 2.12(b) shows the electrical conductivity as a function of time for the PP/PS/MWCNTs composite with 0.3–1 wt.% of MWCNTs. It can be seen that the electrical conductivity starts to increase from the first seconds of treatment and approaches a plateau after 5 min. In this case, the concentration of nanoparticles was sufficient for the creation of a conductive network from the start of the treatment.

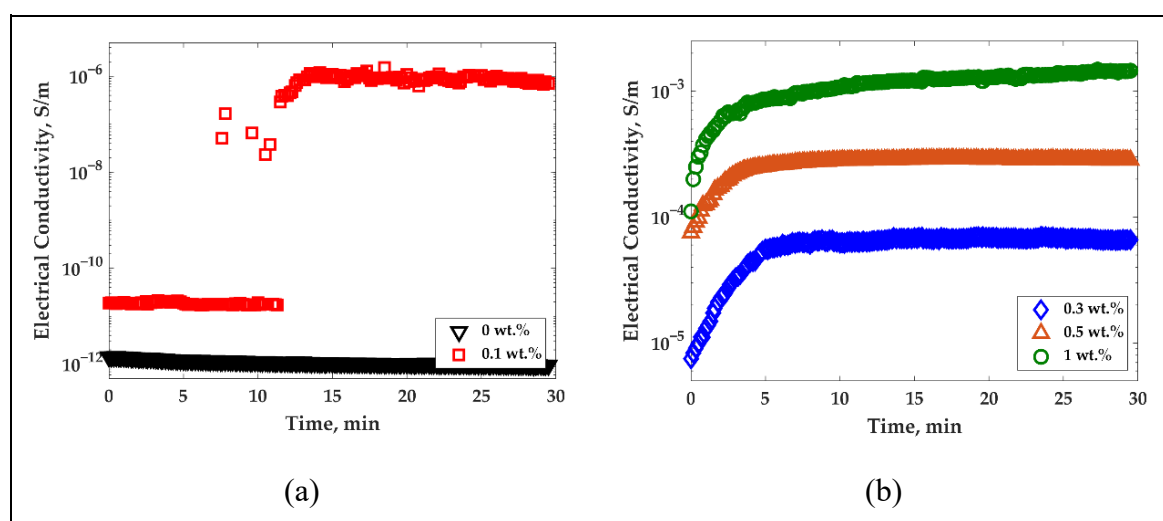


Figure 2.12 Electrical conductivity as a function of time for PP/PS/MWCNTs composite with different concentrations of MWCNTs measured every 10 s at 1 Hz of frequency and 135 °C for: (a) 0–0.1 wt.% of MWCNTs; and (b) 0.3–1 wt.% of MWCNTs

Similar behavior was observed for the electrical conductivity of PP/MWCNTs as a function of time (as can be seen in Figure-A I-4 and Figure-A I-5 in the Supplementary Materials). At very low concentrations of MWCNTs (0.1–0.3 wt.% of MWCNTs—below the percolation threshold), electrical conductivity did not change during the isothermal treatment, and its values were close to those of unfilled PP. However, at MWCNTs concentrations close to the PT and higher (0.5–1 wt.% of MWCNTs), electrical conductivity monotonically increased with time.

2.4 Discussion

There are several ways to reduce the PT of CNT-based thermoplastic composites prepared by melt mixing. One of these ways is to use immiscible polymer blends with a co-continuous morphology as a matrix. In this case, the reduction in PT can be achieved thanks to a double percolation effect, resulting from the co-continuous morphology of the used PB [6,9,24-26]. Furthermore, the reduction in PT can be achieved through both covalent and noncovalent modifications of either CNTs or matrices of CNTs-based thermoplastic composites with co-continuous morphology [7,25,28]. Some researchers suggested adding different nanoparticles to help trap CNTs at the interface [43,47]. Another way is to optimize the mixing parameters (time, mixing speed, ...), as well as use varied post-mixing thermal treatments, as was discussed in the introduction [11,35,49,51]. Table 2.2 summarizes some literature studies in which the ultra-low PT of PB/CNTs composites was achieved along with the employed modifications and treatments. The PT reached in the present work for PP/PS/MWCNTs composites was comparable or even lower than those reported in the literature. The electrical conductivity values, achieved in this study, for several PT concentrations as well as 1 wt.% of CNTs, were greater than those reported in other studies. These values were obtained primarily due to the induced crystallization of PP during the post-mixing thermal treatments. As a result, ultra-low PTs for PP/PS/CNTs composites have been achieved.

The results reported in this work also showed that the thermal treatments did not influence the blend morphology as is the case after an annealing treatment performed above the melting or softening temperature, during which the coarsening of the PB matrix morphology is happening [11,29-31,68].

Table 2.2 Ultra-low PT values of CNT-thermoplastic systems achieved by different modifications and treatments

PT, wt. %	EC at PT, S/m	EC, S/m of with 1 wt.% of CNT	Modification	Reference
0.050	10^{-9}	5.0×10^{-1}	Modification of MWCNT with noncovalent ionic liquid	[7]
0.050	10^{-6}	5.0×10^{-1}	Modification of MWCNT with noncovalent ionic liquid	[28]
0.017	10^{-10}	5.0×10^{-2}	MWCNT functionalization with carboxyl groups	[25]
0.060	10^{-9}	2.0×10^{-5}	Trapping CNT at the interface with the help of 0.3 wt.% of GO	[47]
0.060	10^{-9}	5.0×10^{-5}	Trapping CNT at the interface with the help of 0.1 wt.% of organoclay	[43]
0.025	10^{-9}	2.0×10^{-4}	Adjustment of melt-mixing time	[42]
0.090	10^{-7}	2.0×10^{-1}	2 h of annealing at 200 °C	[68]
0.060	10^{-6}	5.6×10^{-1}	Slow-cooling treatment (takes 50 min)	Our work
0.080	10^{-5}	5.1×10^{-1}	Isothermal treatment (takes 15 min)	Our work

	System
	PS/EVA/IL-CNT (70/30 wt.%)
	PS/PBAT/IL-CNT (50/50 wt.%)
	PS/PMMA/MWCNT- COOH (40/60 wt.%)
	PLLA/EVA/GO0.3/CNT (60/40 wt.%)
	PS/PVDF/Clay0.1/CNT (40/60 wt.%)
	PLA/PCL/MWCNT (50/50 wt.%)
	PP/PMMA/MWCNT (30/70 wt.%)
	PP/PS/MWCNT (50/50 wt.%)
	PP/PS/MWCNT (50/50 wt.%)

The dynamic percolation threshold for the system studied in the present work was also investigated using electrical conductivity measurements. It was found that the electrical conductivity of PP/PS/MWCNTs composites with the lower concentration of 0.1 wt.% of MWCNTs (close to PT concentration) drastically increased after 11.5 min of thermal treatment at 135 °C, as can be observed in Figure 2.12(a). For the samples with a larger MWCNTs concentration, the electrical conductivity monotonically increased with time, depending on the MWCNTs concentration.

Figure 2.13 shows the time which corresponds to the complete crystallization of PP as a function of MWCNTs concentration, as well as the time which the electrical conductivity takes to reach plateau values as a function of the MWCNTs concentration for PP/PS/MWCNTs composites. It can be seen that the electrical conductivity reached plateau values before the crystallization was complete. This is an indication, we believe, of an improvement of MWCNTs particle connections at the PP/PS interface. In this case, MWCNTs were pushed to PP crystals' borders where they stopped by the PS phase which does not crystallize. Generally, the PS phase is more favorable for MWCNTs, but their diffusion into it is significantly impeded upon because the treatment temperature does not provide enough energy to promote MWCNTs diffusion. As a result, due to the accumulation of MWCNTs connections at the PP/PS interface and in the PP phase, the electrical conductivity increases.

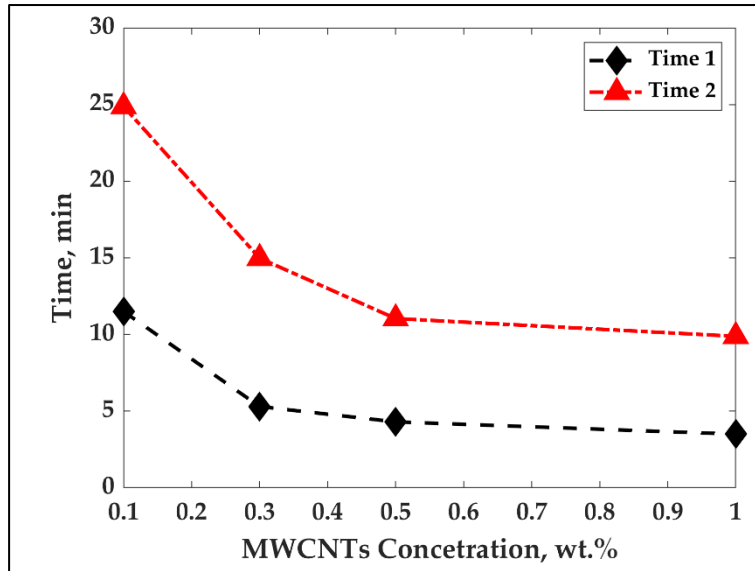


Figure 2.13 Time for complete crystallization of PP (Time 2) and time when electrical conductivity levels off (Time 1) as a function of MWCNTs concentration for PP/PS/MWCNTs composites

2.5 Conclusions

PP/PS/MWCNTs blend composites with co-continuous morphology have been prepared by melt-mixing, using a twin-screw extruder through the dilution of a masterbatch of PP/MWCNTs with PP and PS. Due to the effect of double percolation, the PT of PP/PS/MWCNTs was reduced by over 50% compared to PP/MWCNTs composites. Furthermore, thermal annealing treatments, aimed at enhancing the effect of PP crystal growth on electrical conductivity and PT of PP/PS/MWCNTs composites have been done. It was shown that extremely low PTs of 0.06 wt.% and 0.08 wt.% MWCNTs were obtained after slow-cooling and isothermal treatments, respectively. These treatments promoted the selective localization of MWCNTs due to the PP crystal volume exclusion effect of MWCNTs. Moreover, microscopy observations (SEM) and the characteristic domain sizes calculation of PP/PS/MWCNTs co-continuous morphology confirmed that these treatments have not changed PB morphology in contrast to thermal annealing above the melting or softening temperature.

Supplementary Materials:

The following are available online at www.mdpi.com/xxx/s1, Figure-A I-1: Viscosity as a function of shear rate measured by capillary rheometer for pure PP and PS. Figure-A I-2: Effect of treatments on electrical conductivity as a function of MWCNTs concentration for PP/MWCNTs composites. Figure-A I-3: Image treatment analysis for distinguishing between two phases: (a) original SEM picture for PP/PS/MWCNTs composite with 0.3 wt.% of MWCNTs; (b) image phase separation; (c) final treated image which was used for the estimation of L_{int} —interface length between two phases, which in this case is the perimeter of the white phase (PS phase). Table-A I-1: Percolation threshold and fitting values of experimental data according to Equation (2.6) for PP/MWCNTs composites after each treatment. Figure-A I-4: Electrical conductivity as a function of time for PP/MWCNTs composite with 0–0.3 wt.% of MWCNTs measured every 10 s at 1 Hz of frequency and 135 °C. Figure-A I-5: Electrical conductivity as a function of time for a PP/MWCNTs composite with 1 wt.% of MWCNTs measured every 10 s at 1 Hz of frequency and 135 °C.

Acknowledgments:

Financial supports from the Natural Sciences and Engineering Research Council of Canada (NSERC), PRIMA, and École de technologie supérieure (ÉTS) are gratefully acknowledged.

CHAPTER 3

LINEAR VISCOELASTICITY OF PP/PS/MWCNT COMPOSITES WITH CO-CONTINUOUS MORPHOLOGY

Daria Strugova, Éric David and Nicole R. Demarquette

Mechanical Engineering Department, École de Technologie Supérieure, Montréal, Québec

Paper published in *Journal of Rheology*, May 2022

DOI: <https://doi.org/10.1122/8.0000441>

Abstract

In this work, a study of the linear viscoelastic properties of co-continuous polypropylene/polystyrene blends filled with multiwall carbon nanotubes (MWCNTs) is presented. The YZZ rheological model [89] is employed to correlate the rheological behavior of the blends with their microstructure and electrical properties. A test design involving a sequence of small amplitude oscillatory shear and a time sweep (simulating thermal annealing) is used to evaluate the morphology and evolution of electrical properties. It was shown that the YZZ rheological model could be successfully modified to be able to quantify a co-continuous morphology of filled composites. The calculated characteristic domain size was found to be in good agreement with the experimental data obtained via scanning electron microscopy. Furthermore, it is shown that the characteristic domain size slightly decreased after 30 min of thermal annealing. It was shown, as well, that thermal annealing promoted a reduction in the electrical percolation threshold (wt.% MWCNT) from 0.28 to 0.06.

3.1 Introduction

Over the last few years, it has been shown that through proper processing, the morphology of a blend to which nanoparticles are added can be manipulated to achieve satisfactory engineering properties. For example, it has been shown that the use of nanostructured blends

[26,116-118] or block copolymers [10,29,119] can help in tailoring the location and orientation of nanoparticles affecting properties such as electrical conductivity [11,31,120], electromagnetic interference shielding [26,116], dielectric properties [118], and thermal properties, among others. In particular, it has been shown that the electrical percolation threshold of carbonaceous nanoparticles composites could be greatly reduced by using the so-called double percolation technique that consists of tailoring the location of a conductive filler in one of the components or the interface between both polymers, forming a blend with a co-continuous morphology [11,42,68,120].

However, during processing, such composites are subjected to further deformation, which could result in a change of their morphology. Rheological tests may be used to probe such an evolution [63,98]. Indeed, small amplitude oscillatory shear (SAOS) tests carried out in the linear viscoelastic region can be used to characterize the equilibrium morphology of binary blends [16,24,59-62,121]. Therefore, if a blend is subjected to SAOS–deformation–SAOS, a second SAOS test after deformation will indicate, to some extent, whether the morphology of the blend would have evolved during that deformation. Rigorously, SAOS can only be used to access equilibrium morphology, and whether or not a highly nonlinear deformation, the morphology would not have reached the equilibrium. A more accurate test would be SAOS–deformation–recovery–SAOS. SAOS–deformation–SAOS has been extensively used for dispersed droplet-type polymer blends [99,102,105,108,122] as their rheological behavior in SAOS is well described by the well-known Palierne [59], Gramespacher and Meissner [60], or Bousmina [61] models. However, to our knowledge, such an analysis is scarce in the case of co-continuous morphology-type blends. Proper models relating the rheological behavior of the blend to its co-continuous morphology, quantitatively, are still being developed [29,88,89]. Indeed, several models have been developed to predict the rheological behavior of polymer blends with a co-continuous morphology [29,88-92]; however, only a few allow a quantitative evaluation of morphology from the rheological analysis.

One such model is that developed by Yu et al. [89], referred to as the YZZ model in the present article as well as in their later article [93]. It is based on the basic idea that the complex modulus of a blend $G_{blend}^*(\omega)$ with a co-continuous morphology can be evaluated as the sum of both components' contribution symbolized by $G_{components}^*(\omega)$ and an interface contribution symbolized by $G_{interface}^*(\omega)$ resulting in [59,60]

$$G_{blend}^*(\omega) = G_{components}^*(\omega) + G_{interface}^*(\omega) \quad (3.1)$$

To calculate the contribution of the components, Yu et al. [89] adapted the expression, developed by Veenstra et al. [95], to evaluate the complex and/or storage moduli of a blend with co-continuous morphology. In the present article, both components and interface contributions are used for the storage modulus of a blend with a co-continuous morphology. In their model, Veenstra et al. [95] assumed that the microstructure of the blend with a co-continuous morphology is schematically shown in Figure 3.1. An elementary cell of a co-continuous microstructure is 1/8 of the primary microstructure and is assumed to consist of three connected parallelepiped shape elements of length $l'_c = a' + b' = 1$, square section of edge a' , and $b' = 1 - a'$ as shown in in Figure 3.1(b). If the length of the cell is normalized to 1 and φ_1 is the volume fraction of fluid 1, as shown in in Figure 3.1(c), then φ_1 amounts to:

$$\varphi_1 = 3a'^2 - 2a'^3 \quad (3.2)$$

Using these geometrical assumptions, the storage modulus of the blend can then be written as

$$G'_{components} = \frac{a'^2 b' G_1'^2(\omega) + (a'^3 + 2a' b' + b'^3) G_1'(\omega) G_2'(\omega) + a' b'^2 G_2'(\omega)}{b' G_1'(\omega) + a' G_2'(\omega)} \quad (3.3)$$

where $G_1'(\omega)$ is the storage modulus of component 1 and $G_2'(\omega)$ is the storage modulus of component 2.

To evaluate the contribution of the interface, Yu et al. [89] modified the scheme of Veenstra et al. [95] by considering that the parallelepiped shape elements should be, in fact, cylinders to take into account the minimization of the surface area (see in Figure 3.1(c)). These cylinders are assumed to have radius a and characteristic length l_c with $a' = a/l_c$ and $b' = b/l_c$. Then, they calculated the stress contribution induced by the interfacial deformation of each cylinder. This results in expression (4) for the storage modulus of the interface contribution as

$$G'_{interface} = G'_A{}_{interface} + G'_B{}_{interface} + G'_C{}_{interface} \quad (3.4)$$

where $G'_A{}_{interface}$, $G'_B{}_{interface}$, and $G'_C{}_{interface}$ are the elastic moduli due to interface deformation of the cylinder type A, type B, and type C, respectively.

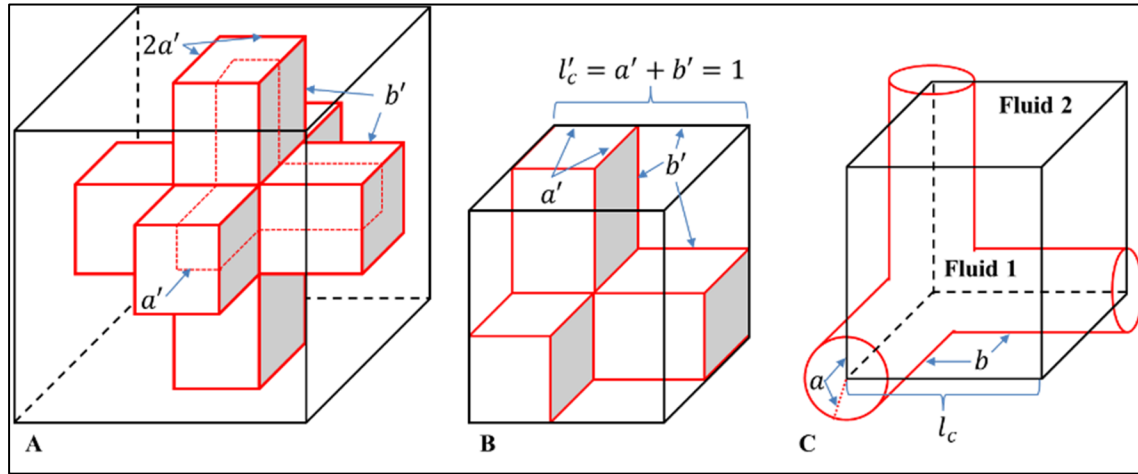


Figure 3.1 A schematic of an ideal co-continuous morphology (redrawn from refs. [89,95])

In doing so, they were able to derive an expression for $G'_{interface}$ as

$$G'_{interface} = \frac{k_C}{6} \alpha S_V \left(\frac{k_B}{k_C} + \frac{3}{4} \frac{f_2 \omega^2 \tau^2}{f_1^2 + \omega^2 \tau^2} \right) \quad (3.5)$$

where α is the interfacial tension, ω is the frequency, and S_V is the specific area, inversely proportional to the characteristic domain size ξ , given by

$$S_V = \frac{3\pi ab}{2l_c^3} = \frac{1}{\xi} \quad (3.6)$$

$$\tau = \frac{\eta_m a}{\alpha} \quad (3.7)$$

$$k_C = -\frac{f_2 \omega^2 \tau^2}{f_1^2 + \omega^2 \tau^2} \gamma_0 \quad (3.8)$$

$$k_B = -\frac{f_1 f_2 \omega \tau}{f_1^2 + \omega^2 \tau^2} \gamma_0 \quad (3.9)$$

with

$$f_1 = \frac{40(p+1)}{(2p+3)(19p+16)} \quad (3.10)$$

and

$$f_2 = \frac{5}{2p+3} \quad (3.11)$$

where p is the viscosity ratio of fluid 1 over fluid 2 and γ_0 is the strain amplitude. k_B and k_C are constants that relate to a random orientation and possible distortion of a co-continuous element, and the ratio $k_B/k_C \leq 1$.

Using Equations (3.1-3.11), the storage modulus of the blend with a co-continuous morphology can be written as:

$$G'_{blend}(\omega) = \frac{a'^2 b' G_1'^2(\omega) + (a'^3 + 2a'b' + b'^3)G_1'(\omega)G_2'(\omega) + a'b'^2 G_2'^2(\omega)}{b'G_1'(\omega) + a'G_2'(\omega)} + \frac{k_C}{6} \alpha S_V \left(\frac{k_B}{k_C} + \frac{3}{4} \frac{f_2 \omega^2 \tau^2}{f_1^2 + \omega^2 \tau^2} \right) \quad (3.12)$$

where G_1' is the storage modulus of component 1, G_2' is the storage modulus of component 2, and more details can be found in the work Yu et al. [89].

However, in the case of the YZZ model, the linear viscoelastic properties are well described just for neat polymer blends with a co-continuous morphology. In the case of blends to which nanoparticles are added, the elastic contribution from the filler network has a significant effect on the elastic modulus of the composite, which was widely observed for different polymer blend/filler systems [2,29,31]. As a result, it can be concluded that the influence of a rigid filler network in the modeling of viscoelastic properties of a co-continuous morphology of polymer blends requires further investigation. Such a tool would enable the study of the stability of a co-continuous blend morphology to which nanoparticles are added as well as of the stability of their electrical properties. Indeed, with such a model, it would be possible to use the response of co-continuous filled nanocomposites subjected to SAOS–deformation–SAOS to evaluate the effect of deformation on their morphology.

In particular, it was shown, in our previous work [120], that it is possible to achieve an electrical percolation threshold using ultralow values of multiwall carbon nanotube (MWCNT) concentrations in polypropylene/polystyrene (PP/PS)/MWCNT composites. This ultralow percolation threshold concentration is achieved by applying a thermal treatment that affect PP crystal growth. However, it is very important to study the stability of the obtained morphologies to avoid loss of properties (in particular, electrical conductivity) during further processing.

In the present article, the YZZ model was modified for systems containing nanoparticles and used to evaluate the effect of thermal annealing on the morphology of the PP/PS/MWCNT composites studied in our previous work.

3.2 Materials and Methods

3.2.1 Materials

PP, grade PP4712E1, from Exxon Mobile and PS, grade MC3650, from PolyOne were used in this work. The characteristics of these polymers are reported in Table 3.1. MWCNTs, grade NC7000™, were purchased from Nanocyl. The nanotubes have an average diameter of 9.5 nm and a length of 1.5 μm with a nominal electrical conductivity of $10^6 \text{ S}\cdot\text{m}^{-1}$.

Table 3.1 Properties of the polymers

Polymers	Melt index	η_0 (Pa·s) at 200 °C	Density ($\text{g}\cdot\text{cm}^{-3}$)
PP	2.8 g/10 min (230°C/2.16kg)	7800	0.9
PS	13 g/10 min (200°C/5kg)	4080	1.04

3.2.2 Composites' preparation

All composites were prepared by a melt-mixing process using a Haake Rheomix OS PTW16 twin-screw extruder (Thermo Fisher Scientific Inc., Waltham, MA, USA). The temperature was fixed at 220 °C in all zones, and the screw speed was adjusted to 100 rpm for all compositions. First, a masterbatch of PP with 10 wt.% of MWCNT was prepared. Second,

PP/PS/MWCNT composites with a MWCNT concentration varying from 0 to 2 wt.% were prepared by diluting the PP/MWCNT masterbatch with PP and PS to the concentration of PP/PS of 50/50 wt.% where a co-continuous morphology was obtained.

A 50/50 wt.% PP/PS concentration was chosen as it would yield a co-continuous morphology based on the analysis of Jordhamo et al. [85], as was explained in our previous work [120].

Samples for rheological, electrical, and morphological analyses were obtained by compression molding. Disks with 25 mm diameter and 1 mm thickness were molded at 200 °C under 0.8 MPa for 10 min, and after that, the pressure was increased to 10 MPa, and samples were molded for additional 10 min at the reached pressure.

3.2.3 Characterizations

3.2.3.1 Rheology

The rheological characterization of all composites was performed using a controlled-stress MCR 501 rotational rheometer (Anton Paar, Graz, Austria). Measurements were carried out under a dry nitrogen atmosphere. A parallel-plate geometry was used with a gap size of 1 mm and a plate diameter of 25 mm. All tests were carried out at 200 °C. First, dynamic strain sweep tests were performed for all composites at three different angular frequencies, 1, 10, and 100 rad/s, in a strain range from 0.01% to 10 % in order to determine the linear viscoelastic region. A strain of 0.3% was chosen as it was found to correspond to the LVE region for all composites in the studied range. Second, time sweep tests were performed for pure PP and PS at 0.05 rad/s for 6 h at the fixed strain of 0.3 % in order to check the thermal stability of the samples. Then, SAOS tests were performed with frequencies ranging from 300 to 0.01 1/s at a fixed strain of 0.3 % for all composites. For each composite, a sequence of SAOS, followed by a time sweep (simulating thermal annealing), followed by another SAOS, as shown in Figure 3.2, was carried out to evaluate the evolution of morphology during thermal annealing. This sequence can be used whether or not an equilibrium morphology is reached after annealing.

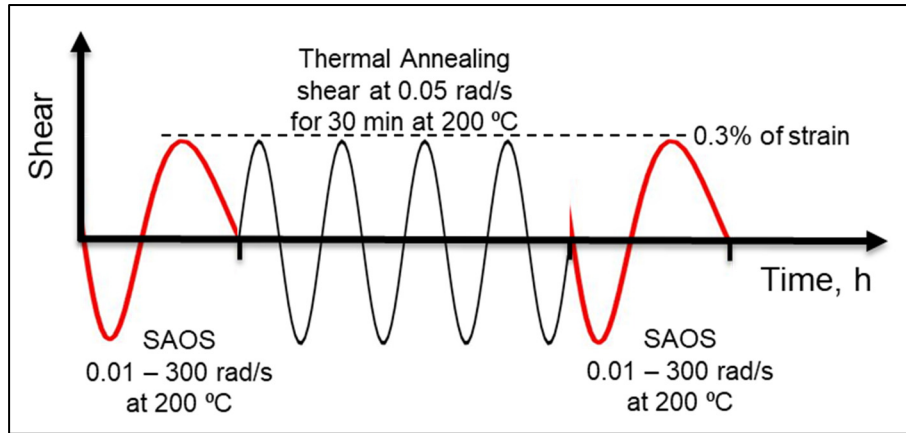


Figure 3.2 Experimental protocol

3.2.3.2 Electrical conductivity

Combined rheological and electrical characterization of the PP/PS/MWCNT composites was carried out during the middle time step using the MCR501 rheometer equipped with a dielectro-rheological device (DRD with ST2826/A high-frequency LCR meter). The time sweep was carried out at an angular frequency equal to 0.05 rad/s. Measurements of electrical properties were performed by applying 20 Hz AC of 1 V_{RMS} across the sample.

The electrical conductivity at 200 °C (see Figure 3.7 in Results and Discussion section) was evaluated from the complex impedance using

$$\sigma' = \frac{1}{Z'} \frac{d}{A} \quad (3.13)$$

where Z' is the real part of the complex impedance, A is the plate area, and d is the distance between the plates.

At room temperature, the electrical conductivity of the obtained composites was rather characterized using a broadband dielectric spectrometer (Novocontrol Technologies GmbH & Co. KG, Montabaur, Germany). The measurements were conducted in a frequency range from 10^{-2} to 3×10^5 Hz under an excitation voltage of 1 V_{RMS} applied across the sample. The

calculation of the electrical conductivity from the complex capacitance has been explained in detail in our previous work [120]. The electrical conductivity values, presented in the Results and Discussion section using this device, refer to the value of $\sigma'(\omega)$ at a frequency of 10^{-2} Hz. Disks of 25 mm in diameter and 1 mm in thickness, covered on both sides with 20 nm of gold, serving as electrodes, were used for measurements.

3.2.3.3 Microscopy analysis

The morphology of PP/PS/MWCNT composites was observed by scanning electron microscopy (SEM) using a S3600 Hitachi microscope (Hitachi, Ltd., Tokyo, Japan), operated at 5 kV in the secondary electrons' mode. The samples were fractured in liquid nitrogen and then the polystyrene was extracted by using butanone at room temperature under continuous stirring for 2 h. Then, the samples were dried under vacuum at room temperature for 12 h. After drying, the samples were covered with gold using a gold sputter coater, model K550X.

The state of dispersion and localization of MWCNT in PP/PS/MWCNT composites before and after thermal annealing was evaluated by transmission electron microscopy (TEM). To obtain 50–100 nm ultrathin sections, the investigated samples were embedded in the epoxy resin, and the sectioning was performed using a Leica Microsystems UC7/FC7 cryoultramicrotome operated at -160 °C. Imaging was carried out with a Thermo Scientific Talos F200X G2 S/TEM at an accelerating voltage of 200 kV.

3.3 Results and Discussion

As mentioned in the Introduction, our previous study had shown that it is possible to obtain electrically conductive PP/PS/MWCNT composites with ultra-low percolation threshold concentrations of 0.06 wt.% and 0.08wt.% of MWCNT after applying thermal treatments. These thermal treatments had the benefit of resulting in a decrease in percolation threshold concentration without affecting the overall blend morphology. The aim of this work is to study the stability of the morphologies obtained. For that, a method to characterize the composites'

morphology from their rheological behavior needed to be developed. This is what is described in Section 3.3.1 of this result section. Then, the tool is used to study the systems after thermal annealing to explain the evolution of their electrical and morphological properties during thermal annealing.

3.3.1 PP/PS/MWCNT composites' morphology and the YZZ model fitting

Figure 3.3 shows the storage modulus as a function of frequency for pure PP, PS, and PP/PS blend of 50/50 wt.% and PP/PS/MWCNT (50/50/x wt.%) composites with different concentrations of MWCNTs. It can be seen that the experimentally obtained storage modulus of the blend, at low frequencies, is higher than the ones for pure components. The reason for the increase in G' for polymer blends originates from an extra contribution of the stress generated by the deformation of the interface [60]. It can be also seen that the storage modulus at low frequencies increases with MWCNT concentration, exhibiting a plateau what indicates a solid-like behavior due to the formation of a rigid nanoparticles network [2,24,31]. Concomitantly, it has been shown that independently of the complexity of the filled composite's matrix, the filler network contributes more to the elastic modulus at low frequencies with frequency-independent elastic modulus – G'_0 compared to the matrix response [97,123,124].

Figure 3.4 shows the rheological behavior of PP/PS 50/50 wt.% blend with the YZZ model fitting (Figure 3.4(a)) and PP/PS blend to which 0.3wt.% of MWCNT (Figure 3.4(b)) was added with the YZZ model fitting. The dashed line in both graphs shows the fit of the YZZ model. The data for storage and loss moduli as a function of frequency for PP/PS/MWCNT (50/50/x wt.%) composites for all concentrations of MWCNT are reported in Figure-A II-1(a) and Figure-A II-1(b) of the supplementary material.

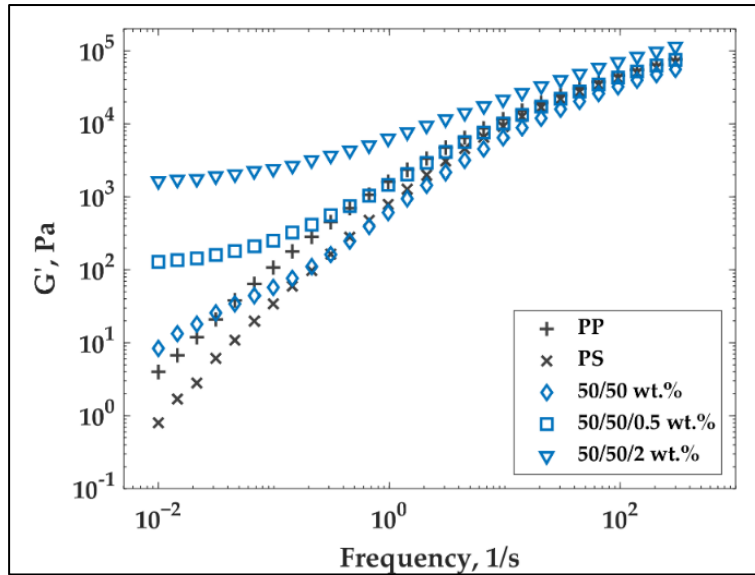


Figure 3.3 Storage modulus as a function of frequency for PP/PS/MWCNT composites with different concentrations of MWCNT at 200 °C. PP, PS, and PP/PS blend of 50/50 wt.%

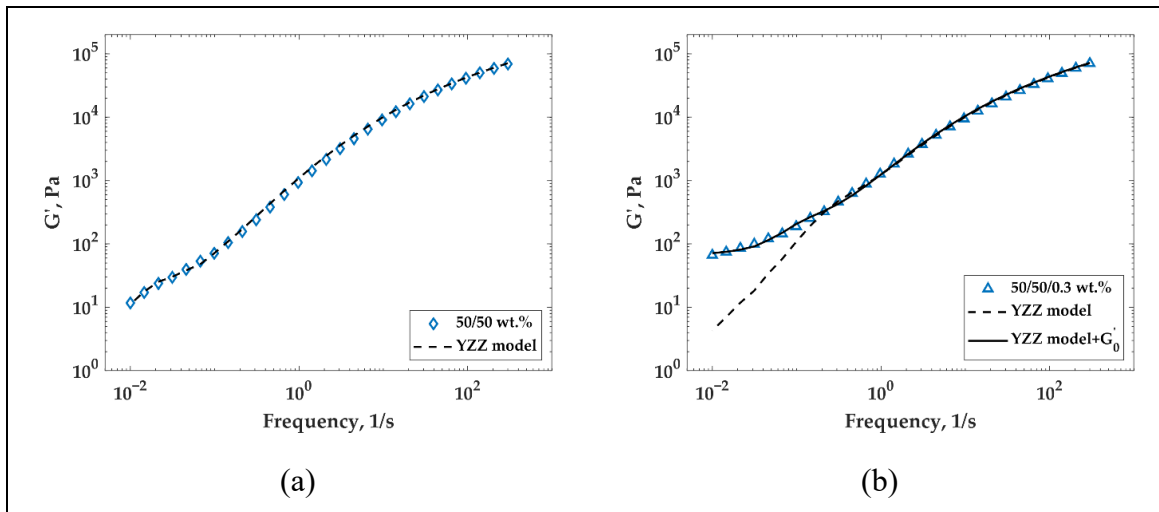


Figure 3.4 Storage modulus as a function of frequency for (a) PP, PS, and PP/PS blend with YZZ model fitting data (dashed line) and (b) PP/PS/MWCNT composite with 0.3 wt.% of MWCNT with model data representing the fit of the YZZ model (dashed line) and model data representing the fit of the Equation (3.15) (solid line)

It can be seen that the YZZ model describes well the experimental data in the absence of MWCNT. It should be noted that fitting the model to the experimental data requires knowledge of the value of the zero-shear viscosity ratio (η_0) and interfacial tension. Zero shear viscosity of neat PP and PS was found by fitting the experimental data to the Carreau model [125,126], using the curve of complex viscosity (Pa·s) versus frequency (rad/s), obtained from SAOS tests. The values of η_0 are presented in Table 3.1. The value for interfacial tension was taken from the literature [127]. Using a viscosity ratio of 0.52 and an interfacial tension of 6 mN/m, fitting the YZZ model to the experimental data resulted in an a value of 4.95 μm . $l_c = a/a'$ was then found to be 10.45 μm . These values are used in Equation (3.6) to obtain the value of $\xi = 8.9 \mu\text{m}$ for the neat blend. This corroborates rather well with morphological characterization, presented in Figure 3.5(a), in which a value of $\xi = 11 \pm 0.8 \mu\text{m}$ was found using the following equation [30,31]:

$$\xi = \frac{A_{SEM}}{L_{int}} \quad (3.14)$$

where A_{SEM} is the total area of the SEM micrograph (Figure 3.5) and L_{int} is the interface length, estimated using a homemade image analysis script (written in MATLAB). (Note that these analyses were done for at least seven images). The MATLAB code for SEM pictures' treatment and calculation of the perimeter of the interface (interfacial length) was written based on the analysis described by Galloway et al. [128]. The steps of the image treatment for interface indication are shown in Figure-A II-3(a) and Figure-A II-3(b) of the supplementary material.

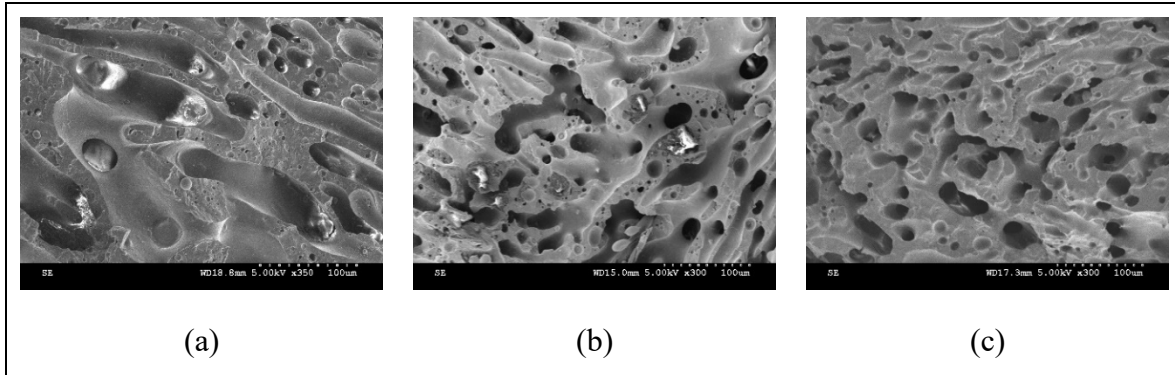


Figure 3.5 Morphology evolution of selected PP/PS/MWCNT composites for (a) 0 wt.% of MWCNT, (b) 0.3 wt.% of MWCNT, and (c) 0.5 wt.% of MWCNT

Figure 3.4(b) shows that the YZZ model fails to describe the rheological behavior at lower frequencies for the PP/PS/MWCNT composite containing 0.3 wt.% MWCNT independently of the value of a used. This was observed for all PP/PS/MWCNT composites. The discrepancy between the experimental values of G' and the ones predicted by the model was much larger at low frequencies. One way to deal with this discrepancy is to add, as was done in this work, a frequency-independent elastic modulus, G'_0 , to the YZZ model resulting in

$$G'_{blend}(\omega) = G'_{components}(\omega) + G'_{interface}(\omega) + G'_0 \quad (3.15)$$

where G'_0 is a constant that takes into account the filler network elasticity.

Using Equation (3.15), it was then possible to achieve a good fit of storage modulus for all PP/PS/MWCNT composites. Two fitting parameters were found when adjusting Equation (3.15) to the experimental data: a and G'_0 . Figure 3.4(b) shows the result of this fit (solid line) for PP/PS/MWCNT with 0.3 wt.% of MWCNT. In this case, the values of G'_0 of 66.2 Pa and a of 1.18 μm were resulted in a value of $\xi = 2.13 \mu\text{m}$ which agrees well with the morphological characterization of Figure 3.5(b) for which a value of $\xi = 1.86 \pm 0.2 \mu\text{m}$ was found.

Equation (3.15) is tested as a tool to quantify the morphology of different composites studied in this work using the data presented in Figure-A II-1 of the supplementary material (model fitting results for all composites are shown in Figure-A II-2 of the supplementary material). A comparison of the characteristic domain size evaluated using the morphological and rheological data is presented in Figure 3.6. It can be seen that a good agreement was obtained for all composites. The larger discrepancy obtained for the neat blend, probably, originated from the non-fully developed co-continuous morphology, which was observed for the neat blend.

It can also be seen that the characteristic domain size drastically decreases from 11 ± 0.8 to 1.3 ± 0.05 μm upon the addition of 0.5 wt.% of MWCNT. A drastic decrease in the characteristic domain size was observed, in the literature, for different blend systems filled with carbon-based nanoparticles, as their presence helps to prevent the coalescence and coarsening of the blend morphology [29,30,120,129].

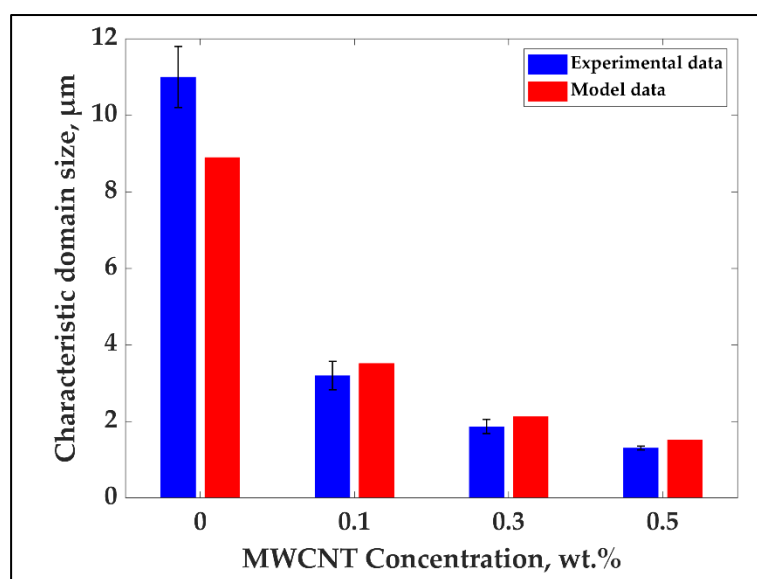


Figure 3.6 Characteristic domain size of PP/PS/MWCNT composites calculated with the help of Equation (3.14) – experimental data and predicted with the YZZ model for

PP/PS/MWCNT with 0-0.1 wt.% of MWCNT and Equation (3.15) for PP/PS/MWCNT with 0.3-0.5 wt.% of MWCNT – model data

3.3.2 Effect of thermal annealing on electrical conductivity and characteristic domain size of co-continuous morphology of PP/PS/MWCNT composites

The PP/PS/MWCNT composites' morphology evolution during thermal annealing was investigated using the experimental protocol presented in Figure 3.2. Figure 3.7 shows the electrical and rheological behavior of PP/PS/MWCNT composites during the middle step – time sweep (simulating thermal annealing, see Figure 3.2). Figure 3.7(a) shows the electrical conductivity of PP/PS/MWCNT composites as a function of time during thermal annealing, performed using the rheometer connected with the DRD cell. Figure 3.7(b) shows the time-dependent evolution of the storage modulus for PP/PS/MWCNT composites.

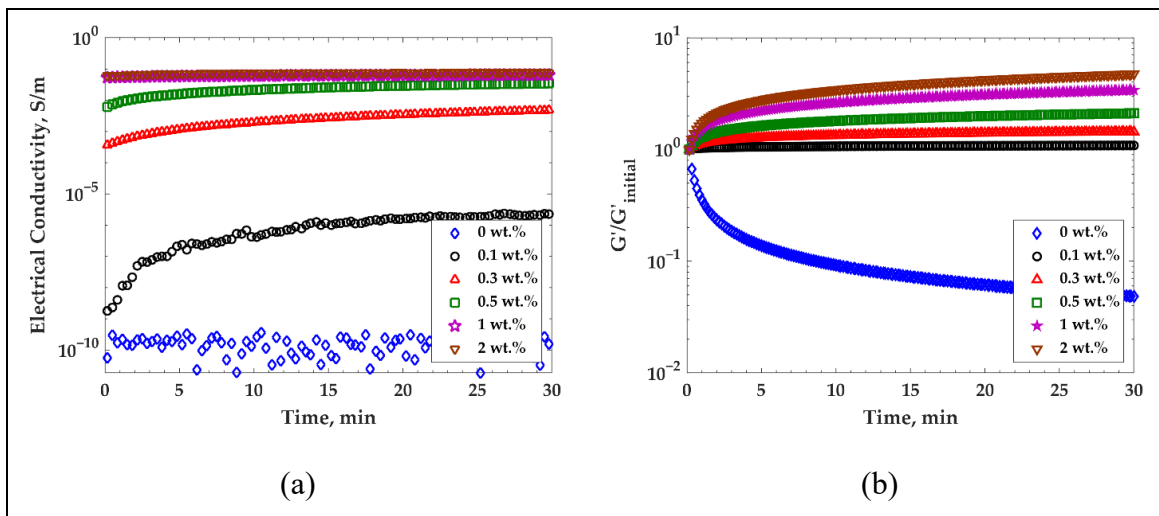
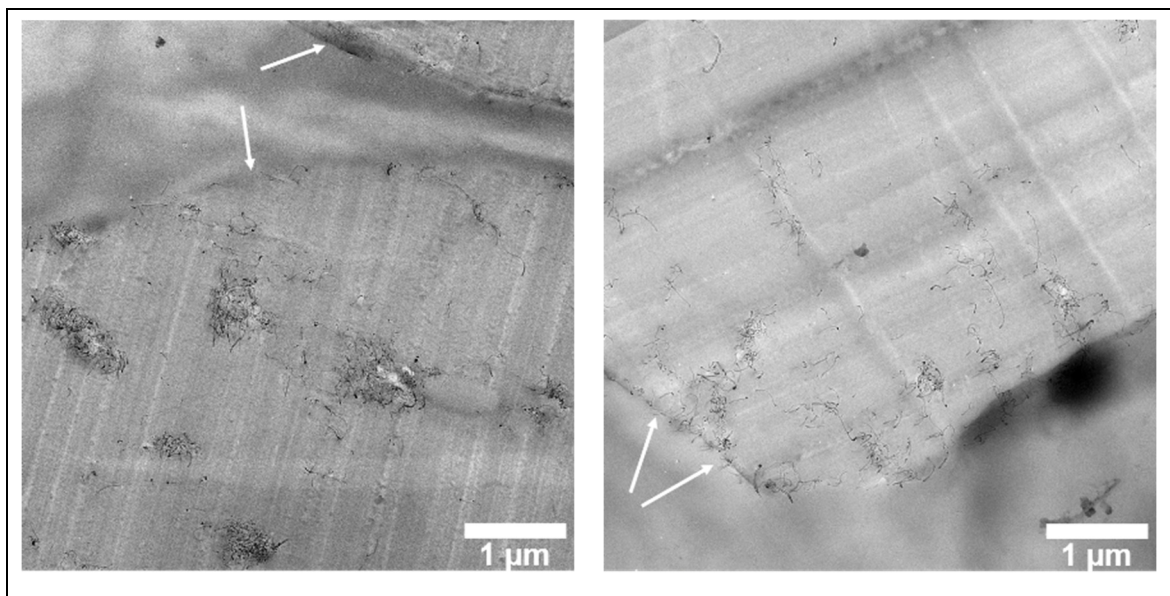


Figure 3.7 (a) Electrical conductivity as a function of time for PP/PS/MWCNT composites with different concentrations of MWCNT measured at 20 Hz of frequency and 200 °C. (b) Time-dependent evolution of storage modulus at 200 °C for PP/PS/MWCNT composites with different MWCNT concentrations

It can be seen, from Figure 3.7(a), that even at a very low concentration of MWCNT, the electrical conductivity starts to increase from the first second and reaches a plateau. The increase could originate from a MWCNT nanoparticles network formation during thermal annealing. Similar behavior was observed by other authors for different polymer pairs such as PaMSAN/PMMA with MWCNT [72] and for PLA/PS filled with reduced graphene oxide [29]. However, in those cases, the authors observed electrical conductivity increase only for a large MWCNT concentration and/or after long annealing times. After thermal annealing, a low value of electrical percolation threshold (PT) was reached. This happened due to the double percolation effect [30,40,42] and due to the destruction of the filler agglomerates and reformation of the electrically conductive network [130], which both reduce the electrical PT. In order to confirm the localization of MWCNT in PP/PS/MWCNT composites before and after thermal annealing, TEM was performed for the PP/PS/MWCNT composite with 0.5 wt.% of MWCNT. Figure 3.8(a) and Figure 3.8(b) show the images corresponding to PP/PS/MWCNT composite with 0.5 wt.% of MWCNT before thermal annealing and Figure 3.8(c) and Figure 3.8(d) show the images corresponding to the same composite after thermal annealing. It was observed that for PP/PS/MWCNT composite with 0.5 wt.% of MWCNT after thermal annealing, the nanoparticles are mostly located at the PP/PS interface.



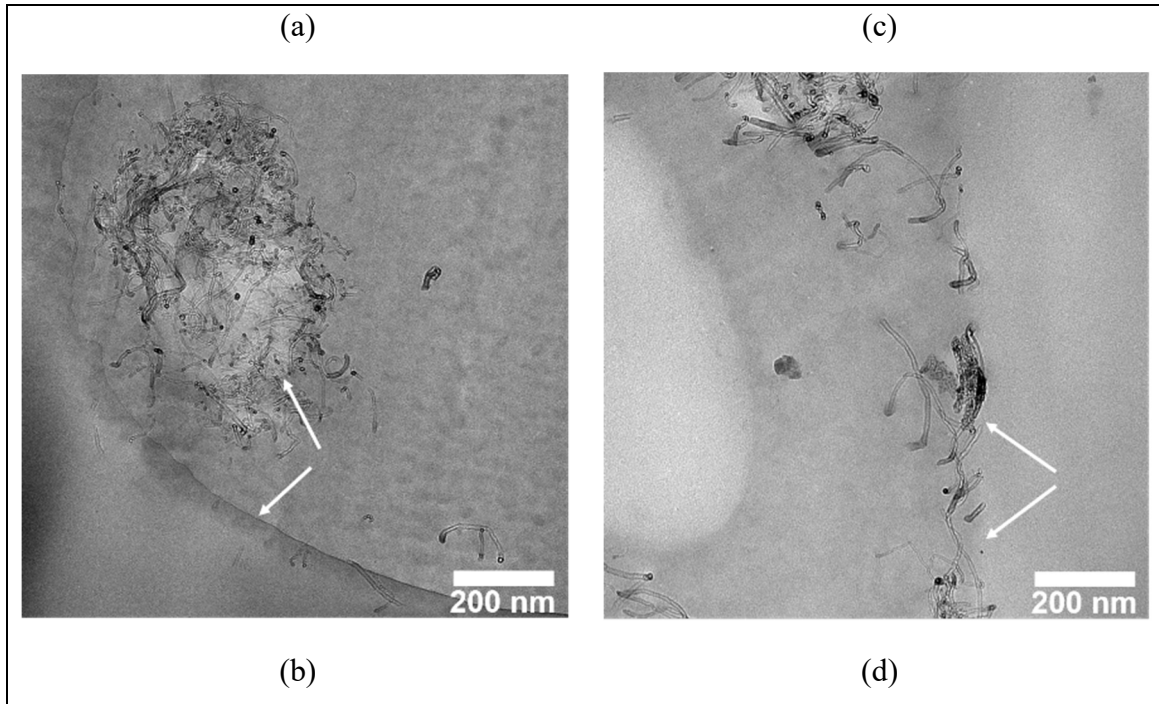


Figure 3.8 TEM of the PP/PS/MWCNT composite with 0.5 wt.% of MWCNT for (a) and (b) before treatment and (c) and (d) after thermal annealing. Arrows show the PP/PS interface

Figure 3.7(b) shows the evolution of the storage modulus during thermal annealing. In this case, the power-law fitting of experimental data is presented. The fitted storage modulus (G') was normalized by its initial value ($G'_{initial}$), which was taken at the beginning of the test. The experimental values of G' were fluctuating during the early stage of thermal annealing (~10 min) (as shown in Figure-A II-4 of the supplementary material); after that, G' values were slightly increasing and then approaching a plateau for filled PP/PS/MWCNT composites. However, in the case of neat PP/PS blend, G' was decreasing drastically during the first 10 min and then approaching a plateau. This behavior can be clearly seen in normalized fitted data. In order to understand these changes in electrical conductivity and evolution of the storage moduli during thermal annealing for the PP/PS/MWCNT composites, the SAOS experiments before and after thermal annealing were analyzed. The YZZ model (Equation (3.12)) was used for the systems containing less than 0.3 wt.% MWCNT. The modified YZZ model (Equation

(3.15)) was used for the systems containing higher concentrations of MWCNT to characterize the morphologies of the blend before and after thermal annealing.

The values predicted by the YZZ model and the modified YZZ model are reported in Table 3.2. These values were used to calculate the characteristic domain size for each PP/PS/MWCNT composite before and after thermal annealing as shown in Figure 3.9.

Table 3.2 Fitting parameters for Equations (3.12) and (3.15)

MWCNT, wt. %	G'_0, Pa, before annealing	G'_0, Pa, after annealing	a, μm, before annealing	a, μm, after annealing
0	-	-	4.95	7.67
0.1	-	-	1.96	1.67
0.3	66	74	1.18	0.91
0.5	124	158	0.85	0.69
1	257	389	0.65	0.53
2	1548	1677	0.59	0.42

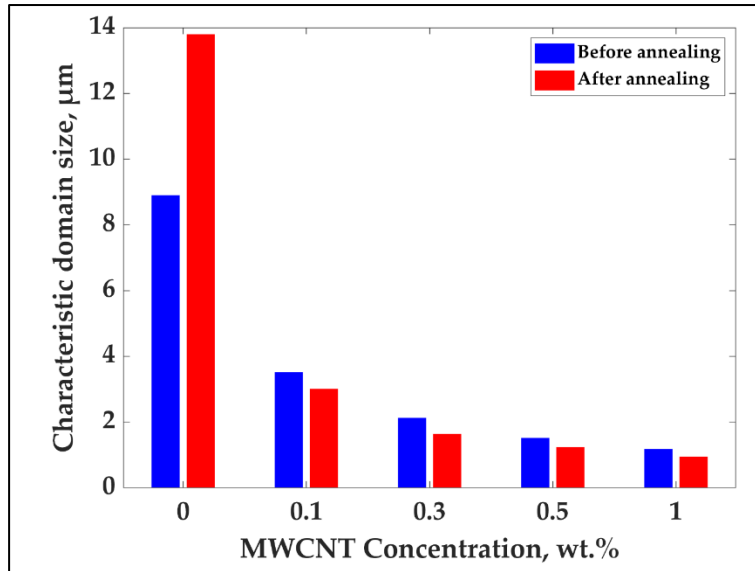


Figure 3.9 Characteristic domain size of PP/PS/MWCNT composites before and after 30 min of annealing calculated with the help of the YZZ model for PP/PS/MWCNT with 0-0.1 wt.% of MWCNT and Equation (3.12) for PP/PS/MWCNT with 0.3-0.5 wt.% of MWCNT

It can be seen, from Figure 3.9, that the characteristic domain size increased from 8.9 to 13.8 μm after 30 min of thermal annealing, for the neat PP/PS blend, indicating a blend morphology coarsening [29,30]. Interestingly, for composites containing MWCNTs, the characteristic domain size slightly decreased after 30 min of thermal annealing. This could indicate that the migration of MWCNTs from the PP to the more favorable PS prevented its coalescence and coarsening. This resulted in a more refined co-continuous morphology.

Data presented in Table 3.2 can help with further investigation of the elastic response mechanism in PP/PS/MWCNT composites and in the estimation of the contribution of the filler network formation after thermal annealing. As was mentioned above, the values of G'_0 for filled composites are constant at low frequencies. These values can be used to estimate the rheological percolation threshold defined as the minimum particle concentration needed for the formation of a filler network as [97]

$$G'_0 = k \cdot (P - P_c)^v \quad (3.16)$$

where G'_0 is the frequency-independent elastic modulus, P is the mass fraction of MWCNT, P_c is the percolation threshold, v is a fitted exponent that depends, only, on the dimensionality of the system, and k is a scaling factor responsible for strength of the filler network. It should be noted that this equation is valid for $P > P_c$.

A linear regression of $\log(G'_0)$ versus $\log(P - P_c)$ was used to determine the rheological percolation threshold of the blends, studied in this work. The same calculations were done for the electrical conductivity before and after thermal annealing to determine the electrical percolation threshold. The experimental data for PP/PS/MWCNT composites before and after thermal annealing were fitted to Equation (3.16), and the results are presented in Figure 3.10 for both the rheological (Figure 3.10(a)) and the electrical (Figure 3.10(b)) percolation thresholds (where values of σ' instead of G'_0 were used for the calculation of electrical PT). Both rheological and electrical percolation thresholds were decreased by thermal annealing: from 0.03 wt.% to 0.009 wt.% of MWCNTs for rheological PT and from 0.28 wt.% to 0.06 wt.% of MWCNTs for electrical PT. It can be seen that rheological PT is smaller than the electrical one. This could indicate that adding a rigid filler to the polymer matrix can impede the movement of the polymer chains even at a ultralow MWCNT concentration due to the strong interaction between the filler and polymer chains. However, in the case of electrical conductivity, MWCNT-MWCNT contacts have to be dominant for easier charge transfer [131]. Therefore, the electrical PT is higher than the rheological one. It is worth noting that the stiffness of the network for both rheological and electrical PT is higher than that after thermal annealing. Rheological PT was found to be 367 Pa before compared to 487 Pa after thermal annealing. Similarly, electrical PT increased from 8×10^{-4} S/m before to 6.4×10^{-1} S/m after thermal annealing. This is attributed to the increase in the fraction of MWCNT located at the PP/PS interface after thermal annealing. The same behavior was observed for LLDPE/EVA co-continuous polymer blend containing graphene [31].

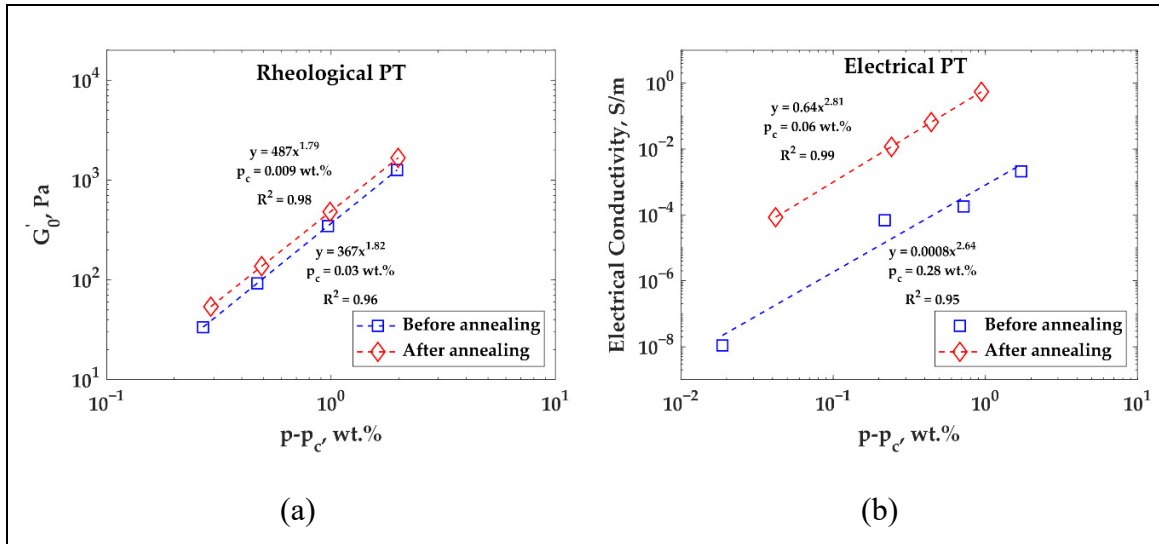


Figure 3.10 Network elasticity as a function of reduced filler content related to PP/PS/MWCNT composites (solid squares) and power-law fitting to the experimental data (solid lines) for composites before and after thermal annealing: (a) rheological PT – G'_0 versus $(P - P_c)$ plots and (b) electrical PT σ' versus $(P - P_c)$ plots

3.4 Conclusion

In this study, the linear viscoelastic behavior of a co-continuous PP/PS blend containing an electrically conductive filler – MWCNT was investigated. PP/PS/MWCNT composites were prepared by melt-mixing using a twin-screw extruder by the dilution of a masterbatch of PP/MWCNT with PP and PS. The linear viscoelastic behavior of PP/PS/MWCNT composites was investigated by the YZZ model. It was shown that this model fails to describe the rheological behavior of highly filled composites at lower frequencies. The discrepancy between the experimental values of the storage modulus and the one predicted by the YZZ model is due to a significant contribution of filler network elasticity to the dynamic modulus. To consider this contribution, a modified YZZ model is proposed in this work for PP/PS/MWCNT composites. By using the modified YZZ model, it was possible to quantify the co-continuous morphology of PP/PS/MWCNT composites. It was shown that a good agreement between the characteristic domain size, predicted by this model, and that calculated

via a statistical analysis of SEM images was achieved. Furthermore, the modified YZZ model was used to study the evolution of the co-continuous morphology of PP/PS/MWCNT composites after thermal annealing. It was observed that the characteristic domain size, calculated with the modified YZZ model, slightly decreased after 30 min of thermal annealing. This resulted in a more refined co-continuous morphology. This is in good agreement with the measured electrical properties of these composites. It was shown that the electrical percolation threshold was reduced by over 70% as a result of thermal annealing.

Supplementary Material:

See supplementary material for the additional information of experimental data: storage and loss moduli as a function of frequency for PP/PS/MWCNT composites with different concentrations of MWCNT. The model fitting data; SEM image treatment analysis; time-dependent evolution of storage modulus; and electrical conductivity as a function of time for PP/PS/MWCNT and PP/MWCNT composites.

Acknowledgments:

Financial supports from the Natural Sciences and Engineering Research Council of Canada (NSERC), PRIMA and École de technologie supérieure (ÉTS) are gratefully acknowledged. The help of Mazen Samara in reviewing English is highly appreciated.

CHAPTER 4

EFFECT OF STEADY SHEAR DEFORMATION ON ELECTRICALLY CONDUCTIVE PP/PS/MWCNT COMPOSITES

Daria Strugova, Éric David and Nicole R. Demarquette

Mechanical Engineering Department, École de Technologie Supérieure, Montréal, Québec

Paper submitted for publication, February 2023

Abstract

Conductive polymeric materials are commonly obtained adding conductive nanoparticles to blends of immiscible polymers that form a co-continuous morphology. However, during processing, morphology changes affecting materials properties. This study investigates the impact of steady shear deformation on the morphological and electrical properties of a model system consisting of polypropylene/polystyrene/multiwall carbon nanotubes (PP/PS/MWCNT). The findings reveal that the deformation results in coarsening of the blend morphology and disruption of the electrical network, increasing both the rheological and electrical percolation threshold concentrations. The evolution of both electrical and morphological properties depends on MWCNT concentration, strain amplitude, and shear rate. MWCNT concentration, below a certain level, leads to a disruption in electrical conductivity at high shear rates. However, if the MWCNT concentration is above 1 wt.%, the balance between filler network breakup and nanoparticle diffusion is maintained, resulting in stable electrical conductivity and morphology.

4.1 Introduction

Blending two polymers, along with a nanoparticles' filler, can be an effective way to enhance the properties of thermoplastic nanocomposites, as it provides a tool to engineer the distribution of the nanoparticles within the matrix. For example, adding electrically conductive

nanofillers to blends with a co-continuous morphology can lower the electrical percolation threshold (PT), which is the fillers' concentration at which the material conducts electricity. Indeed, if two immiscible polymers with appropriate rheological properties are mixed in the right proportions, a blend forming a co-continuous morphology is obtained [84,85]. If conductive particles are added to the blend, in such a way that they end up locating in one of the blend components or at the interface between the two polymers, the percolation threshold decreases drastically. This phenomenon is known as double percolation [1,4,11,13-22,25,26,29-31,38,51,120], was observed in several studies using various carbonaceous nanofillers, such as carbon black (CB) [13-23], carbon nanotubes (CNT) [2-8,24-28], or graphene [12,29-37].

The potential for low percolation threshold, predicted by the double percolation theory, can be hampered by changes to the co-continuous morphology during both processing and post-processing stages. In particular, the characteristic domain size can coarsen resulting in a decrease of electrical conductivity [19,30,42,71,118,132]. Overall, achieving good electrical properties in composites with a double percolation structure requires careful control of processing and post-processing parameters to mitigate the negative effects of morphology changes on the conductive filler network. Optimizing post-treatment temperature and duration can positively alter the electrical conductivity of the composite and decrease the percolation threshold concentration [29,133]. In practice, however, it can be challenging to control all relevant parameters. Therefore, further research is needed to fully understand the effects of processing and post-processing on the electrical properties, in order to develop effective strategies to control the morphology and achieve optimal electrical conductivity.

Several strategies have been proposed in the literature to mitigate the negative effects of morphology changes on the electrical properties of composites with double percolation structures, including increasing filler content [29,118], using different fillers, or applying thermal treatments [29,117,118,134]. The success of these strategies, however, is influenced by various factors, such as the type or geometry of the employed filler [29,35,117,133], as well

as the post-processing temperature and duration. For example, in a study involving a polylactic acid/polystyrene (PLA/PS) co-continuous blend, filled with thermally reduced graphene oxide (r-GO), after 30 min of annealing at 180 °C the characteristic domain size increased significantly for composites containing 0-0.28 vol.% r-GO (it increased, for example, from ~2.5 μm to ~23 μm for composite with r-GO concentration of 0.028 vol.%), but remained unchanged for composites containing 0.56-1.12 vol.% r-GO [29]. In our previous work [133], we demonstrated that the characteristic domain size was slightly reduced after 30 min of annealing at 200 °C for a polypropylene/polystyrene (PP/PS) blend filled with different concentrations of MWCNT presenting a co-continuous morphology [133]. This reduction in domain size was attributed to a refinement of the co-continuous morphology. This refinement led to an increase in the specific interfacial area between the two polymers, which is inversely proportional to the domain size. Our previous work has demonstrated progress in this field by introducing a tool/technique that correlates morphology and electrical properties in filled polymer composites with a co-continuous morphology [133]. Further investigation of the evolution of double percolation-type morphologies, however, is necessary to develop effective strategies for optimizing the electrical properties of such composites.

To investigate the evolution of properties during, as well as, after applying deformation, a series of steps must be taken. A test design consisting of three steps should be carried out. The first step is to use small amplitude oscillatory shear (SAOS) tests within the linear viscoelastic region, which are commonly employed to characterize the morphology of polymer blends by fitting the data to appropriate constitutive equations [16,24,59-62,121]. The second step is to apply a deformation. The third step is to use another SAOS to assess the evolution of the blend's morphology as a result of the applied deformations.

This strategy has been widely used to study the evolution of dispersed droplet shape morphology [63,98,99,102,105,108,122], using the well-known Palierne's model and its derivatives [59,60]. This approach can be used to investigate the evolution of a double-percolation morphology. The rheological behavior of the filled blend-based composite with a

co-continuous morphology is subjected to SAOS and fitted to a modified Yu et al. (YZZ) model (4.1):

$$G'_{blend}(\omega) = G'_{components}(\omega) + G'_{interface}(\omega) + G'_0 \quad (4.1)$$

The contribution of components, denoted by $G'_{components}(\omega)$, can be calculated using equation (4) presented in reference [95], which takes into account the storage moduli of each polymer in the polymer blend, as well as geometrical parameters of a simplified co-continuous morphology. The contribution of the interface, denoted by $G'_{interface}(\omega)$ can be calculated using equation (15) presented in reference [89]. The calculation of $G'_{interface}(\omega)$ takes into account both the geometrical parameters of the co-continuous morphology and the physical properties of the components in the polymer blend, such as the viscosity of each polymer and the interfacial tension between them. Finally, an adjustable constant, denoted by G'_0 is included to account the rigidity of the filler network, as described in references [94,133]. More details can be found in Yu et al. and Strugova et al. [89,133].

As mentioned above, the evolution of the blend morphology that is subjected to a deformation flow depends on the kinematics and kinetics of the undergone deformation. In the case of dispersed droplet morphology, the magnitude of the shear rate will either result in a droplet break-up or droplet coalescence [63,98,102,106,135]. The shear rate value which determines the transition from coalescence to break-up can be calculated using the well-known Grace diagram [110] (presented in Figure-A III-1 of the Supplementary material). This diagram provides the critical capillary number $Ca = \frac{F_{viscous}}{F_{interfacial}} = \frac{\eta_m \dot{\gamma} R_v}{\alpha}$ as a function of the viscosity ratio, $p = \frac{\eta_d}{\eta_m}$, for rotational shear. Here η_m is the viscosity of the matrix, η_d is the viscosity of the dispersed phase, $\dot{\gamma}$ is the shear rate, R_v is the volume average radius of the drops, and α is the interfacial tension [109]. The capillary number is a function of shear rate, therefore, the transition, for a certain viscosity ratio can be predicted by the shear rate value or the capillary number. The value of the transition, from coalescence to breakup, capillary number, was

measured by Grace [110], by gradually increasing the strain rate up to breakup. Tucker et al. [111] suggested an empirical fit to Grace's data shown in Figure-A III-1, according to Equation (4.2):

$$\text{Log}(Ca_c) = -0.506 - 0.0995 \log(p) + 0.124(\log(p))^2 - \frac{0.115}{\log(p) - \log(4.08)} \quad (4.2)$$

While this theory was developed for a dispersed droplet type morphology it can be used to, approximately, determine the critical transition shear rate, from coalescence to breakup.

In the present work, PP/PS/MWCNT composites manifesting double percolation, with MWCNT concentrations equal to or above the PT, were subjected to different sequences of SAOS-steady shear-SAOS tests. The values of steady shear rate to which the blends were subjected during deformation were chosen to promote coalescence and break-up in order to induce two types of morphology evolution. The evolution of morphology of the blend during deformation was evaluated using the modified YZZ model [133]. The electrical properties of the materials were monitored during the deformation step and were attributed to the morphology evolution. The possibility of recovering the morphological and electrical properties after applied deformation was also investigated.

4.2 Materials and Methods

4.2.1 Materials

The study employed PP (PP4712E1 grade) from ExxonMobil and PS (MC3650 grade) from PolyOne. Their respective characteristics are detailed in Table 4.1. Additionally, MWCNT (NC7000™ grade) with an average diameter of 9.5 nm and length of 1.5 μm, and a nominal electrical conductivity of 10⁶ Sm⁻¹, were obtained from Nanocyl.

Table 4.1 Properties of the polymers

Polymers	M_w (g/mol)	M_w/M_n	Density ($\text{g}\cdot\text{cm}^{-3}$)	η_0 (Pa·s) at 200 °C
PP	317 420	6.65	0.9	7 800
PS	105 000	2.37	1.04	4 080

* η_0 – zero-shear viscosity. Zero shear viscosity of neat PP and PS was found by fitting the experimental data to the Carreau model [125,126].

4.2.2 Composites preparation

In this study, PP/PS/MWCNT composites with 50/50/x wt.% (where x is the weight concentration of MWCNT ranging from 0 to 5 wt.%) were prepared using a melt-mixing process with a Haake Rheomix OS PTW16 twin-screw extruder. The compositions were prepared by initially producing a masterbatch of PP containing 10 wt.% MWCNT, which was then diluted with PP and PS to achieve the desired MWCNT concentrations in PP/PS/MWCNT composites. During extrusion, a temperature of 220 °C was maintained in all zones, and the screw speed was fixed at 100 rpm for all compositions.

To promote MWCNT migration to the interface, the MWCNT was added to the PP phase, as it exhibited better affinity towards PS. Young's equation was utilized to predict the preferred location of MWCNT in the PP/PS blend, by estimating the wetting coefficient [26,44,51].

Further details regarding the selection of PP and PS weight fractions in order to obtain a co-continuous morphology can be found in our previous works [120,133].

4.2.3 Characterizations

4.2.3.1 Rheological analysis

The rheological properties of the composites were evaluated using a controlled-stress MCR 501 rotational rheometer from Anton Paar (Graz, Austria), in a dry nitrogen atmosphere. The experiments were conducted using a parallel-plate geometry with a 1 mm gap and 25 mm diameter plates, with all tests performed at a temperature of 200 °C. To determine the linear viscoelastic (LVE) region of the composites, dynamic strain sweep tests (DSST) were conducted. Following the DSST, a strain of 0.3% was selected for all subsequent tests, as it corresponds to the LVE region of the composite. The thermal stability of polymers was tested using time sweep tests on pure PP and PS. The employed polymers were found to be thermally stable for 6 hours. SAOS tests were carried out to investigate the morphology evolution. The parameters for all the above-mentioned tests can be found in Table-A III-1 of the supplementary materials.

Rheological properties' evolution can be investigated by using sequences of SAOS, followed by a steady shear (simulating deformation), followed by another SAOS, as shown in Figure 4.1(a) [63,98,136]. Parameters for the steady shear steps were chosen in order to perform/mimic coalescence and break-up phenomena of a dispersed droplet morphology type blend, composed of the same polymers (see Table 4.2, below). To assess any possible relaxation of the morphology after steady shear a stress relaxation step consisting of 30 min of rotation at 0.05 rad/s was added to the sequence (depicted in Figure 4.1(a)). The parameters of the stress relaxation step are similar to the parameters of annealing, explained in our previous work [133].

It is important to note that the parallel-plate geometry is not ideal for performing deformation tests to assess the morphology of polymer blends because the shear rate across the sample is not uniform. However, when measuring electrical properties at the same time as rheological properties under applied deformation, the parallel-plate geometry is the most suitable option as it allows for simpler extraction of electrical properties. Although the parallel-plate geometry may not be ideal for characterizing the morphology, we assumed that we could study the evolution of morphology using this geometry since we are measuring bulk properties rather

than point-specific properties. To obtain a more comprehensive understanding of the co-continuous morphology, the samples for scanning electron microscopy were broken across the diameter. The observed morphology of the cross-sections was uniform across the diameter. To determine the presence of a slip effect, the viscosity of the composites (pure blend and filled with 0.5 wt.% of MWCNT) was measured at a constant shear rate of 0.05 s^{-1} for 2000s (100% of shear strain) for two plate-plate gaps: 1 mm and 2 mm. It was found that no significant change in viscosity was observed. The data for this experiment is presented in Figure-A III-2(a) and Figure-A III-2(b) of the supplementary material.

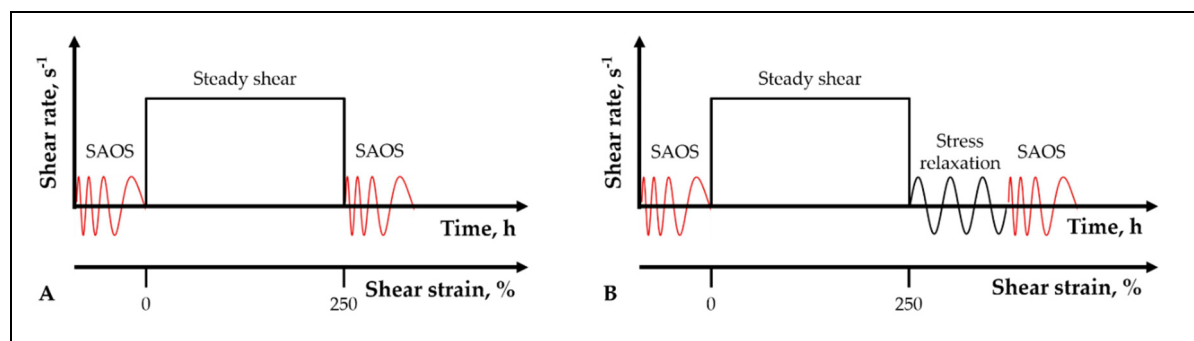


Figure 4.1 Experimental protocols

Equation (4.2) was used to determine the critical shear rate ($\dot{\gamma}_c$), above and below which break-up or coalescence occurs. Although this theory was originally developed for dispersed droplets morphology, calculating the critical shear rates for a co-continuous morphology can be done by estimating of the critical shear rates for different ratios of the dispersion. This would yield a curve of the of shear rate versus dispersion approaching a plateau. The plateau value of the shear rate is considered to be the critical shear rate for the co-continuous morphology. For this purpose, PP/PS blends with PS disperse phase ranging from 0 to 30 wt.% were prepared. 30wt.% of PS was deemed adequate since the co-continuous range was approached. The droplets volume average radius (R_v) for each blend was measured by scanning electron microscopy (SEM). The interfacial tension value was taken from the literature [127]. Table 4.2 summarizes the experimental data required for the proposed experimental protocol.

Table 4.2 Experimental data for PP/PS blend with different weight concentration of components

PP/PS wt. %	Ca_c	α , mNm	R_v , μm	$\dot{\gamma}_c$, s^{-1}
90/10			0.76	0.5
80/20	0.46	6	3.2	0.1
70/30			4.9	0.07
50/50			-	-

Values of steady shear rate for the experimental protocol presented in Figure 4.1(a) and Figure 4.1(b) are reported in Table 4.3. These values were chosen based on the experimental data presented in Table 4.2.

Table 4.3 Parameters of the experimental protocol presented in Figure 4.1

Coalescence		Break-up	
Shear strain, %	$\dot{\gamma}$, s^{-1}	Shear strain, %	$\dot{\gamma}$, s^{-1}
0		0	
10		10	
25	0.05	25	1
100		100	
250		250	

4.2.3.2 Electrical conductivity analysis

Electrical characterization, in conjunction with a rheological one, was carried out, using the MCR501 rheometer equipped with a dielectro-rheological device (DRD with ST2826/A high-frequency LCR meter). The plates of the parallel-plate geometry are made of stainless steel. In the employed arrangement two ceramic insulating discs about 5mm in height are added to both

shafts holding the plates to provide electrical insulation. Electrical conductivity was measured during the steady shear and stress relaxation steps, see Figure 4.1(a) and Figure 4.1(b). More technical details for electrical conductivity measurements can be found in our previous work [133].

4.2.3.3 Microscopy analysis

The morphology of PP/PS/MWCNT 50/50/x wt.% composites, before and after 250% of applied shear strain at two steady shear rates, one corresponding to coalescence, 0.05 s^{-1} , and other to breakup, 1 s^{-1} , was observed by scanning electron microscopy (SEM) using a S3600 Hitachi microscope (Hitachi, Ltd., Tokyo, Japan), operated at 5 kV in the secondary electrons mode. The samples, deformed in the rheometer, were quenched by opening the rheometer oven and cooling them, by convection, with compressed air. The cooling time was around 30 s which was not enough for the sample to undergo a change of morphology. More details for sample preparation can be found in Strugova et al. [120,133].

The state of dispersion and localization of MWCNT in PP/PS/MWCNT composites were evaluated by transmission electron microscopy (TEM). The investigated samples were embedded in an epoxy resin in order to obtain 50–100 nm ultrathin sections. The sectioning was performed using a Leica Microsystems UC7/FC7 cryo-ultramicrotome operated at $-160\text{ }^{\circ}\text{C}$. Imaging was carried out with a Thermo Scientific Talos F200X G2 S/TEM at an accelerating voltage of 200 kV.

4.3 Results

Figure 4.2(a) and Figure 4.2(b) depict the co-continuous morphology of PP/PS 50/50 wt.% and PP/PS/MWCNT 50/50/0.5 wt.%. Figure 4.2(c) and Figure 4.2(d) illustrate the localization of MWCNT in PP/PS/MWCNT 50/50/0.5 wt.% composite. It was observed that the addition of MWCNT refined the co-continuous morphology of the 50/50 wt.% PP/PS matrix, as

previously observed in our earlier works [120,133]. Moreover, due to MWCNT's thermodynamic affinity to PS, it tends to move towards that more favorable phase.

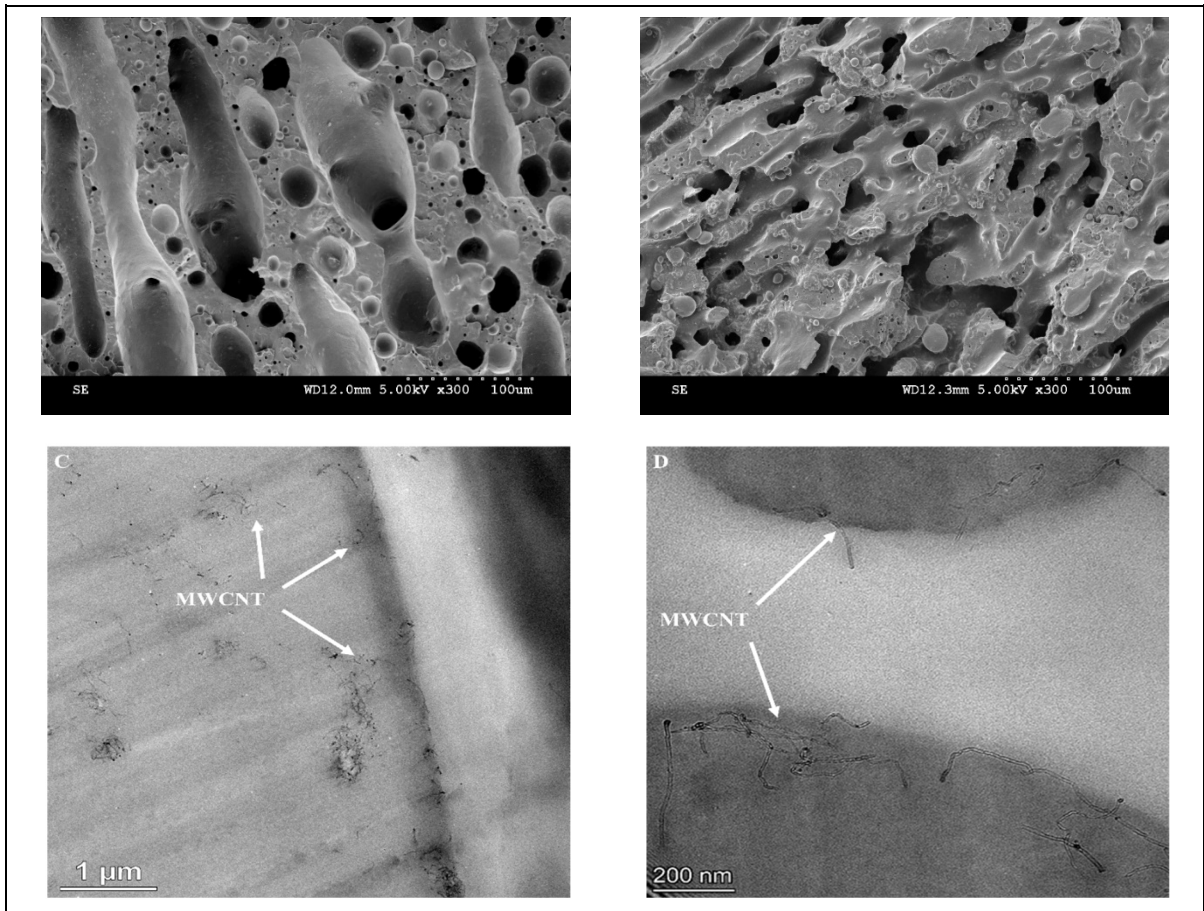


Figure 4.2 SEM observations for (a) PP/PS 50/50 wt.% and (b) PP/PS/MWCNT 50/50/0.5 wt.%. TEM of PP/PS/MWCNT 50/50/0.5 wt.% composite with different magnification

Figure 4.3(a) and Figure 4.3(b) show electrical conductivity versus shear strain at steady shear rates of 0.05 s^{-1} and 1 s^{-1} , respectively. The results demonstrate a significant impact of the MWCNT concentration on the electrical conductivity of composites during the steady shear step. For the composite containing 0.3 wt.% MWCNT, the electrical conductivity decreased noticeably in the early stages of deformation for both studied steady shear rates. It eventually levelled off at a value close to the one for pure PP/PS matrix, exhibiting a dielectric behavior.

However, for a steady shear rate of 0.05 s^{-1} , corresponding to coalescence, the electrical conductivity gradually decreased at a much lower pace, while for a steady shear rate of 1 s^{-1} , corresponding to break-up, the conductivity decreased very sharply to within 75% of its value. The electrical conductivity of composites with 0.5wt.% and 1 wt.% of MWCNT decreased by two orders of magnitude (or four orders of magnitude for the composite containing 0.5 wt.% of MWCNT sheared at a shear rate of 1 s^{-1}), while composites containing 2 wt.% and 5 wt.% of MWCNT showed either no change or an increase in electrical conductivity during steady shear. Figure 4.12 (presented later in the paper) provides a clear illustration of the effect of morphology coarsening during applied deformation on the distribution of the filler within the matrix, and the resulting impact on electrical conductivity of the composites. Similar behavior of electrical conductivity for polycarbonate/MWCNT composites containing 0.75, 1, and 1.5 wt.% of MWCNT was observed by Skipa et al. [137]. For these concentrations of MWCNT, electrical conductivity decreased with increasing deformation time, within the first 300 s, and within the following 300 s, it stabilized and approached a plateau [137].

Transient shear viscosity behavior versus shear strain is presented in Figure 4.3(c) and Figure 4.3(d) for composites deformed at a steady shear rate of 0.05 s^{-1} and 1 s^{-1} , respectively. To aid visualization, the results are presented for the first 50% of applied deformation only. This is because, beyond this point, the transient viscosity reaches a plateau for both steady shear rates. Figure-A III-3(a) and Figure-A III-3(b) in the supplementary material illustrate this trend. The results show that the composites subjected to a deformation rate of 1 s^{-1} exhibit a stress overshoot, whereas the ones subjected to a deformation rate of 0.05 s^{-1} do not. This stress overshoot corresponds to reorientation of the MWCNT network [94]. Its magnitude is larger for the larger compositions of MWCNT as the network is expected to be more robust.

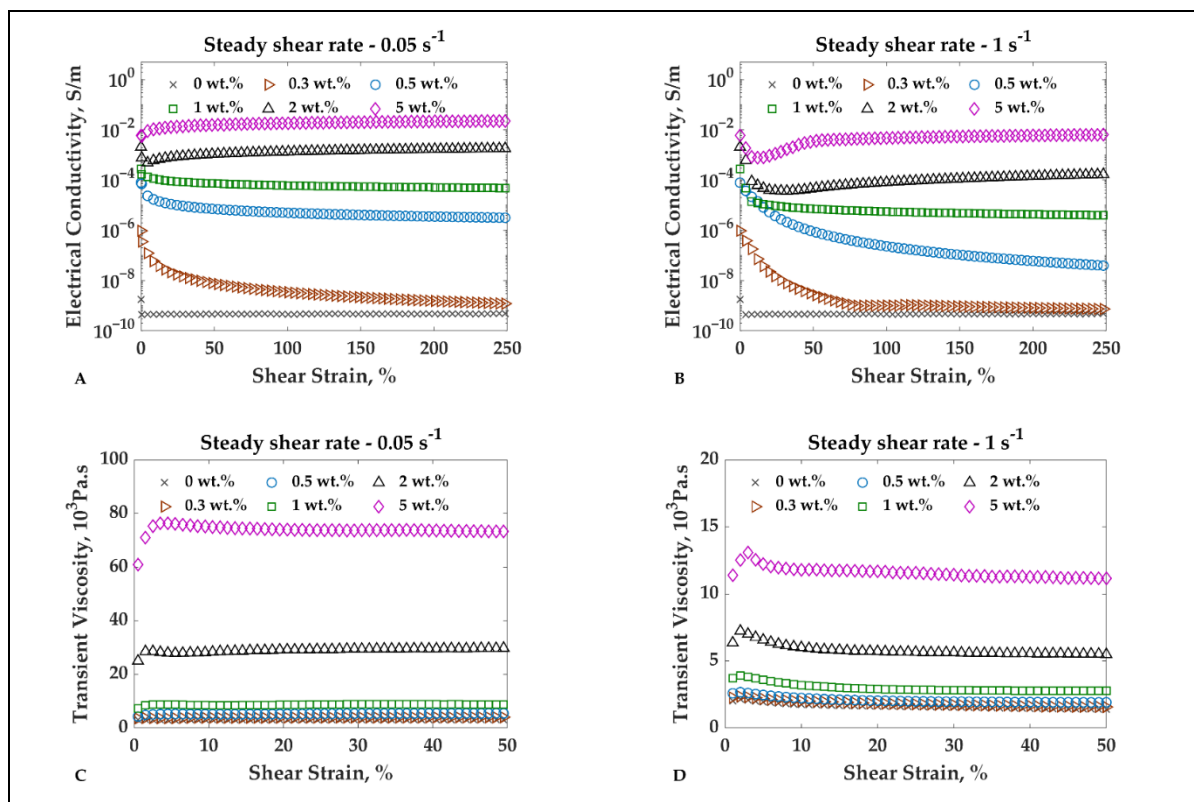


Figure 4.3 Electrical conductivity and transient shear viscosity vs. applied shear strain for PP/PS/MWCNTs 50/50/x wt.% composites at 200 °C at: (a) and (c) steady shear rate of 0.05 s⁻¹; (b) and (d) steady shear rate of 1 s⁻¹

The DC electrical conductivity of PP/PS/MWCNT composites before and after applying 250% of shear strain at steady shear rates of 0.05 s⁻¹ and 1 s⁻¹ is presented in Figure 4.4. In comparison to the undeformed composites, the results indicate that the behavior of the electrical conductivity of deformed composites can be categorized into three distinct groups based on MWCNT concentration. Composites with 0.3 wt.% MWCNT and below experienced a significant decrease in electrical conductivity, exhibiting dielectric behavior. For composites containing 0.5-1 wt.% MWCNT, the electrical conductivity decreased by one order of magnitude when subjected to steady shear at a shear rate of 0.05 s⁻¹, and by 2-3 orders of magnitude at a shear rate of 1 s⁻¹, compared to composites before any deformation. Finally, composites containing 2 wt.% and 5 wt.% of MWCNT either demonstrated no change or exhibited an increase in electrical conductivity after 250% of applied deformation at both shear

rates. The observed results suggest that the effect of shear strain on the electrical conductivity of PP/PS/MWCNT composites is highly dependent on the MWCNT concentration. Additionally, the applied shear rate also plays a crucial role in determining the behavior of electrical conductivity. The decrease in electrical conductivity for composites with lower MWCNT wt.% can be attributed to the reduction in MWCNT network connectivity caused by the deformation. However, for composites with higher MWCNT wt.%, the increase in electrical conductivity can be attributed to the alignment and re-orientation of the MWCNT network, resulting in enhanced connectivity.

The percolation threshold concentrations for PP/PS/MWCNT (50/50/x wt.%) composites, subjected to 250% of applied deformation at both 0.05 s^{-1} and 1 s^{-1} shear rates, were evaluated using Equation (4.3) and the data presented in Figure 4.4.

$$\sigma = k \cdot (p - p_c)^t, \text{ with } p > p_c, \quad (4.3)$$

where σ is the electrical conductivity of PP/PS/MWCNT 50/50/x wt.% composite, p is the mass fraction of MWCNT, p_c is the percolation threshold concentration, t is a fitted exponent that depends, only, on the dimensionality of the system, and k is a scaling factor. The fitting parameters are presented in Table 4.4 and in Figure-A III-4 of the supplementary material.

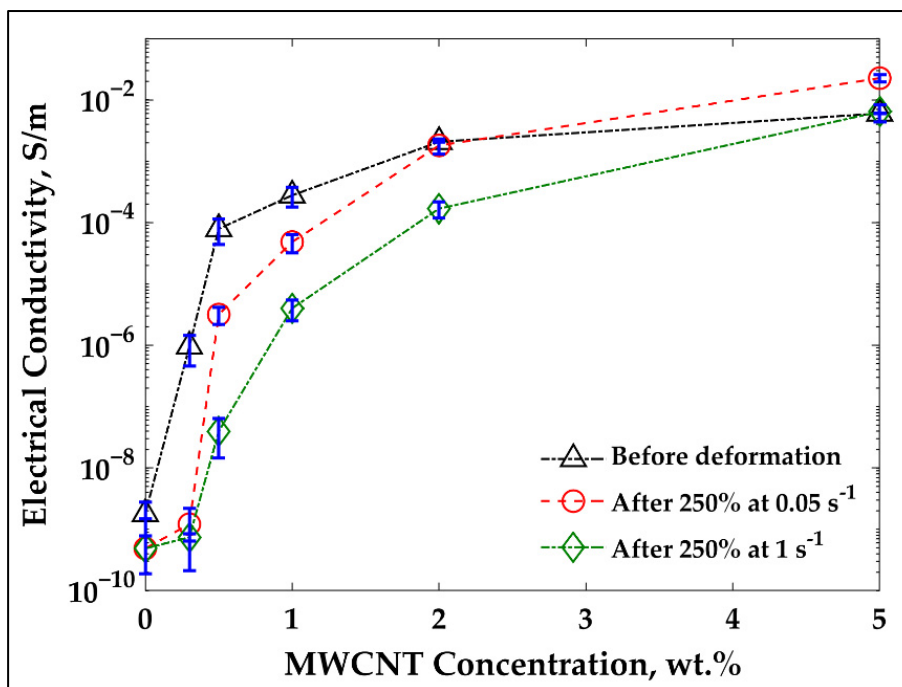


Figure 4.4 Electrical conductivity vs. MWCNT wt.% for composites before and after 250% of applied shear strain at different steady shear rates

Table 4.4 p_c and fitted coefficients for PP/PS/MWCNT composites before and after 250% of shear strain applied at different steady shear rates

Parameters	Before deformation	After 250% of shear strain at a steady shear rate of:	
		0.05 s ⁻¹	1 s ⁻¹
p_c , wt.%	0.29	0.43	0.75
k , S/m	7×10^{-4}	6×10^{-4}	1×10^{-4}
t	1.4	2.2	2.6
R^2	0.99	0.96	0.99

As presented in Figure 4.4 and Table 4.4, an increase in the percolation threshold concentration was observed after the application of 250% shear strain at both shear rates. The concentration increased to 0.43 wt.% and 0.75 wt.% compared to 0.29 wt.% MWCNT for composites

subjected to 250% applied strain at shear rates of 0.05 s^{-1} and 1 s^{-1} , respectively. Nevertheless, the filler network was not completely destroyed for highly filled composites containing more than 1 wt.% MWCNT, even in composites subjected to a shear rate of 1 s^{-1} , as the electrical conductivity of these composites exhibited minimal reduction. In the following section, the changes in electrical properties are elucidated in terms of the morphological evolution, as assessed by rheological measurements.

Figure 4.5 shows a typical example of the frequency-dependent evolution of the storage modulus ($G'(\omega)$) after subjecting the composites to a certain shear strain at steady shear rates of 0.05 s^{-1} (Figure 4.5(a) and Figure 4.5(c)), and 1 s^{-1} (Figure 4.5(b) and Figure 4.5(d)). The $G'(\omega)$ behavior for PP/PS/MWCNT 50/50/0.5 wt.% and 50/50/2 wt.% composites is shown in this case, although similar behavior was observed for the other samples, as presented in Figure-A III-5 of the supplementary material.

Notably, a nonterminal behavior characterized by the presence of a plateau of $G'(\omega)$ is observed at low frequencies, indicating the presence of a rigid nanoparticle network [2,24,31], independently of the shear conditions to which the samples were exposed. However, the magnitude of this plateau modulus decreases with increasing shear strain indicating that the strength of the MWCNT network decreases, although it was not fully destroyed during the applied deformation. Similar results were observed for all composites with MWCNT concentration above 0.5 wt.% (see Figure-A III-5 of the supplementary material), except for the composites containing 2 wt.% and 5wt.% of MWCNT, subjected to steady shear at a shear rate of 0.05 s^{-1} , for which plateau values of $G'(\omega)$ remains nearly unchanged or even increased as a function of applied shear strain.

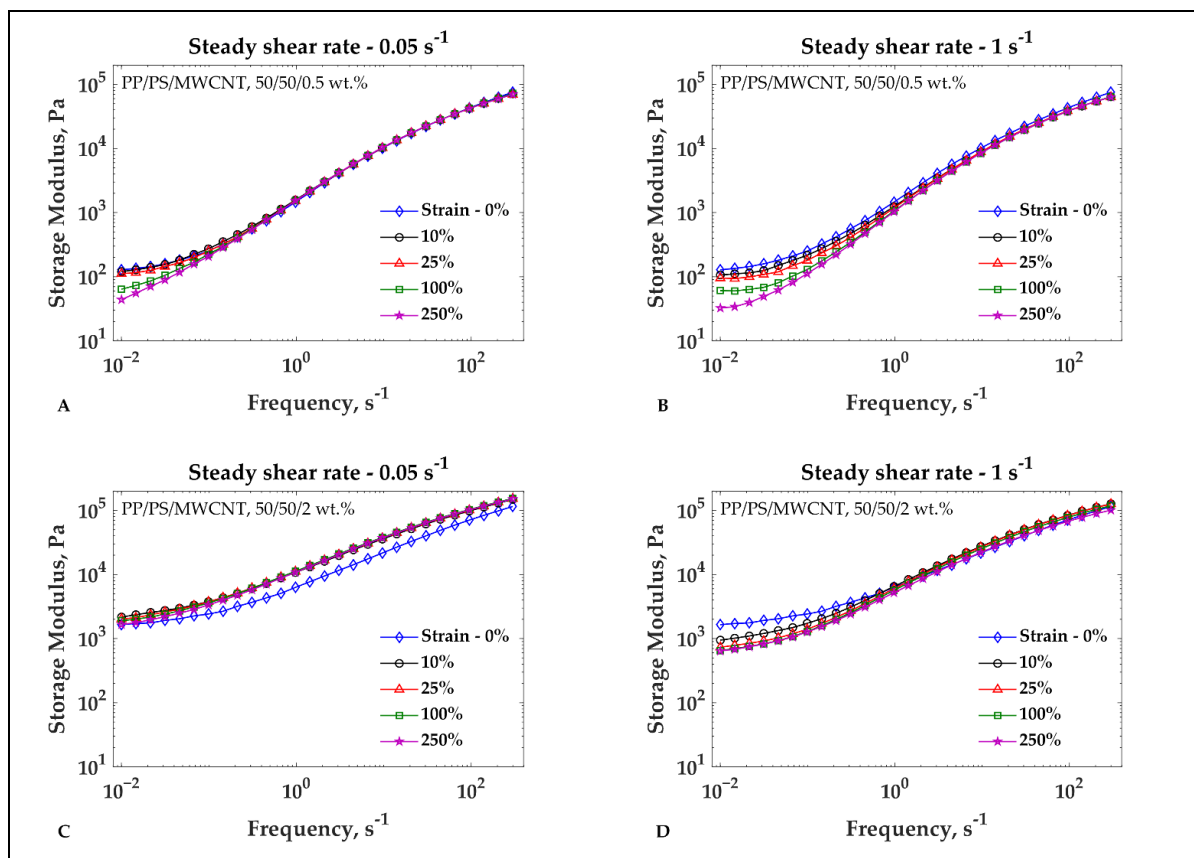
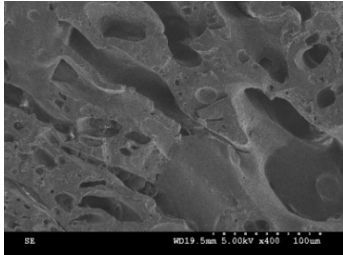
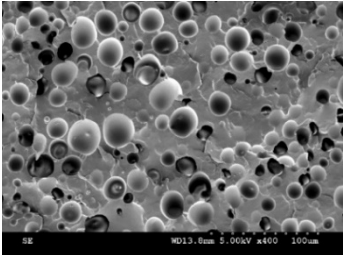
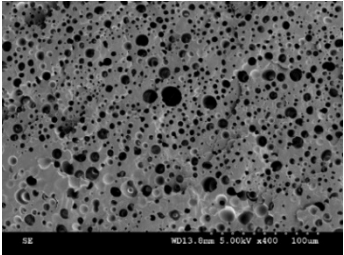
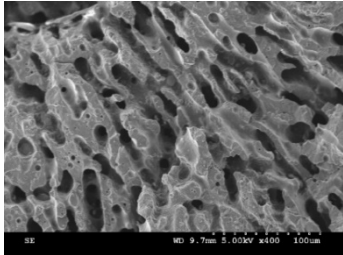
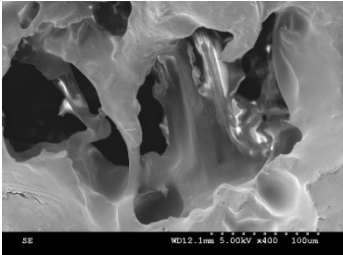
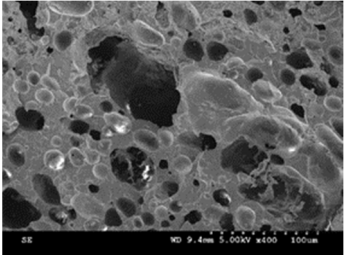
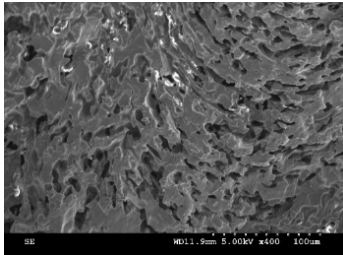
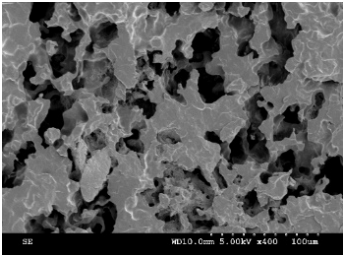
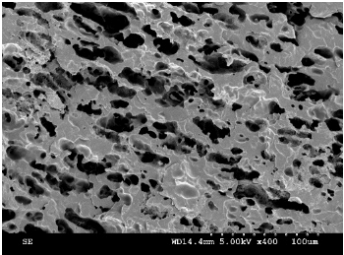


Figure 4.5 G' versus frequency for PP/PS/MWCNT composites with 0.5 and 2 wt.% of MWCNT after shear strain applied at a steady shear rate of: (a) and (c) 0.05 s^{-1} , and (b) and (d) 1 s^{-1}

Table 4.5 presents SEM observations of co-continuous morphology evolution in neat PP/PS (50/50 wt.%) blend, as well as PP/PS/MWCNT composites with 0.5 wt.% and 2 wt.% of MWCNT, before and after 250% of applied shear strain, at steady shear rates of 0.05 s^{-1} and 1 s^{-1} . The results indicate that the co-continuous morphology of the 50/50 wt.% PP/PS blend transforms into a droplet-type morphology following 250% of applied shear strain at both shear rates. However, when MWCNT are added into the blend, this transformation does not occur. Instead, the co-continuous morphology undergoes coarsening following the applied shear strain but does not lose its continuity.

Table 4.5 Morphology of neat PP/PS, 50/50 wt.% blend and PP/PS/MWCNT composites, containing 0.5 wt.% and 2 wt.% of MWCNT wt.% before any deformation and after 250% of shear strain at different steady shear rates

	Before any deformation	After 250% at 0.05 s^{-1}	After 250% at 1 s^{-1}
PP/PS, 50/50 wt.%			
	(a)	(b)	(c)
50/50/0.5 wt.%			
	(d)	ε	(f)
50/50/2 wt.%			
	(g)	(h)	(i)

To study the rate of morphology coarsening following deformation at different shear rates, the characteristic domain size was determined by fitting the storage moduli data to Equation (4.1) for all the sheared composites, except for composites containing 5 wt.% of MWCNT. This is because in such composites, the behavior of $G'(\omega)$ at low frequencies was largely dominated by the MWCNT network, making the modelling method less sensitive to the assessment of the

morphology. Furthermore, for the neat blend without MWCNT and the blend containing 0.3 wt.% MWCNT, the characteristic domain size could not be calculated for shear strains equal to or greater than 100% and 250%, respectively. This was because the morphology of these blends transformed from a co-continuous structure to a dispersed droplet type one, which made the calculation of the characteristic domain size impossible.

Figure 4.6(a) and Figure 4.6(b) show the characteristic domain size (ξ) as a function of shear strain applied at steady shear rates of 0.05 s^{-1} (Figure 4.6(a)), and 1 s^{-1} (Figure 4.6(b)), for composites with different MWCNT concentrations. The neat blend showed no change in morphology when sheared at sheared at a shear rate of 0.05 s^{-1} , but refinement was observed when sheared at a shear rate of 1 s^{-1} . In contrast, all composites containing MWCNT exhibited an increase in the characteristic domain sizes, indicating morphology coarsening. However, the degree of coarsening was less pronounced for composites with higher MWCNT concentrations, and almost absent at a concentration of 2 wt.%, indicating that 2 wt.% MWCNT stabilizes the morphology.

Table 4.5 shows variations in morphologies for composites containing 2 wt.% MWCNT following 250% of shear strain at different shear rates, although the values of the characteristic domain size for these composites are close. The variations in morphology were primarily due to slight orientation along the direction of shear at the higher rate of $1/\text{s}$, which was observed for composites with high MWCNT loadings (1-2 wt.%). As a result, co-continuous domains of the composites appear to be slightly elongated, but the specific surface area values remain relatively constant, as well as the characteristic domain size, which is inversely proportional to it.

The results also indicate that all filled composites exhibit a greater increment in the characteristic domain when sheared at a steady shear rate of 0.05 s^{-1} compared to 1 s^{-1} . This can be attributed to the longer time required to achieve a strain of 250% at a lower shear rate, allowing more time for morphology evolution/coarsening. Moreover, the increase in

characteristic domain size is dependent on the MWCNT concentration, with a greater increase observed for lower concentrations. Interestingly, the coarsening observed at different shear rates can lead to either an increase or decrease in electrical conductivity. The results reveal that when the deformation is applied at a shear rate of 0.05 s^{-1} , the electrical conductivity of the composites increases, whereas it decreases when the deformation is applied at a shear rate of 1 s^{-1} . These results indicate that the evolution of electrical conductivity depends on a delicate balance between changes in blend morphology, leading to the destruction of the conductive network, and the diffusion of MWCNT particles toward the interface.

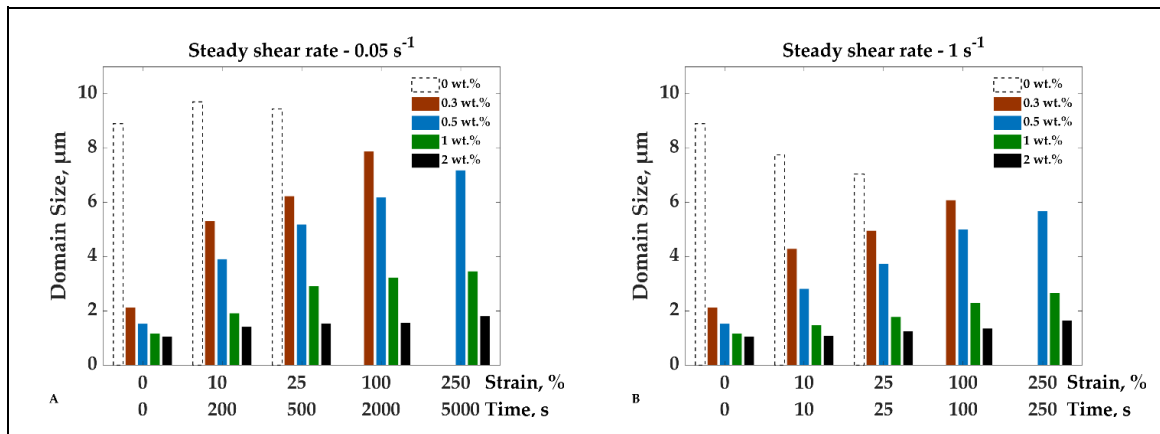


Figure 4.6 ξ vs. applied shear strain for all composites at a steady shear rate of: (a) 0.05 s^{-1} , and (b) 1 s^{-1}

The stability of the filler network of the PP/PS/MWCNT composites can be investigated by fitting the values of G'_0 , the frequency-independent elastic modulus, obtained by fitting the SAOS data to Equation (4.1), to the following equation (values predicted by the modified YZZ [133]) [97]:

$$G'_0 = k \cdot (\gamma - \gamma_c)^{-\nu} \quad (4.4)$$

where γ is the applied shear strain, γ_c is the critical shear strain at which MWCNT rheological network is destroyed, ν is a fitted exponent that depends, only, on the dimensionality of the system, and k is a scaling factor responsible for strength of the filler network.

The G'_0 data for PP/PS/MWCNT composites with different MWCNT concentrations, subjected to deformation at 0.05 s^{-1} and 1 s^{-1} are presented in Table-A III-2 and Table-A III-3 of the Supplementary material, respectively. Linear regression analysis was used to obtain critical shear strains, represented by the equation, $\log(G'_0) = \log(\gamma - \gamma_c)$. The results of these regressions, for PP/PS/MWCNT composites with varying concentrations of 0.5 wt.%, 1 wt.%, and 2 wt.% MWCNT, deformed at 0.05 s^{-1} and 1 s^{-1} , are illustrated in Figure-A III-6(a-c) of the Supplementary material. The critical shear strain values for composites sheared at steady shear rates of 0.05 s^{-1} and 1 s^{-1} are reported in Table 4.6.

It can be seen that the critical strain at which the rheological network is destroyed increases with increasing MWCNT concentration and decreases with increasing shear rate. However, it should be noted that the critical strain values obtained indicate that the rheological network is destroyed at lower strains compared to the electrical network.

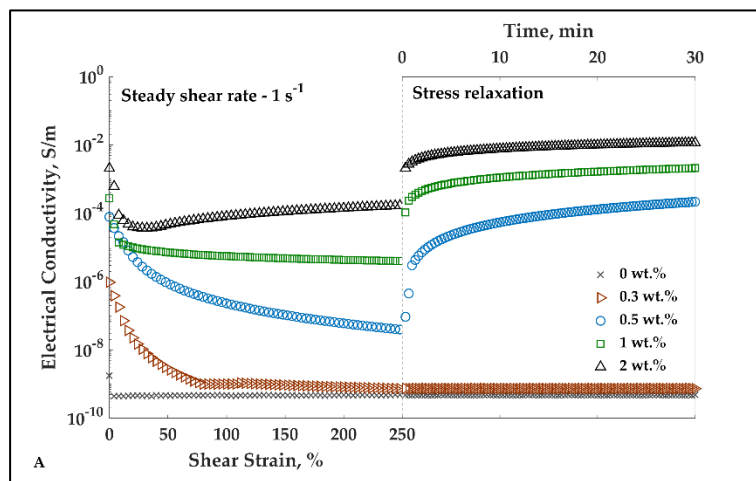
Table 4.6 Critical shear strain for composites sheared at 0.05 s^{-1} and 1 s^{-1} of steady shear rates

MWCNT, wt.%	γ_c , %	
	0.05 s^{-1}	1 s^{-1}
0.5	9	5
1	18	10
2	53	25

Figure 4.7(a) presents the electrical conductivity as a function of shear strain of PP/PS/MWCNT 50/50/x wt.% composites sheared at 1 s^{-1} , as well as a function of time during the stress relaxation step (see to Figure 4.1(b) for the deformation history). It can be seen that

for composites with MWCNT concentrations above 0.5 wt.%, the electrical conductivity increases during stress relaxation, reaching values even greater than those prior to shearing as shown in Figure 4.8.

Figure 4.7(b) shows the shear stress growth function during steady shear at $1/s$ and stress relaxation for the first 10 minutes. The results indicate that there is a significant relaxation step following the steady shear step that occurs within the first few seconds. Furthermore, the relaxation takes longer in the PP/PS/MWCNT composites filled with MWCNT compared to the neat PP/PS blend. This behavior of stress is likely due to the presence of a rigid filler network, which is building-up during the stress relaxation step and this process incorporates long time relaxation mechanisms into the system.



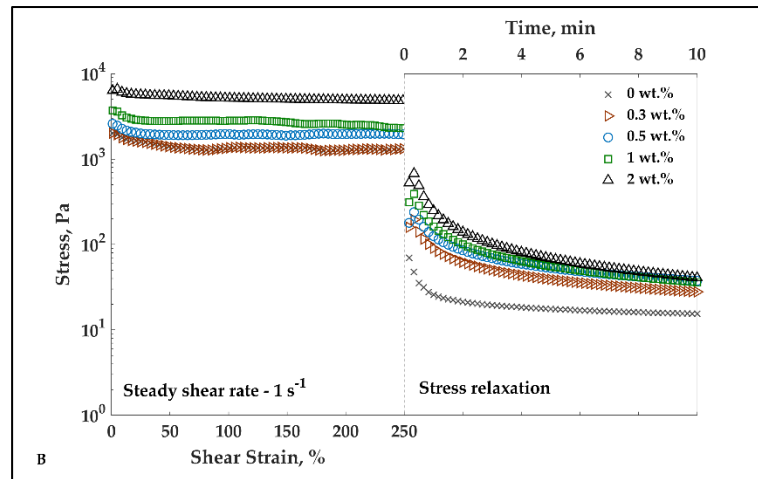


Figure 4.7 (a) Electrical conductivity vs. shear strain at a steady shear step and as a function of time at a stress relaxation step for all composites; (b) Stress vs. shear strain and time for all composites

Figure 4.8 presents the DC electrical conductivity as a function of MWCNT wt.% before any deformation, after 250% shear strain applied at steady shear rate of 1 s^{-1} , and after 250% shear strain applied at steady shear rate of 1 s^{-1} plus 30 min of stress relaxation step at an angular velocity of 0.05 rad/s . As previously mentioned, the electrical conductivity values for composites containing 0.5 wt.% or more MWCNT after deformation and stress relaxation are even greater than those prior to deformation. For PP/PS/MWCNT composite containing 2 wt.% of MWCNT, the electrical conductivity after 250 % of applied shear strain plus 30 min of stress relaxation at 0.05 rad/s is 0.015 S/m , compared to 0.002 S/m and 0.00017 S/m prior to deformation and just after 250 % of applied strain at 1 s^{-1} , respectively. This indicates that the filler network rebuilds and strengthen itself although it was partially destroyed during the deformation steps [130,131,137]. Moreover, the co-continuous morphology of the composite undergoes further refinement after the stress relaxation step, resulting in improved connections of the filler particles trapped at the interphase (the illustration of the effect of morphology coarsening during applied deformation and morphology refinement after the stress relaxation step can be seen in Figure 4.12).

Similar results on the electrical conductivity behavior were obtained by other researchers who worked with a single polymer containing MWCNT. In particular, in a study conducted by Alig et al., using polycarbonate (PC)/MWCNT composites, the electrical conductivity after steady shear decreased from 4×10^{-5} S/m to 3×10^{-8} S/m but recovered to a value of 2×10^{-2} S/m [130]. Similarly, in another investigation of the PC/MWCNT composites containing 0.75 to 1.5 wt.% MWCNT, Skipa et al. observed a decrease in electrical conductivity with increasing deformation time at an angular velocity of 0.02 rad/s for 600s. However, the electrical conductivity bounced back to its initial value after 600 s of stress relaxation step, which was equivalent to the deformation time [137].

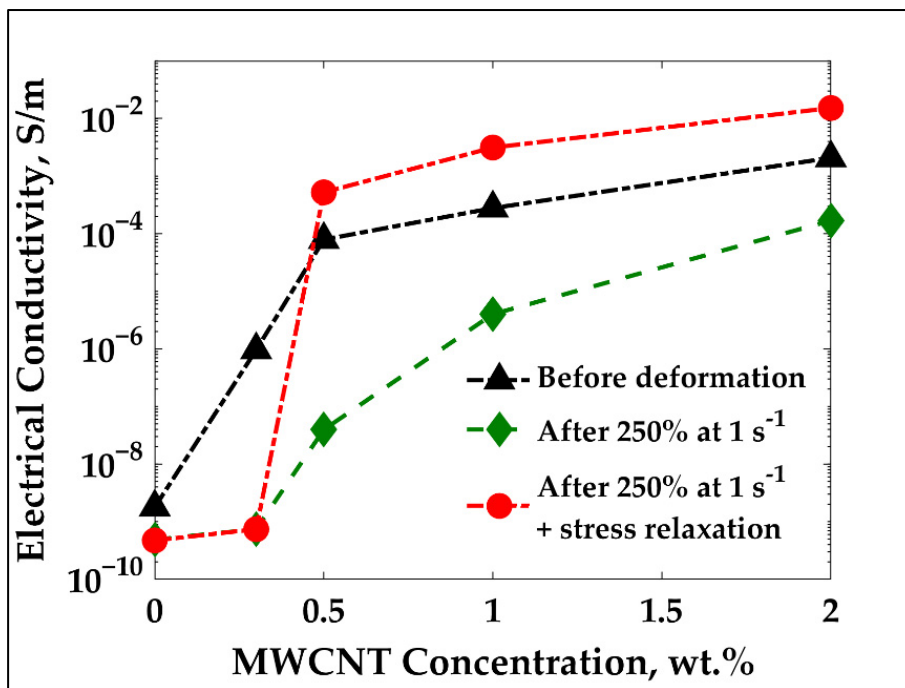


Figure 4.8 Electrical conductivity vs. MWCNT wt.% for composites before, after 250% of applied shear strain at 1 s^{-1} , and after 250% of applied shear strain at 1 s^{-1} plus 30 min of stress relaxation at 0.05 rad/s

Figure 4.9 shows a comparison of characteristic domain sizes for PP/PS/MWNT composite containing 0.5 wt.% MWCNT before deformation, after deformation following the protocol of

Figure 4.1(a), and after deformation along with 30 minutes of stress relaxation, see Figure 4.1(b). Figure 4.10 shows the morphology of the composites at the same conditions. Such analysis was performed to visualize the evolution of the morphology and electrical conductivity of the blends containing 0.5 wt.% MWCNT, as both parameters showed the most significant changes after steady shear (see Figure 4.6) and stress relaxation (see Figure 4.7(a)). The results indicate that the stress relaxation step led to a refinement of the co-continuous morphology. Specifically, the characteristic domain size decreased from 5.7 μm to 3 μm after the stress relaxation step was applied. However, it did not reach the initial value of 1.5 μm observed in the composites before deformation. Notably, as shown in Figure 4.10(c), the morphology remains continuous after the stress relaxation step.

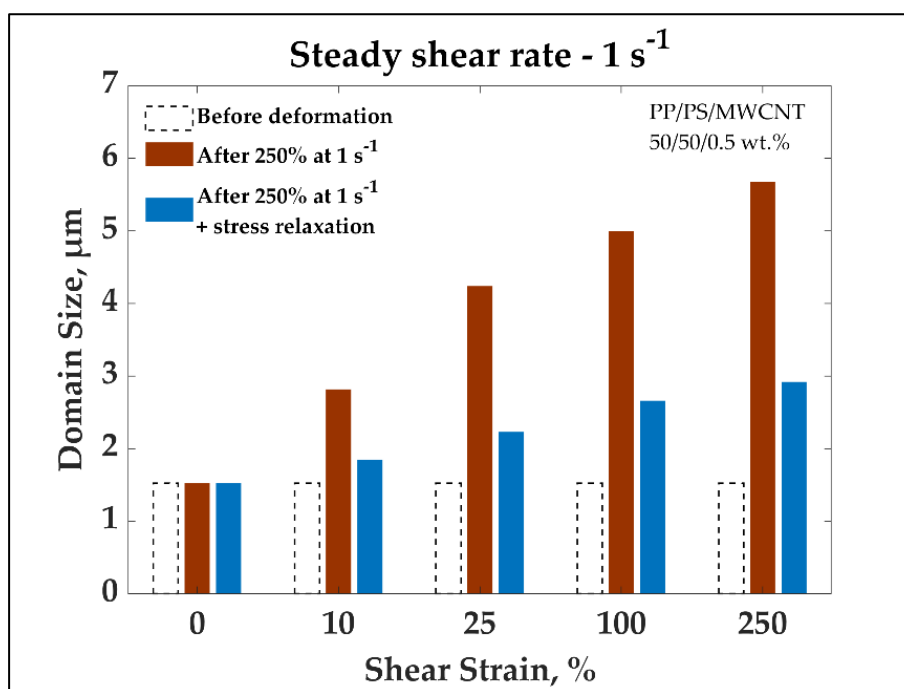


Figure 4.9 Evolution of characteristic domain size for PP/PS/MWCNT 50/50/0.5 wt.% composite before any deformation, after shear strain applied at a steady shear rate of 1 s^{-1} , and after shear strain applied at a steady shear rate of 1 s^{-1} plus stress relaxation step of 10 min

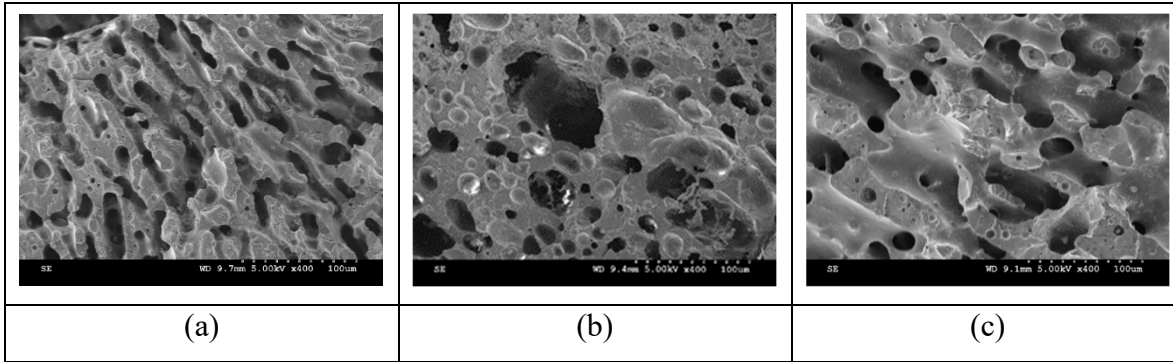


Figure 4.10 Morphology of PP/PS/MWCNT 50/50/0.5 wt.% composite: (a) before any deformation, (b) after 250% of shear strain at a shear rate of 1 s^{-1} , and (c) after 250% of shear strain at a shear rate of 1 s^{-1} + 30 min of stress relaxation step

4.4 Discussion

The experimental results found in this work indicate that the evolution of the electrical conductivity of the composites, when subjected to steady shear, depends on the carbon nanotubes concentration, as well as, the rate (steady shear rate), and amplitude (strain) of deformation. In turn, those three variables will affect 1) the blend morphology, 2) the coverage of interface by conductive nanoparticles, 3) the diffusion of conductive nanoparticles towards the interface. Indeed, the evolution of electrical conductivity during deformation and/or stress relaxation depends on both the evolution of morphology of the blend and location of the filler [11,29-31,120,133].

The maximum interface coverage (Σ), assuming that all MWCNT are at the PP/PS interface can be found as:

$$\Sigma = \frac{A_{MWCNT}}{S_V} * wt. \%PS * 100\% \quad (4.5)$$

where A_{MWCNT} is the total area of a triangular array which is created by MWCNT as shown in Figure 4.11, S_V is the specific interphase area per weight fraction of PS.

In order to determine the maximum area covered by the MWCNT within the composite we assumed that the carbon nanotubes formed a triangular array as illustrated in Figure 4.11. The total surface area of the array, denoted as A_{MWCNT} , was calculated by multiplying the area of a single triangular unit by the total number of triangular units in the array, taking into account the surface fraction of the network. By knowing the concentration of the nanotubes in the composites, as well as their length and density, it was possible to determine the number of nanotubes within a composite. This allowed us to calculate the area occupied by the nanotubes when arranged in the triangular array configuration as shown in Figure 4.11.

Table 4.7 presents the MWCNT weight concentrations, S_V , A_{MWCNT} , and Σ .

Table 4.7 Maximum surface coverage of PP/PS/MWCNT 50/50/x wt.% composite interface by MWCNT mesh

MWCNT, wt. %	S_V , m ² /g, for pure PP/PS	A_{MWCNT} , m ²	Σ , %
0.1		509	23
0.3		1528	68
0.5	112364	2547	113
1		5093	227
2		10187	453

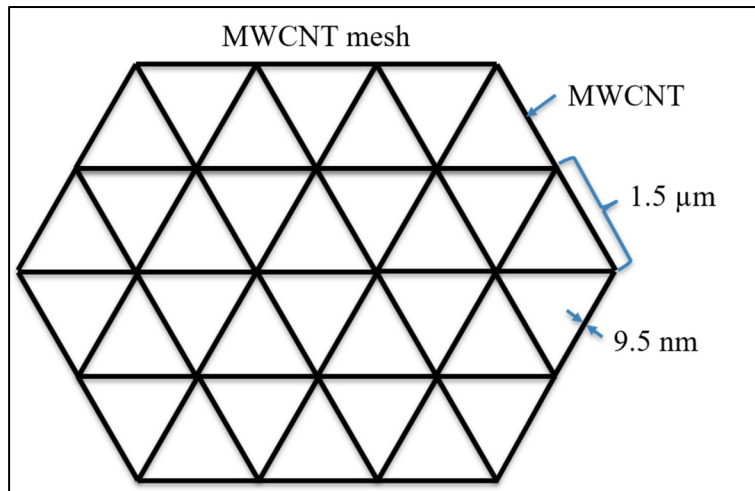


Figure 4.11 Schematic of a triangular array of MWCNT

The results presented in Table 4.7 suggest that a complete surface coverage can be reached with as little as 0.5 wt.% of MWCNT and that a surface coverage of 68% is sufficient to reach the percolation threshold concentration of 0.3 wt.% for these composites. However, it is important to note that our assumption of complete coverage by MWCNT at the interface is not a common occurrence, as it is often difficult to achieve. Nonetheless, we do believe that a complete surface coverage can be achieved with a less dense MWCNT array, as the creation of a conductive pathway through the sample volume does not necessarily require interconnections in the array once the pathway has been established.

Figure 4.12 provides a summary of the results obtained in this work. It presents a sketch of the co-continuous morphology and of the conductive filler network evolutions for composites containing three MWCNT concentrations (0, 0.5 and 2 wt.%) before and after undergoing 250% deformation (strain) under steady shear rates of 0.05 s^{-1} and 1 s^{-1} , as well as after a stress relaxation step following the strain. The corresponding electrical conductivity values are also reported. The chosen concentrations correspond to a blend without addition of MWCNT, a blend with complete coverage of the PP/PS interface by MWCNT (0.5 wt.%), as was calculated using Equation (4.5), and a blend with high MWCNT concentration (2 wt.%) in order to illustrate the effects of deformation and MWCNT concentration on morphology coarsening and electrical conductivity changes. Note that MWCNT were always present in the PP phase.

The results showed that when no MWCNT were added to the blend, the co-continuous morphology transformed into a droplet type morphology after undergoing 250% strain at both steady shear rates (0.05 s^{-1} and 1 s^{-1}), as shown in Table 4.5. When 0.5 wt.% of MWCNT were added to the blend, the morphology coarsened, and the distance between MWCNT at the PP/PS interface increased, resulting in a decrease in electrical conductivity. However, during stress relaxation, the remaining MWCNT in PP were able to migrate to the interface, leading to a recovery of the electrical conductivity to its pre-deformation values. While the morphology was able to recover, it did not return to its initial state. When 2 wt.% MWCNT were added to the blend, the morphology was stabilized by the presence of MWCNT. However, when a high shear rate (1 s^{-1}) was applied in order to deform the blend, the electrical conductivity decreased slightly, most likely due to a disruption of the electrical network. Nonetheless, during stress relaxation, the MWCNTs were once again able to migrate to the interface and contribute to an increase in electrical conductivity, as a large amount of MWCNTs remained at the interphase at all times, preventing any morphology coarsening.

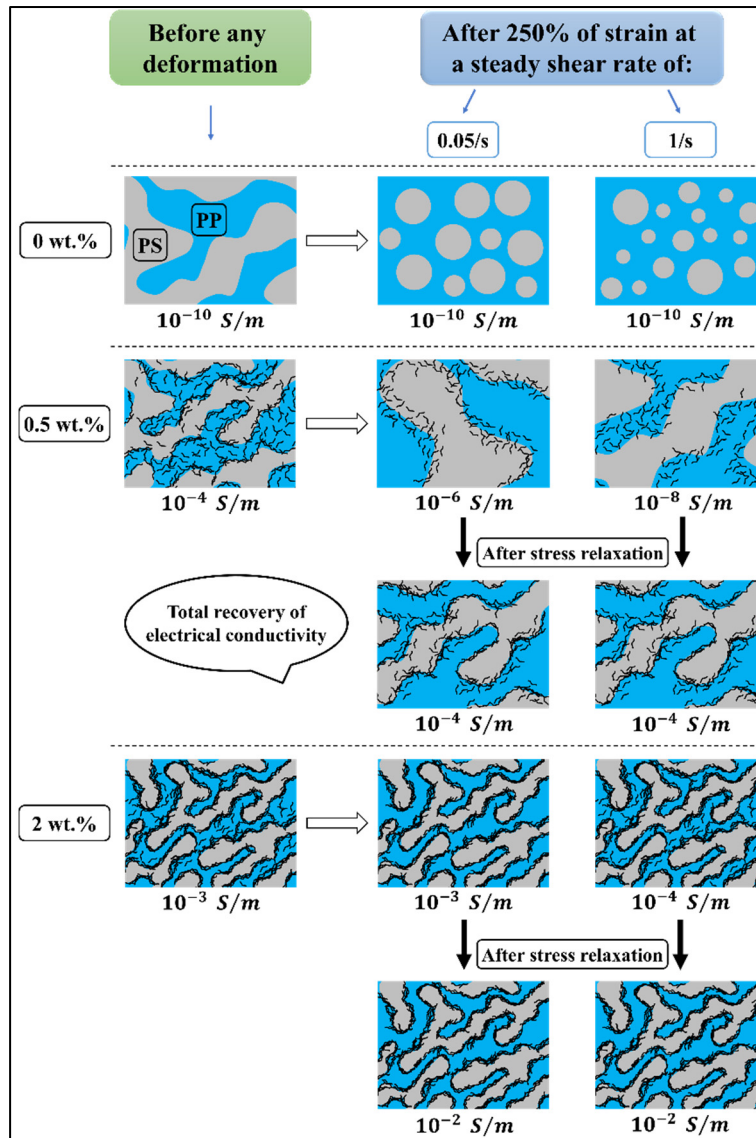


Figure 4.12 Schematic summary of the results

The results of this study are general and can be applied to a broad range of blend systems based on thermoplastic polymers that exhibit a co-continuous morphology, provided that the viscosity ratio between the components does not exceed 3. This is due to the fact that a higher viscosity ratio would hinder the droplets break-up and coalescence, and it will not be possible to mimic droplets break-up and coalescence in order to perform steady shear deformation tests which are critical for predicting morphological and electrical properties evolutions.

Moreover, the results of this study can be extended to any commonly added conductive filler.

It should be emphasized that these findings have significant industrial implications, as they offer a reliable and cost-effective way to predict and optimize the electrical conductivity of polymer composites during processing. This can be particularly relevant for the development of advanced materials for a broad range of applications, such as electromagnetic shielding, energy storage and conversion, and sensing technologies.

4.5 Conclusion

Blends consisting of two immiscible polymers and presenting a co-continuous morphology have been widely used to obtain electrically conductive polymeric materials. The morphology of such blends is characterized by a double percolation of the polymer and filler phases, which significantly reduces the concentration of electrically conductive fillers required to attain conductivity, known as the percolation threshold. However, the morphology of multiphase materials is prone to evolution during processing involving various flows at different magnitudes and speeds. These changes in morphology can lead to a negative impact on materials properties and need to be understood and ultimately controlled. In this study, the effect of steady shear deformation on the morphological and electrical properties of a model system, polypropylene/polystyrene/multiwall carbon nanotubes (PP/PS/MWCNT), which presents a double percolation morphology, was investigated.

The results obtained in this work showed that deformation results in evolutions of blend morphology (coarsening) and electrical network, leading to an increase in both the rheological and electrical percolation thresholds. These evolutions depend on three key factors: MWCNT concentration, strain, and shear rate applied on the composites. High shear rates can have a disruptive effect on composites with low MWCNT concentration, causing coarsening of the blend morphology and a drastic reduction in electrical conductivity. Once the MWCNT

concentration reaches a certain critical level, where the surface coverage is high enough, the co-continuous morphology and electrical network are stabilized. However, even if the morphology coarsens and the electrical network is disrupted, resulting in a decrease in electrical conductivity, it is possible to restore both the morphology and electrical conductivity through a stress relaxation if the MWCNT concentration is large enough. This can be achieved by promoting the diffusion of nanoparticles towards the PP/PS interface by applying thermal treatments. Nonetheless, when the MWCNT concentration is very low, it becomes impossible to recover from the disruptive effects of applied strain and shear rate. The changes in electrical conductivity and co-continuous morphology are governed by the balance between the breakup of the filler network and nanoparticles diffusion.

Acknowledgments:

Financial support from the Natural Sciences and Engineering Research Council of Canada (NSERC), PRIMA and École de technologie supérieure (ÉTS) are gratefully acknowledged. The help of Mazen Samara in reviewing the English in this paper is highly appreciated.

CONCLUSION

In this section, a summary of the main findings of this project are presented following the order of their presentation in the thesis. At the end of the section, the overall conclusion of this PhD thesis is presented.

In the first part of this project, PP/PS/MWCNT composites with MWCNT concentration ranging from 0 to 2 wt.% were studied with the aim to reach a very low percolation threshold concentration (PTC) without altering the matrix morphology. A co-continuous morphology of PP/PS matrix was used in order to reach a double percolation effect. Further, a thermal treatment based on the crystallization kinetics of PP was proposed to enhance the volume exclusion effect of PP crystals which in turn led to further reduction of PTC. It was found that:

- The PTC for PP/PS/MWCNT composites was significantly reduced from 0.6 wt.% to 0.28 wt.% when compared to that of PP/MWCNT composites due to the double percolation effect of selective filler locations in the PP continuous phase of PP/PS co-continuous matrix.
- It was possible to lower PTC to 0.06 wt.% MWCNT upon the performance of a thermal treatment of PP/PS/MWCNT composites, based on the volume exclusion effect of PP crystals, which favored the growth of a larger crystalline structure.
- The electrical conductivity values at PTC, as well as, for 1 wt.% of MWCNTs, were greater than those reported in other studies, as a result of the treatment.
- Furthermore, microscopy observations, as well as calculation of characteristic domain sizes of the co-continuous morphology of PP/PS/MWCNT composites confirmed that the proposed treatment did not alter the PP/PS morphology, in contrast to thermal annealing above the melting or softening temperature.

Additionally, in this study, we investigated the effect of fillers on the crystallization kinetics of semi-crystalline polymers in PP/MWCT and PP/PS/MWCNT composites, during the

proposed thermal treatment. We aimed to consider all factors that may affect the electrical properties of these composites during the treatment. Our findings indicate that:

- Increasing MWCNT concentration from 0 to 1 wt.% in PP/MWCNT and PP/PS/MWCNT composites raises the peak crystallization temperature (T_c) from 112 °C to 126 °C and 117 °C to 122 °C, respectively. This is attributed to MWCNTs' nucleating effect. The effect is more significant in PP/MWCNT composites, possibly because in the case of PP/PS/MWCNT composites some amount of MWCNT is located at the interface between PP and PS.
- Adding MWCNT to PP/MWCNT composites reduces the crystallization half time, indicating a MWCNT' nucleating effect as well. For PP/PS/MWCNT composites, the crystallization half time remains mostly unchanged with increased MWCNT concentration and is about twice as long as that for PP/MWCNT composites, potentially due to selective localization of MWCNT at the interface in the PP/PS matrix, weakening the nucleation effect.
- Cooling rate affects crystal sizes, as observed by polarized optical microscopy. Fast cooling produces smaller crystals that are difficult to identify, while isothermal and slow-cooling treatments yield big crystals of around 100 μm for both pure PP and PP/MWCNT composites.

In the second part of this project, an existing rheological model was modified in order to correlate the rheological behavior of PP/PS/MWCNT composites, subjected to small amplitude oscillatory shear (SAOS), with their microstructure. The modified model allows the quantification of a blend co-continuous morphology, and the establishment of a correlation between the morphological properties of PP/PS/MWCNT composites and their electrical properties. It was found that:

- The already existing model (known as the YZZ model), used to predict storage modulus and quantify the co-continuous morphology of pure polymer blends, fails to describe

the rheological behavior of filled composites at lower frequencies, due to a significant contribution of the filler network elasticity to the dynamic modulus.

- The YZZ model was modified by adding an elastic contribution to the predicted storage modulus. The modified YZZ model successfully predicted the storage moduli of PP/PS/MWCNT composites and quantified their morphology.
- The model was used to predict the evolution of morphology of PP/PS/MWCNT, which were subjected to thermal annealing. The characteristic domain size, calculated using the proposed model, exhibited a slight decrease following 30 minutes of thermal annealing, leading to a more refined co-continuous morphology.
- The electrical properties of the PP/PS/MWCNT composites which were subjected to annealing showed significant improvement. The PTC was reduced from 0.28 wt.% to 0.08 wt.% MWCNT.

Finally, the third part of this project aimed to investigate the evolution and stabilization of the rheological, morphological, and electrical properties of co-continuous PP/PS/MWCNT composites under a deformation flow at varying shear rates. In order to investigate properties evolution and their possible stabilization, all PP/PS/MWCNT composites were subjected to a SAOS – steady shear (deformation flow) – SAOS – recovery test sequence. The SAOS data were used to characterize the morphology before and after deformation. The electrical conductivity was monitored during both the deformation and recovery. It was found that:

- The effect of the applied deformation on both rheological and electrical percolation threshold concentrations is significant, leading to an increase in the percolation threshold concentrations with an increase in the applied deformation.
- The stability of the morphology and electrical network depends on three factors: MWCNT concentration, strain, and shear rate. A higher MWCNT concentration results in a more stable co-continuous morphology and filler network. However, a high shear rate can have a disruptive effect, especially for composites with low MWCNT concentration.

- Once the MWCNT concentration reaches a certain critical level, when the surface coverage is high enough, both the co-continuous morphology and electrical network become stable.
- For composites with a certain critical level of MWCNT concentration, it is possible to recover the morphology and electrical conductivity after the disruptive effects of the applied strain and shear rate are removed. This can be achieved by promoting the diffusion of nanoparticles towards the PP/PS interface.
- Below a certain MWCNT concentration, it is not possible to recover from the disruptive effects of an applied strain and shear rate.
- The changes of electrical conductivity and co-continuous morphology are governed by the balance between filler network breakup and nanoparticles diffusion.

General conclusion

In conclusion, highly conductive PP/PS/MWCNT composites with a low percolation threshold concentration were successfully developed in this project. The double percolation effect in the co-continuous PP/PS system was observed, and further reduction of PTC was achieved through thermal treatments based on both volume expulsion effect and dynamic particle diffusion – thermal annealing. The investigation of the morphological and electrical properties evolution played a crucial role in the project. The new tool/technique developed in this study facilitated the correlation between the rheological and electrical properties of filled polymer composites, paving the way for further advancements in this area of research. This represented a significant progress in the field, as a comprehensive investigation of the electrical and morphological properties of these composites during and post deformation had not been carried out previously.

RECOMMENDATIONS

Like most research work, there is always room for further development and exploration. The perspectives resulting from our work lie in the continuation of this research to deepen our understanding of the relationship between rheological, morphological, and electrical properties of composites with double percolated structures. This will help to extend the potential applications of these materials. In light of this, we propose the following recommendations for future work:

- Once a very low PTC is achieved through the use of the volume exclusion effect of polymer crystals, it is advantageous to incorporate rheological investigations into the study of these composites because SAOS tests are sufficiently sensitive to capture the elastic contribution of the filler network that was formed during crystallization. By conducting these investigations, it is possible to evaluate the stability of the filler network for further processing.
- The PP/PS blend system is a well-established model system with known rheological behavior. Additionally, the use of a filler with well-defined geometrical parameters, such as MWCNT, simplifies the task at hand. However, in order to further advance the field, it is recommended to investigate the behavior of composites with other conductive particles. Varying the viscosity ratio or polarity of the blends could also generate valuable insights into the effects of particle affinity on the evolution of rheological, morphological, and electrical properties during applied shear deformations. By exploring these parameters, a deeper understanding of the underlying mechanisms that govern the behavior of these composites can be obtained, which will facilitate the development of novel materials with tailored properties for specific applications.
- When the MWCNT concentration is increased, the plateau G' value will completely mask the contribution of the blend interface and the G' curve in the SAOS will consist

of a high frequency response dominated by the components contribution and a low frequency plateau resulting from the particle network. Hence, it is expected that the model used in the second part of the project, would become less sensitive to the morphology at high MWCNT concentrations (and thus extracting the morphological information would not be possible anymore). It is proposed to further address this question. Particularly, one way of extension model uses is to investigate the concentration at which this effect occurs for different types of nanoparticles.

- In the proposed model, the effect of filler network elasticity on the rheological behavior of filled composites with co-continuous morphology was assumed to be frequency-independent due to the fact that the presence of a filler network essentially affects the rheological behavior at low frequencies where frequency dependent G' of the whole system has constant plateau values. However, considering that all other contributions are frequency-dependent, it would be interesting to develop a more comprehensive model that takes into account the frequency-dependent contribution of filler network elasticity. This would allow for the development of more precise and effective models for predicting and optimizing the rheological properties of filled composites with co-continuous morphology. Furthermore, it can solve the problem explained in the above statement.
- During processing, polymer blends are subjected to large deformation, which could result in changes to their morphology and electrical properties. Therefore, it is crucial to investigate the effect of processing on these properties. It is recommended to study the effect of extensional flow in addition to shear flow on the morphological and electrical properties of these blends.

ANNEX I

SUPPORTING ELECTRONIC INFORMATION FOR ARTICLE 1

Ultra-Low Percolation Threshold Induced by Thermal Treatments in Co-Continuous Blend-Based PP/PS/MWCNTs Nanocomposites

Daria Strugova, José Carlos Ferreira Junior, Éric David and Nicole R. Demarquette *

Mechanical Engineering Department, École de Technologie Supérieure, Montréal, Québec H3C 1K3, Canada;

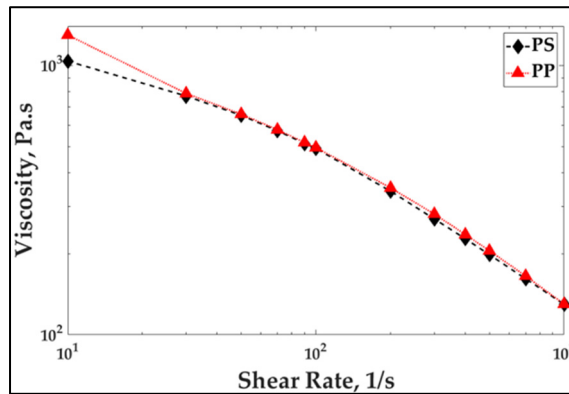


Figure-A I-1 Viscosity as a function of shear rate measured by capillary rheometer for pure PP and PS

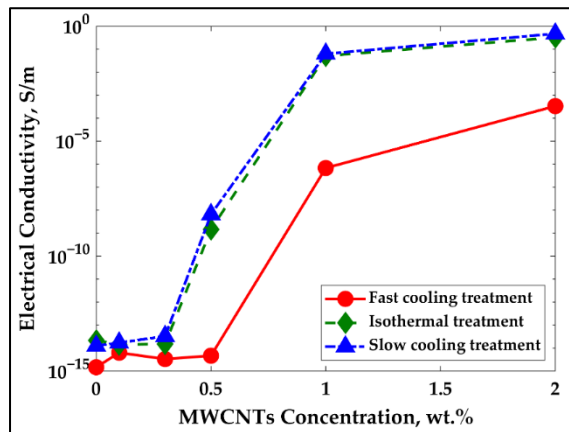


Figure-A I-2 Effect of treatments on electrical conductivity as a function of MWCNTs concentration for PP/MWCNTs composites

Table-A I-1 Percolation threshold and fitting values of experimental data according to the Equation (2.6) for PP/MWCNTs composites after each treatment

Parameters	Fast cooling treatment	Isothermal treatment	Slow cooling treatment
P_c, wt.%	0.6	0.44	0.38
k, S/m	6.5×10^{-5}	0.15	0.17
t	4.9	1.8	2.1
R²	1	0.95	0.93

Table-A I-2 Melting and crystallization temperatures, onset and end of crystallization and degree of crystallinity for PP/MWCNTs and PP/PS/MWCNTs nanocomposites

Material	CNTs, wt.%	Peak of T _m , °C	Peak of T _c , °C	Onset T _c , °C	End T _c , °C	X _c , %
PP/CNTs	0	166 ± 0.2	112 ± 0.1	117 ± 0.2	107 ± 1.2	47 ± 0.09
	0.1	165 ± 0.2	121 ± 0.1	126 ± 0.2	118 ± 0.1	48 ± 0.08
	0.3	166 ± 0.3	124 ± 0.2	128 ± 0.1	120 ± 0.2	47 ± 0.1
	0.5	167 ± 0.9	126 ± 0.2	130 ± 0.1	121 ± 1.2	49 ± 1.8
PP/PS/CNTs	0	166 ± 0.5	117 ± 0.1	122 ± 0.1	113 ± 0.1	52 ± 1.4
	0.1	165 ± 1.3	119 ± 0.2	123 ± 0.1	114 ± 0.4	51 ± 0.2
	0.3	167 ± 0.3	121 ± 0.2	126 ± 0.5	116 ± 0.1	48 ± 0.8
	0.5	168 ± 0.2	122 ± 0.2	127 ± 0.4	117 ± 0.1	52 ± 0.6

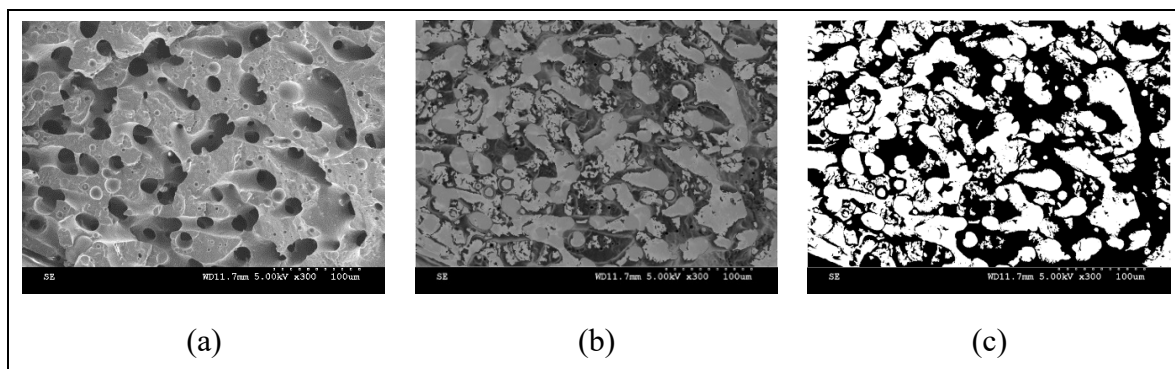


Figure-A I-3 Image treatment analysis for distinguishing between two phases: (a) original SEM picture for PP/PS/MWCNTs composite with 0.3 wt.% of MWCNTs; (b) image phase separation; (c) final treated image which was used for the estimation of L_{int} - interface length between two phases, which in this case is the perimeter of white phase

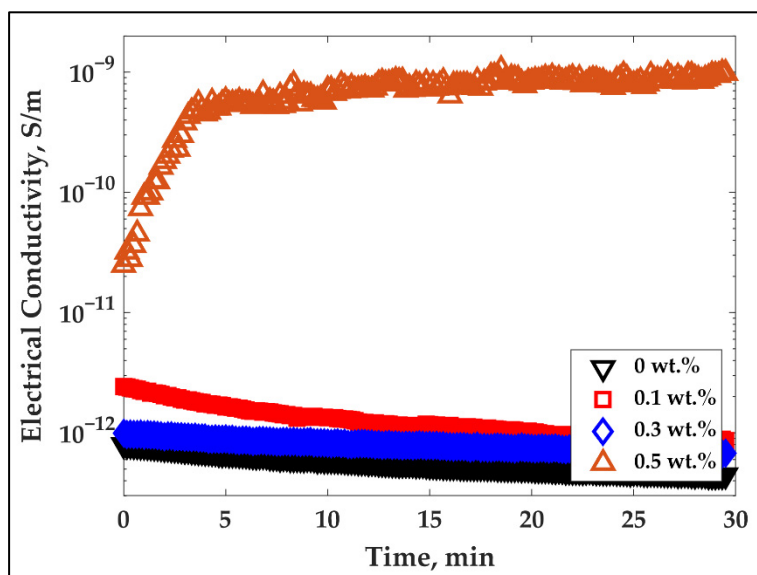


Figure-A I-4 Electrical conductivity as a function of time for PP/MWCNTs composite with 0-0.3 wt.% of MWCNTs measured every 10 s at 1 Hz of frequency and 135 °C

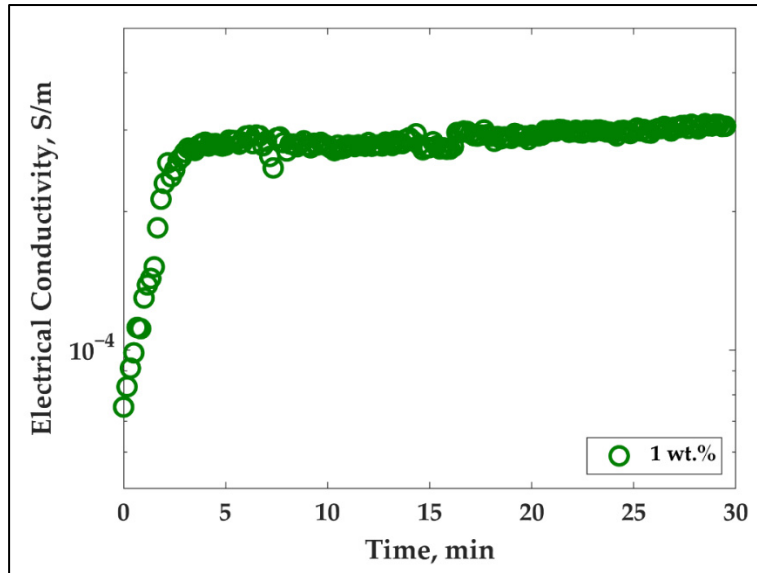


Figure-A I-5 Electrical conductivity as a function of time for PP/MWCNTs composite with 1 wt.% of MWCNTs measured every 10 s at 1 Hz of frequency and 135 °C

ANNEX II

SUPPORTING ELECTRONIC INFORMATION FOR ARTICLE 2

Linear viscoelasticity of PP/PS/MWCNT composites with co-continuous morphology

Daria Strugova, Éric David and Nicole R. Demarquette *

Mechanical Engineering Department, École de Technologie Supérieure, Montréal, Québec
H3C 1K3, Canada;

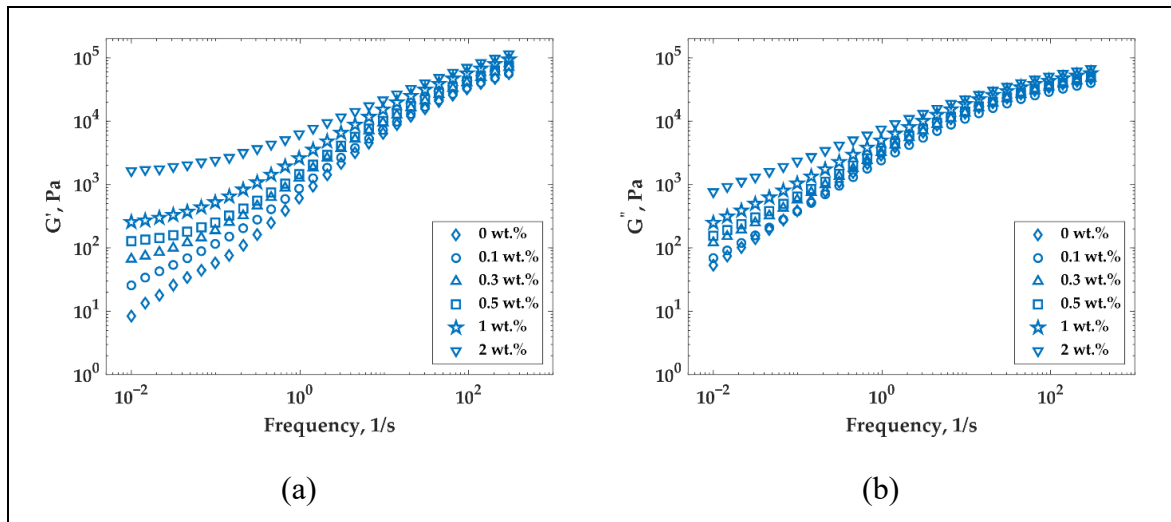


Figure-A II-1 (a) G' and (b) G'' as a function of frequency for PP/PS/MWCNT composites with different concentrations of MWCNT at 200 °C

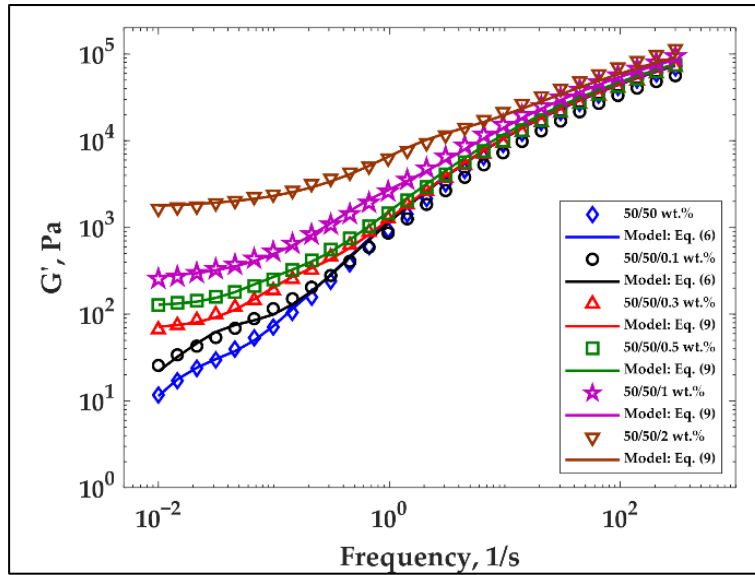


Figure-A II-2 Experimental G' as a function of frequency and its prediction by the YZZ model and the modified YZZ model for PP/PS/MWCNT composites with different concentrations of MWCNT at 200 °C

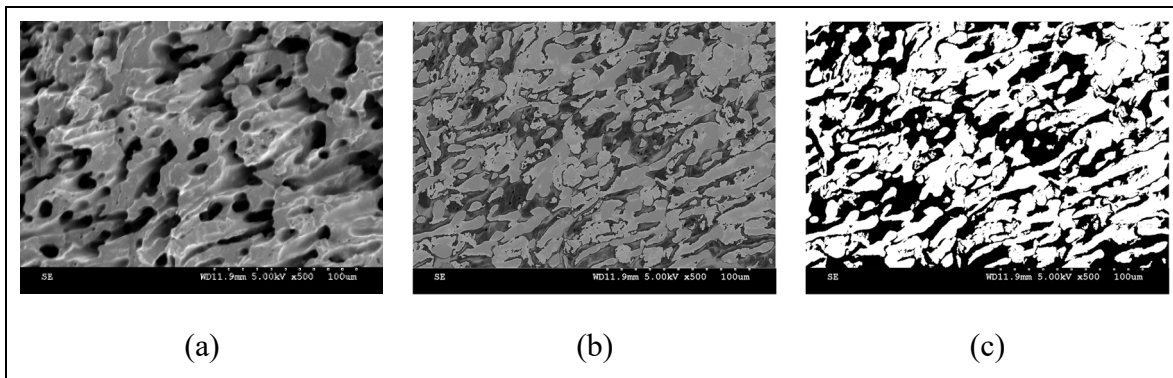


Figure-A II-3 Image treatment analysis for distinguishing between two phases: (a) original SEM picture for PP/PS/MWCNT composite with 1 wt.% of MWCNT; (b) image phase separation; (c) final treated image which was used for the estimation of L_{int} – interface length between two phases, which in this case is the perimeter of white phase

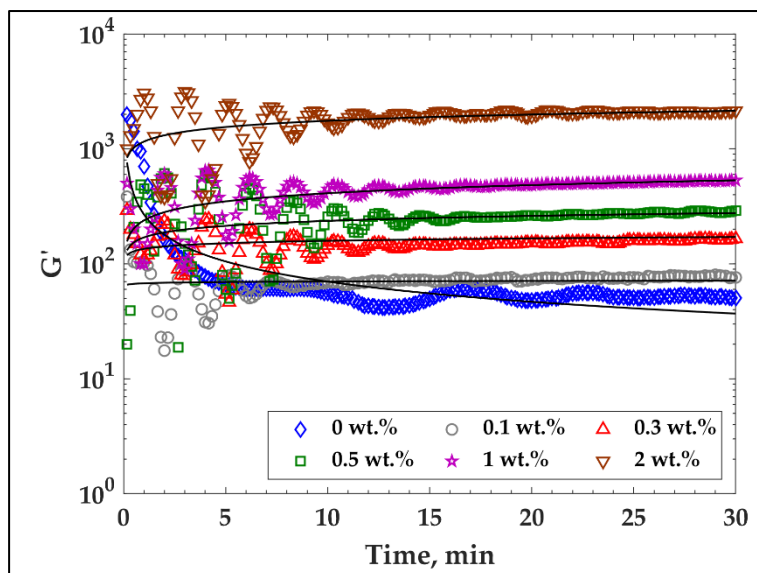


Figure-A II-4 Time-dependent evolution of storage modulus at 200 °C for PP/PS/MWCNT composites with different MWCNT concentration. Solid lines are power-law fits

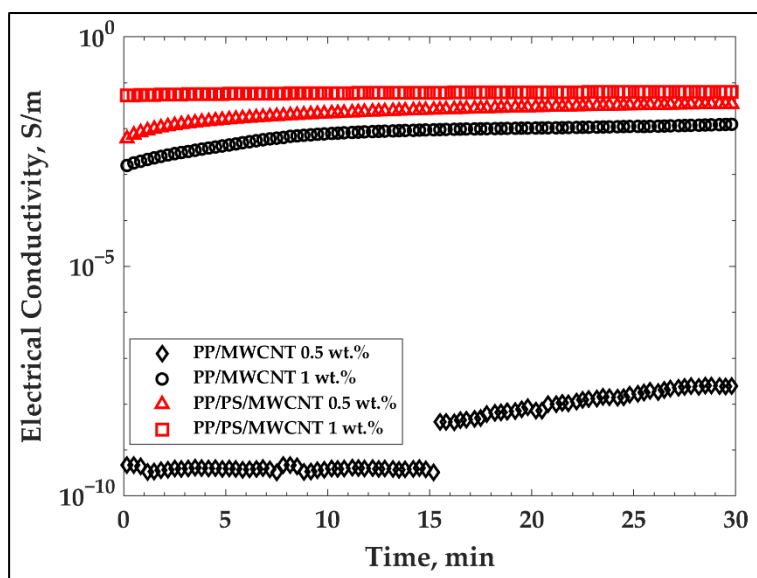


Figure-A II-5 Electrical conductivity as a function of time for PP/PS/MWCNT and PP/MWCNT composites with 0.5 wt.% and 1wt.% of MWCNT measured at 20 Hz of frequency and 200 °C

ANNEX III

SUPPORTING ELECTRONIC INFORMATION FOR ARTICLE 3

Effect of steady shear deformation electrically conductive PP/PS/MWCNT composites

Daria Strugova, Éric David and Nicole R. Demarquette *

Mechanical Engineering Department, École de Technologie Supérieure, Montréal, Québec
H3C 1K3, Canada;

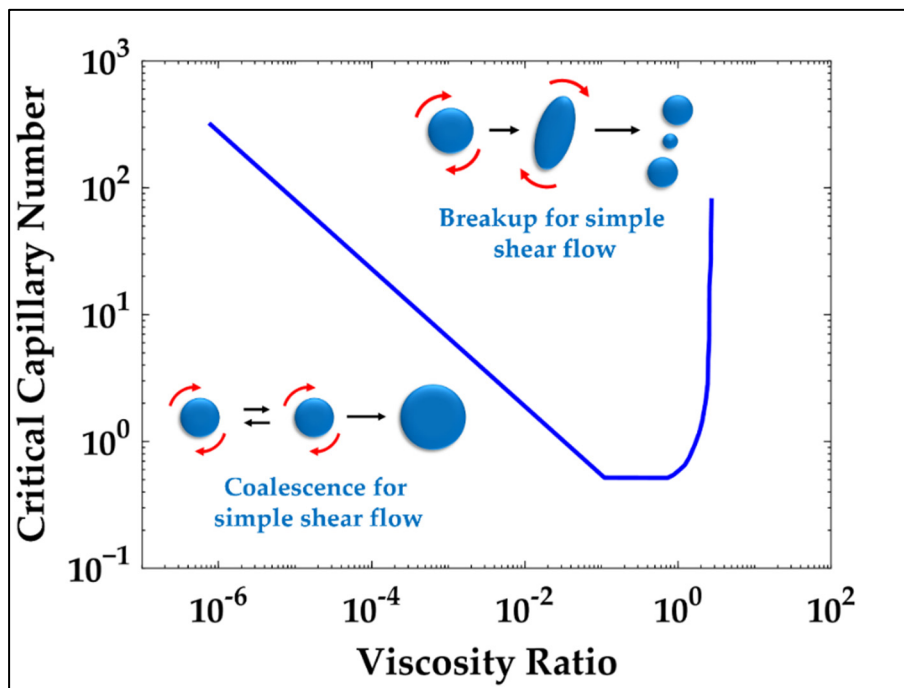


Figure-A III-1 Ca_c vs. $p = \frac{\eta_d}{\eta_m}$ in a rotational shear

(adapted from Grace [110])

Table-A III-1 shows the DSST, time sweep, and SAOS test parameters.

Table-A III-1 Tests parameters

Parameters Tests	Angular frequency, rad/s	Strain, %	Time, h	Temperature, °C
DSST	100	0.01 – 10	-	200
	10			
Time sweep	1	0.3	6	200
	0.05			
SAOS	0.01-300 s ⁻¹	0.3	-	

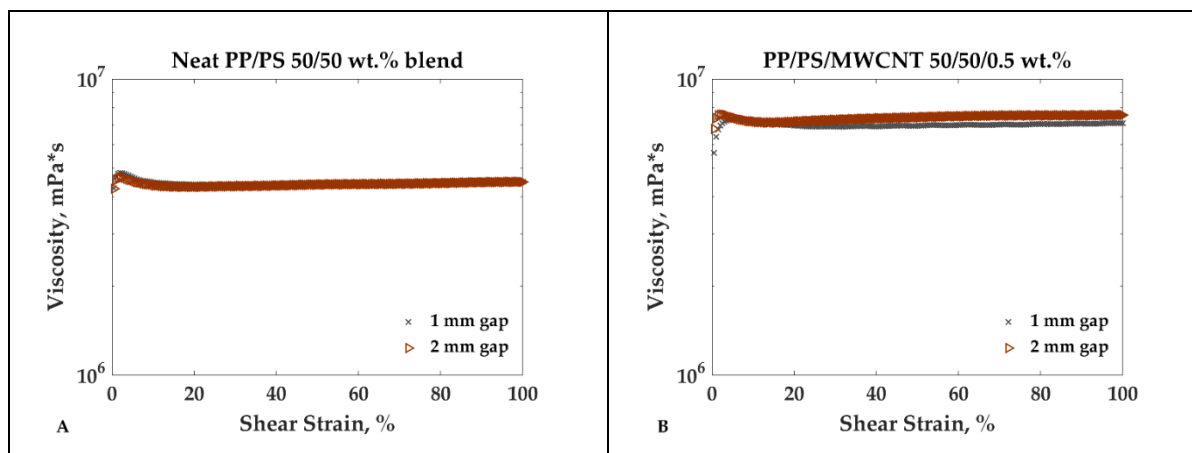


Figure-A III-2 Viscosity of: (a) pure blend and (b) filled with 0.5 wt.% of MWCNT. It was measured at a constant shear rate of 0.05 s⁻¹ for 2000s (100% of shear strain) for two plate-plate gaps: 1 mm and 2 mm

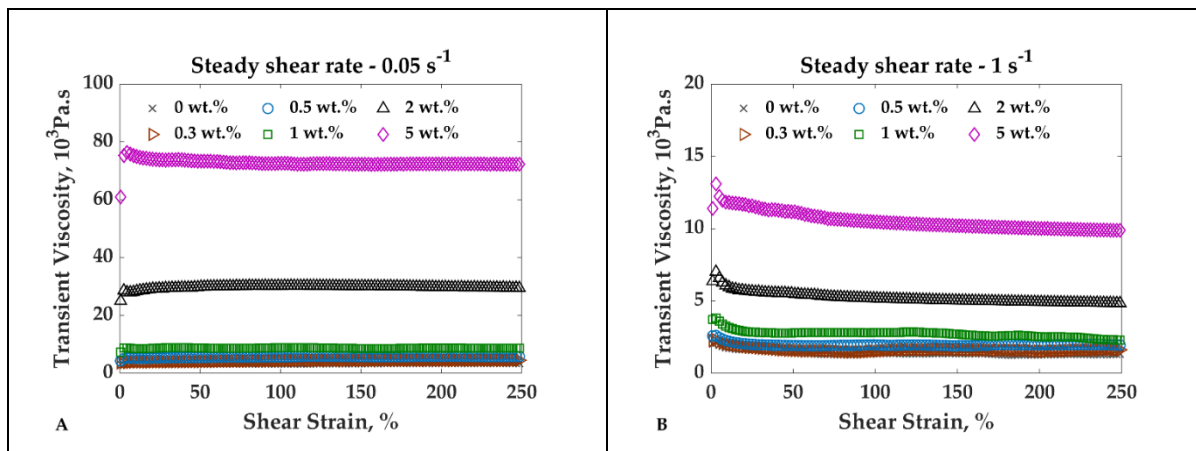


Figure-A III-3 Transient shear viscosity vs. applied shear strain for PP/PS/MWCNTs 50/50/x wt.% composites at 200 °C at: (a) steady shear rate of 0.05 s⁻¹; (b) steady shear rate of 1 s⁻¹

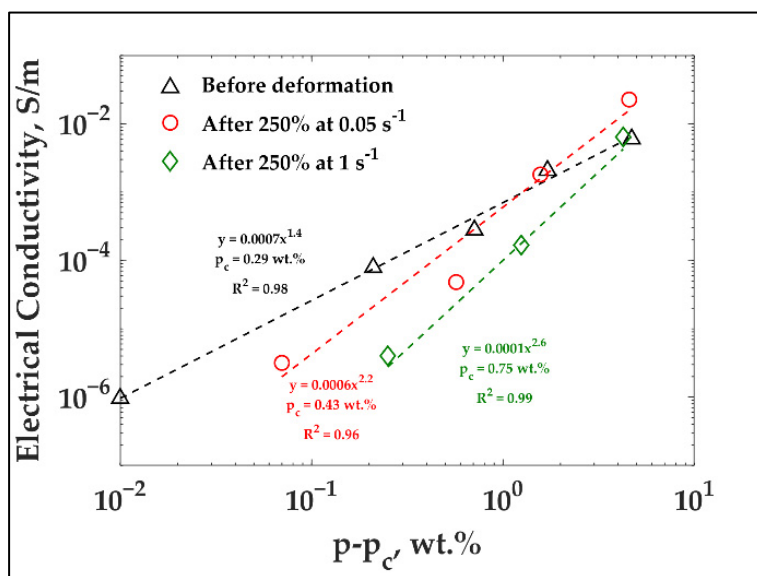


Figure-A III-4 Electrical conductivity versus reduced filler content

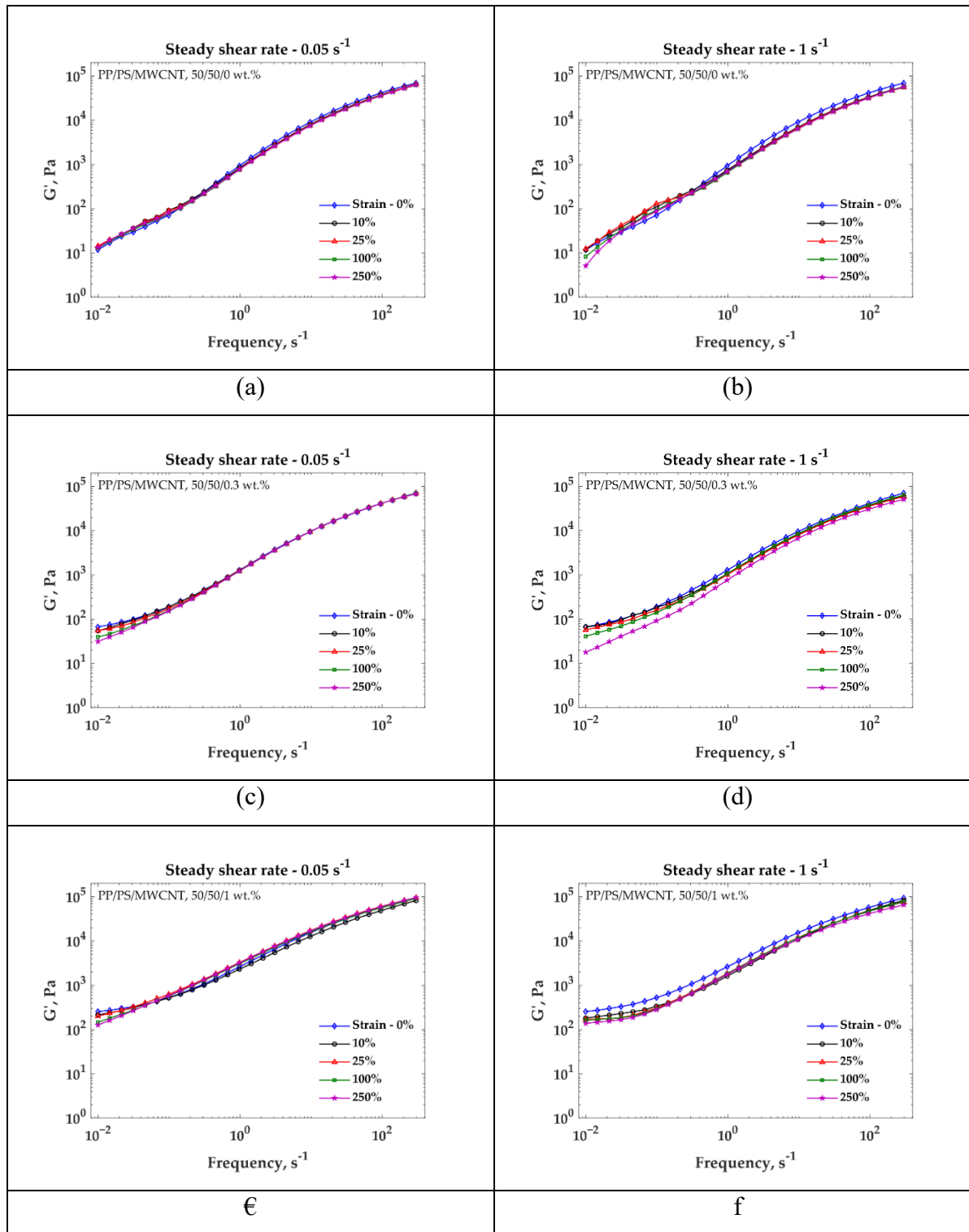


Figure-A III-5 Storage modulus as a function of frequency for PP/PS/MWCNT composites with 0 wt.%, 0.3 wt.%, and 1 wt.% of MWCNT after shear strain applied at a steady shear rate of: (a-e) 0.05 s^{-1} , and (b-f) 1 s^{-1}

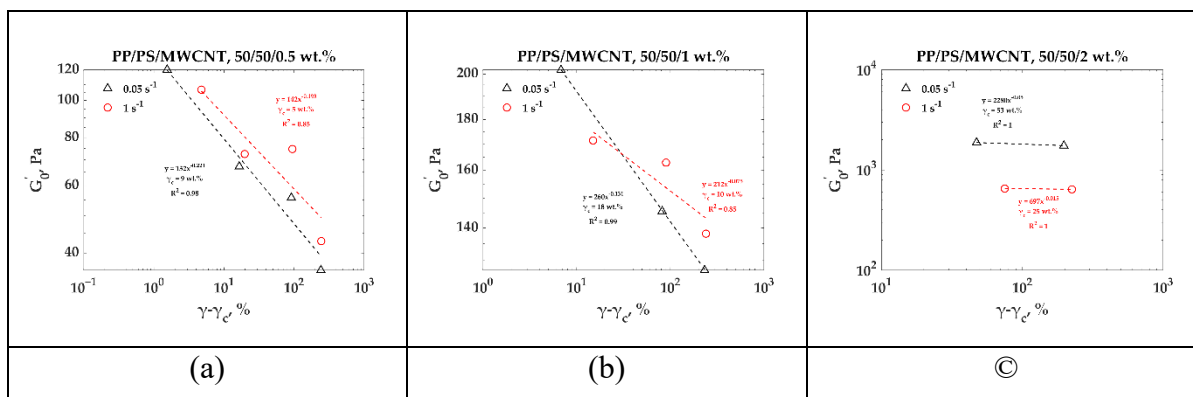


Figure-A III-6 Network elasticity as a function of reduced shear strain related to PP/PS/MWCNT composites (solid signs) and power-law fitting to the experimental data (solid lines) for composites, deformed at 0.05 s^{-1} and 1 s^{-1} for composites containing: (a) 0.5 wt.% MWCNT, (b) 1 wt.% MWCNT, (c) 2 wt.% MWCNT

Table-A III-2 Fitting parameter G'_0 of Equation (4.1) for PP/PS/MWCNT composites with varying concentrations of 0.5 wt.%, 1 wt.%, and 2 wt.% of MWCNT, deformed at 0.05 s^{-1}

Strain (γ), %	G'_0 , Pa		
	0.5 wt.%	1 wt.%	2 wt.%
0	128	256	1650
10	120	216	2168
25	67	202	2099
100	56	146	1878
250	36	127	1748

Table-A III-3 Fitting parameter G'_0 of Equation (4.1) for PP/PS/MWCNT composites with varying concentrations of 0.5 wt.%, 1 wt.%, and 2 wt.% of MWCNT, deformed at 1 s^{-1}

Strain (γ), %	G'_0 , Pa		
	0.5 wt.%	1 wt.%	2 wt.%
0	128	256	1650
10	107	182	947
25	73	172	734
100	75	163	652
250	43	138	641

APPENDIX

VITA

EDUCATION

- *Doctor of Philosophy* – École de Technologie Supérieure (ÉTS). Supervisor: Prof. Nicole R. Demarquette, Co-supervisor: Prof. Eric David. From September 2017 to May 2023. Montréal, QC – Canada.
- *Master of Science in Materials Science and Technologies of Materials* – National University of Science and Technology "MISIS" (NUST MISIS). Supervisor: Prof. Vladislav Y. Zadorozhnyy. From September 2013 to June 2015. Moscow – Russia.
- *Specialist degree in Medical Physics* – Orenburg State University (OSU). Supervisor: Prof. Tatiana M. Chmereva. From September 2012 to June 2013. Orenburg – Russia.
- *Bachelor of Science in Medical Physics* – Orenburg State University (OSU). From September 2008 to June 2012. Orenburg – Russia.

AWARDS AND SCHOLARSHIPS

- Bourse Substance de diffusion de la recherche award – École de Technologie Supérieure (ÉTS), Montréal, Canada, 2023.
- Mitacs Accelerate research project – École de Technologie Supérieure (ÉTS) and VPM Research Inc., Montréal, Canada, 2022-2023.
- Circular Economy Seed Funding – École de Technologie Supérieure (ÉTS), Montréal, Canada, 2022.
- Conference travel award – Society of Plastics Engineers (SPE), Montréal, Canada, 2022.
- Conference travel award – École de Technologie Supérieure (ÉTS), Montréal, Canada, 2022.

- Conference travel award – Society of Plastics Engineers (SPE), Montréal, Canada, 2022.
- Full ride scholarship and excellence Ph.D. award for international students. École de Technologie Supérieure (ÉTS), Montréal, Canada, 2017-2022.
- State grant of the Government of the Russian Federation for graduate students, Moscow, Russia, 2016-2017.
- Grant for young scientists. Participant of youth scientifically-innovative competition «Y.M.N.I.K» (the winner), Moscow, Russia, 2014-2015.
- State grant of the Government of the Russian Federation for graduate students, Moscow, Russia, 2013-2015.

JOURNAL PUBLICATIONS

- Strugova, D., David, E., and Demarquette N., Effect of steady shear deformation electrically conductive PP/PS/MWCNT composites. *Journal of Rheology* (submitted, under review).
- Strugova, D., David, E., and Demarquette N., Linear viscoelasticity of PP/PS/MWCNT composites with co-continuous morphology. *Journal of Rheology* 2022, 66(4), 671-681.
- Strugova, D.; Ferreira Junior, J.C.; David, É.; Demarquette, N.R. Ultra-Low Percolation Threshold Induced by Thermal Treatments in Co-Continuous Blend-Based PP/PS/MWCNTs Nanocomposites. *Nanomaterials-Basel* 2021, 11, 1620.
- Strugova, D.; Zadorozhnyy, M.Y.; Berdonosova, E.; Yablokova, M.Y.; Konik, P.; Zheleznyi, M.; Semenov, D.; Milovzorov, G.; Padaki, M.; Kaloshkin, S. Novel process for preparation of metal-polymer composite membranes for hydrogen separation. *International Journal of Hydrogen Energy* 2018, 43, 12146-12152.
- Zadorozhnyy, V.Y.; Shelekhov, E.; Milovzorov, G.; Strugova, D.; Zinnurova, L.K. Analysis of the background temperature during the mechanical alloying of metal

powders in the planetary ball mill. *Inorganic Materials: Applied Research* 2018, 9, 559-565.

- Zadorozhnyy, V.Y.; Milovzorov, G.; Klyamkin, S.; Zadorozhnyy, M.Y.; Strugova, D.; Gorshenkov, M.; Kaloshkin, S. Preparation and hydrogen storage properties of nanocrystalline TiFe synthesized by mechanical alloying. *Progress in Natural Science: Materials International* 2017, 27, 149-155.
- Zadorozhnyy, V.Y.; Klyamkin, S.; Zadorozhnyy, M.Y.; Strugova, D.; Milovzorov, G.; Louzguine-Luzgin, D.; Kaloshkin, S. Effect of mechanical activation on compactibility of metal hydride materials. *Journal of Alloys and Compounds* 2017, 707, 214-219.
- Zadorozhnyy, M.Y.; Klyamkin, S.; Strugova, D.; Olifirov, L.; Milovzorov, G.; Kaloshkin, S.; Zadorozhnyy, V.Y. Deposition of polymer coating on metallic powder through ball milling: application to hydrogen storage intermetallics. *International Journal of Energy Research* 2016, 40, 273-279.

CONFERENCE PRESENTATIONS

- D. Strugova, E. David, and N.R. Demarquette, Linear viscoelasticity of PP/PS/MWCNTs composites: co-continuous morphology evolution and filler network stability investigation / IX BRAZILIAN CONFERENCE ON RHEOLOGY (BCR 2022). São Paulo, Brazil. – December 2022. (Talk)
- D. Strugova, E. David, and N.R. Demarquette, Linear viscoelastic properties and electrical conductivity evolution of PP/PS/CNT composites during steady shear / The 93rd Annual Meeting of The Society of Rheology (SOR93). Chicago, Illinois, USA. – October 2022. (Talk)
- D. Strugova, E. David, and N.R. Demarquette, Linear viscoelasticity of PP/PS/MWCNTs composites: investigating of co-continuous morphology evolution and filler network stability during steady shear / Annual European Rheology Conference (AERC 2022). Seville, Spain. – April 2022. (Talk)

- D. Strugova, E. David, and N.R. Demarquette, Use of Tailored Blend Morphologies to Obtain Electrically Conductive Composites / The 92nd Annual Meeting of The Society of Rheology (SOR92). Bangor, Maine, USA. – October 2021. (Talk)
- D. Strugova, J.C. Ferreira Junior, E. David, and N.R. Demarquette, Reduction of the Percolation Threshold in CNTs/Polymer Composites Using Thermal Treatments / 36th International Conference of the Polymer Processing Society (PPS36). Montréal, Quebec, Canada. – September 2021. (Talk)
- D. Strugova, E. David, and N.R. Demarquette, Use of tailored blend morphologies to obtain composites for electromagnetic interference shielding / COLLOQUE ÉTUDIANT CREPEC. Amphithéâtre Bernard-Lamarre, Polytechnique Montréal, Canada. – June 2019. (Poster)
- D. Strugova et al., Novel process for preparation of metal-polymer composite membranes for hydrogen separation / 22nd World Hydrogen Energy Conference (WHEC 2018). Rio de Janeiro, Brazil. – June 2018. (Talk)

LIST OF BIBLIOGRAPHICAL REFERENCES

1. Shi, Y.; He, L.; Chen, D.; Wang, Q.; Shen, J.; Guo, S. Simultaneously improved electromagnetic interference shielding and flame retarding properties of poly (butylene succinate)/thermoplastic polyurethane blends by constructing segregated flame retardants and multi-walled carbon nanotubes double network. *Composites Part A: Applied Science and Manufacturing* **2020**, *137*, 106037.
2. Chen, J.; Liao, X.; Li, S.; Wang, W.; Guo, F.; Li, G. A promising strategy for efficient electromagnetic interference shielding by designing a porous double-percolated structure in MWCNT/polymer-based composites. *Composites Part A: Applied Science and Manufacturing* **2020**, *138*, 106059.
3. Liu, T.; Huang, R.; Qi, X.; Dong, P.; Fu, Q. Facile preparation of rapidly electro-active shape memory thermoplastic polyurethane/polylactide blends via phase morphology control and incorporation of conductive fillers. *Polymer* **2017**, *114*, 28-35.
4. Yang, Y.; Feng, C.; Zhou, Y.; Zha, X.; Bao, R.; Ke, K.; Yang, M.; Tan, C.; Yang, W. Achieving improved electromagnetic interference shielding performance and balanced mechanical properties in polyketone nanocomposites via a composite MWCNTs carrier. *Composites Part A: Applied Science and Manufacturing* **2020**, *136*, 105967.
5. Ellingford, C.; Smith, H.; Yan, X.; Bowen, C.; Figiel, Ł.; McNally, T.; Wan, C. Electrical dual-percolation in MWCNTs/SBS/PVDF based thermoplastic elastomer (TPE) composites and the effect of mechanical stretching. *Eur Polym J* **2019**, *112*, 504-514.
6. Bizhani, H.; Nayyeri, V.; Katbab, A.; Jalali-Arani, A.; Nazockdast, H. Double percolated MWCNTs loaded PC/SAN nanocomposites as an absorbing electromagnetic shield. *Eur Polym J* **2018**, *100*, 209-218.
7. Soares, B.G.; Calheiros, L.F.; Silva, A.A.; Indrusiak, T.; Barra, G.M.; Livi, S. Conducting melt blending of polystyrene and EVA copolymer with carbon nanotube assisted by phosphonium-based ionic liquid. *J Appl Polym Sci* **2018**, *135*, 45564.
8. Soares, B.G.; Cordeiro, E.; Maia, J.; Pereira, E.C.; Silva, A.A. The effect of the noncovalent functionalization of CNT by ionic liquid on electrical conductivity and electromagnetic interference shielding effectiveness of semi-biodegradable polypropylene/poly (lactic acid) composites. *Polym Composite* **2020**, *41*, 82-93.
9. Kar, G.P.; Biswas, S.; Rohini, R.; Bose, S. Tailoring the dispersion of multiwall carbon nanotubes in co-continuous PVDF/ABS blends to design materials with enhanced electromagnetic interference shielding. *J Mater Chem A* **2015**, *3*, 7974-7985.

10. Kuester, S.; Demarquette, N.R.; Ferreira Jr, J.C.; Soares, B.G.; Barra, G.M. Hybrid nanocomposites of thermoplastic elastomer and carbon nanoadditives for electromagnetic shielding. *Eur Polym J* **2017**, *88*, 328-339.
11. Kurusu, R.S.; Helal, E.; Moghimian, N.; David, E.; Demarquette, N. The role of selectively located commercial graphene nanoplatelets in the electrical properties, morphology, and stability of EVA/LLDPE blends. *Macromolecular Materials and Engineering* **2018**, *303*, 1800187.
12. Lin, Y.; Liu, S.; Chen, S.; Wei, Y.; Dong, X.; Liu, L. A highly stretchable and sensitive strain sensor based on graphene–elastomer composites with a novel double-interconnected network. *J Mater Chem C* **2016**, *4*, 6345-6352.
13. Zhang, Q.; Zhang, B.-Y.; Guo, Z.-X.; Yu, J. Comparison between the efficiencies of two conductive networks formed in carbon black-filled ternary polymer blends by different hierarchical structures. *Polym Test* **2017**, *63*, 141-149.
14. Sun, X.-R.; Gong, T.; Pu, J.-H.; Bao, R.-Y.; Xie, B.-H.; Yang, M.-B.; Yang, W. Effect of phase coarsening under melt annealing on the electrical performance of polymer composites with a double percolation structure. *Phys Chem Chem Phys* **2018**, *20*, 137-147.
15. Soares, B.G.; Touchaleaume, F.; Calheiros, L.F.; Barra, G.M. Effect of double percolation on the electrical properties and electromagnetic interference shielding effectiveness of carbon-black-loaded polystyrene/ethylene vinyl acetate copolymer blends. *J Appl Polym Sci* **2016**, *133*.
16. Scherzer, S.L.; Pavlova, E.; Esper, J.D.; Starý, Z. Phase structure, rheology and electrical conductivity of co-continuous polystyrene/polymethylmethacrylate blends filled with carbon black. *Compos Sci Technol* **2015**, *119*, 138-147.
17. Qi, X.; Xiu, H.; Wei, Y.; Zhou, Y.; Guo, Y.; Huang, R.; Bai, H.; Fu, Q. Enhanced shape memory property of polylactide/thermoplastic poly (ether) urethane composites via carbon black self-networking induced co-continuous structure. *Compos Sci Technol* **2017**, *139*, 8-16.
18. Pan, Y.; Liu, X.; Hao, X.; Starý, Z.; Schubert, D.W. Enhancing the electrical conductivity of carbon black-filled immiscible polymer blends by tuning the morphology. *Eur Polym J* **2016**, *78*, 106-115.
19. Luo, Y.; Xiong, S.Y.; Zhang, F.; He, X.X.; Lu, X.; Peng, R.T. Preparation of conductive polylactic acid/high density polyethylene/carbon black composites with low percolation threshold by locating the carbon black at the Interface of co-continuous blends. *J Appl Polym Sci* **2021**, *138*, 50291.

20. Gong, T.; Peng, S.-P.; Bao, R.-Y.; Yang, W.; Xie, B.-H.; Yang, M.-B. Low percolation threshold and balanced electrical and mechanical performances in polypropylene/carbon black composites with a continuous segregated structure. *Composites Part B: Engineering* **2016**, *99*, 348-357.
21. Gao, C.; Zhang, S.; Lin, Y.; Li, F.; Guan, S.; Jiang, Z. High-performance conductive materials based on the selective location of carbon black in poly (ether ether ketone)/polyimide matrix. *Composites Part B: Engineering* **2015**, *79*, 124-131.
22. Chen, J.; Cui, X.; Sui, K.; Zhu, Y.; Jiang, W. Balance the electrical properties and mechanical properties of carbon black filled immiscible polymer blends with a double percolation structure. *Compos Sci Technol* **2017**, *140*, 99-105.
23. Calberg, C.; Blacher, S.; Gubbels, F.; Brouers, F.; Deltour, R.; Jérôme, R. Electrical and dielectric properties of carbon black filled co-continuous two-phase polymer blends. *Journal of Physics D: Applied Physics* **1999**, *32*, 1517.
24. Bose, S.; Bhattacharyya, A.R.; Kulkarni, A.R.; Pötschke, P. Electrical, rheological and morphological studies in co-continuous blends of polyamide 6 and acrylonitrile-butadiene-styrene with multiwall carbon nanotubes prepared by melt blending. *Compos Sci Technol* **2009**, *69*, 365-372.
25. Chen, J.; Cui, X.; Zhu, Y.; Jiang, W.; Sui, K. Design of superior conductive polymer composite with precisely controlling carbon nanotubes at the interface of a co-continuous polymer blend via a balance of π - π interactions and dipole-dipole interactions. *Carbon* **2017**, *114*, 441-448, doi:<https://doi.org/10.1016/j.carbon.2016.12.048>.
26. Otero-Navas, I.; Arjmand, M.; Sundararaj, U. Carbon nanotube induced double percolation in polymer blends: Morphology, rheology and broadband dielectric properties. *Polymer* **2017**, *114*, 122-134, doi:<https://doi.org/10.1016/j.polymer.2017.02.082>.
27. Roman, C.; García-Morales, M.; Gupta, J.; McNally, T. On the phase affinity of multi-walled carbon nanotubes in PMMA: LDPE immiscible polymer blends. *Polymer* **2017**, *118*, 1-11.
28. Soares da Silva, J.P.; Soares, B.G.; Silva, A.A.; Livi, S. Double Percolation of Melt-Mixed PS/PBAT Blends Loaded With Carbon Nanotube: Effect of Molding Temperature and the Non-covalent Functionalization of the Filler by Ionic Liquid. *Frontiers in Materials* **2019**, *6*, 191.
29. Bai, L.; He, S.; Fruehwirth, J.W.; Stein, A.; Macosko, C.W.; Cheng, X. Localizing graphene at the interface of cocontinuous polymer blends: Morphology, rheology, and conductivity of cocontinuous conductive polymer composites. *J Rheol* **2017**, *61*, 575-587.

30. Bai, L.; Sharma, R.; Cheng, X.; Macosko, C.W. Kinetic control of graphene localization in co-continuous polymer blends via melt compounding. *Langmuir* **2018**, *34*, 1073-1083.
31. Helal, E.; Kurusu, R.S.; Moghimian, N.; Gutierrez, G.; David, E.; Demarquette, N.R. Correlation between morphology, rheological behavior, and electrical behavior of conductive cocontinuous LLDPE/EVA blends containing commercial graphene nanoplatelets. *J Rheol* **2019**, *63*, 961-976.
32. Lan, Y.; Liu, H.; Cao, X.; Zhao, S.; Dai, K.; Yan, X.; Zheng, G.; Liu, C.; Shen, C.; Guo, Z. Electrically conductive thermoplastic polyurethane/polypropylene nanocomposites with selectively distributed graphene. *Polymer* **2016**, *97*, 11-19.
33. Mao, C.; Zhu, Y.; Jiang, W. Design of electrical conductive composites: tuning the morphology to improve the electrical properties of graphene filled immiscible polymer blends. *Acs Appl Mater Inter* **2012**, *4*, 5281-5286.
34. Rafeie, O.; Razavi Aghjeh, M.; Tavakoli, A.; Salami Kalajahi, M.; Jameie Oskooie, A. Conductive poly (vinylidene fluoride)/polyethylene/graphene blend-nanocomposites: Relationship between rheology, morphology, and electrical conductivity. *J Appl Polym Sci* **2018**, *135*, 46333.
35. Mun, S.C.; Kim, M.J.; Cobos, M.; Gu, L.; Macosko, C.W. Strategies for interfacial localization of graphene/polyethylene-based cocontinuous blends for electrical percolation. *AIChE Journal* **2019**, *65*, e16579.
36. Sadeghi, A.; Moeini, R.; Yeganeh, J.K. Highly conductive PP/PET polymer blends with high electromagnetic interference shielding performances in the presence of thermally reduced graphene nanosheets prepared through melt compounding. *Polym Composite* **2019**, *40*, E1461-E1469.
37. Shen, Y.; Zhang, T.T.; Yang, J.H.; Zhang, N.; Huang, T.; Wang, Y. Selective localization of reduced graphene oxides at the interface of PLA/EVA blend and its resultant electrical resistivity. *Polym Composite* **2017**, *38*, 1982-1991.
38. Zhang, H.; Chen, J.; Cui, X.; Hu, Y.; Lei, L.; Zhu, Y.; Jiang, W. Thermal annealing induced enhancement of electrical properties of a co-continuous polymer blend filled with carbon nanotubes. *Compos Sci Technol* **2018**, *167*, 522-528.
39. Liu, Z.; Bai, H.; Luo, Y.; Zhang, Q.; Fu, Q. Achieving a low electrical percolation threshold and superior mechanical performance in poly (L-lactide)/thermoplastic polyurethane/carbon nanotubes composites via tailoring phase morphology with the aid of stereocomplex crystallites. *Rsc Adv* **2017**, *7*, 11076-11084.

40. Nasti, G.; Gentile, G.; Cerruti, P.; Carfagna, C.; Ambrogi, V. Double percolation of multiwalled carbon nanotubes in polystyrene/polylactic acid blends. *Polymer* **2016**, *99*, 193-203.
41. Zhao, X.; Zhao, J.; Cao, J.-P.; Wang, D.; Hu, G.-H.; Chen, F.; Dang, Z.-M. Effect of the selective localization of carbon nanotubes in polystyrene/poly (vinylidene fluoride) blends on their dielectric, thermal, and mechanical properties. *Materials & Design (1980-2015)* **2014**, *56*, 807-815.
42. Huang, J.; Mao, C.; Zhu, Y.; Jiang, W.; Yang, X. Control of carbon nanotubes at the interface of a co-continuous immiscible polymer blend to fabricate conductive composites with ultralow percolation thresholds. *Carbon* **2014**, *73*, 267-274.
43. Chen, J.; Lu, H.-y.; Yang, J.-h.; Wang, Y.; Zheng, X.-t.; Zhang, C.-l.; Yuan, G.-p. Effect of organoclay on morphology and electrical conductivity of PC/PVDF/CNT blend composites. *Compos Sci Technol* **2014**, *94*, 30-38.
44. Chen, J.; Hou, Y.B.; Zhang, M.L.; Liu, D.; Yang, J.H.; Wang, Y.; Zhou, Z.W.; Yuan, G.P. Combined effect of compatibilizer and carbon nanotubes on the morphology and electrical conductivity of PP/PS blend. *Polym Advan Technol* **2014**, *25*, 624-630.
45. Shi, Y.-y.; Yang, J.-h.; Huang, T.; Zhang, N.; Chen, C.; Wang, Y. Selective localization of carbon nanotubes at the interface of poly (L-lactide)/ethylene-co-vinyl acetate resulting in lowered electrical resistivity. *Composites Part B: Engineering* **2013**, *55*, 463-469.
46. Maiti, S.; Suin, S.; Shrivastava, N.K.; Khatua, B. Low percolation threshold in melt-blended PC/MWCNT nanocomposites in the presence of styrene acrylonitrile (SAN) copolymer: preparation and characterizations. *Synthetic Met* **2013**, *165*, 40-50.
47. Chen, J.; Shen, Y.; Yang, J.-h.; Zhang, N.; Huang, T.; Wang, Y.; Zhou, Z.-w. Trapping carbon nanotubes at the interface of a polymer blend through adding graphene oxide: a facile strategy to reduce electrical resistivity. *J Mater Chem C* **2013**, *1*, 7808-7811.
48. Chen, J.; Du, X.-C.; Zhang, W.-B.; Yang, J.-H.; Zhang, N.; Huang, T.; Wang, Y. Synergistic effect of carbon nanotubes and carbon black on electrical conductivity of PA6/ABS blend. *Compos Sci Technol* **2013**, *81*, 1-8.
49. Cardinaud, R.; McNally, T. Localization of MWCNTs in PET/LDPE blends. *Eur Polym J* **2013**, *49*, 1287-1297.

50. Yuan, J.-K.; Yao, S.-H.; Sylvestre, A.; Bai, J. Biphasic polymer blends containing carbon nanotubes: heterogeneous nanotube distribution and its influence on the dielectric properties. *The Journal of Physical Chemistry C* **2012**, *116*, 2051-2058.
51. Hwang, T.Y.; Yoo, Y.; Lee, J.W. Electrical conductivity, phase behavior, and rheology of polypropylene/polystyrene blends with multi-walled carbon nanotube. *Rheol Acta* **2012**, *51*, 623-636.
52. Xu, Z.; Zhang, Y.; Wang, Z.; Sun, N.; Li, H. Enhancement of electrical conductivity by changing phase morphology for composites consisting of polylactide and poly (ϵ -caprolactone) filled with acid-oxidized multiwalled carbon nanotubes. *Acs Appl Mater Inter* **2011**, *3*, 4858-4864.
53. Su, C.; Xu, L.; Zhang, C.; Zhu, J. Selective location and conductive network formation of multiwalled carbon nanotubes in polycarbonate/poly (vinylidene fluoride) blends. *Compos Sci Technol* **2011**, *71*, 1016-1021.
54. Gültner, M.; Göldel, A.; Pötschke, P. Tuning the localization of functionalized MWCNTs in SAN/PC blends by a reactive component. *Compos Sci Technol* **2011**, *72*, 41-48.
55. Göldel, A.; Kasaliwal, G.; Pötschke, P. Selective localization and migration of multiwalled carbon nanotubes in blends of polycarbonate and poly (styrene-acrylonitrile). *Macromol Rapid Comm* **2009**, *30*, 423-429.
56. Pötschke, P.; Kretzschmar, B.; Janke, A. Use of carbon nanotube filled polycarbonate in blends with montmorillonite filled polypropylene. *Compos Sci Technol* **2007**, *67*, 855-860.
57. Pötschke, P.; Bhattacharyya, A.R.; Janke, A. Carbon nanotube-filled polycarbonate composites produced by melt mixing and their use in blends with polyethylene. *Carbon* **2004**, *42*, 965-969.
58. Meincke, O.; Kaempfer, D.; Weickmann, H.; Friedrich, C.; Vathauer, M.; Warth, H. Mechanical properties and electrical conductivity of carbon-nanotube filled polyamide-6 and its blends with acrylonitrile/butadiene/styrene. *Polymer* **2004**, *45*, 739-748.
59. Palierno, J. Linear rheology of viscoelastic emulsions with interfacial tension. *Rheol Acta* **1990**, *29*, 204-214.
60. Gramespacher, H.; Meissner, J. Interfacial tension between polymer melts measured by shear oscillations of their blends. *J Rheol* **1992**, *36*, 1127-1141.
61. Bousmina, M. Effect of interfacial tension on linear viscoelastic behavior of immiscible polymer blends. *Rheol Acta* **1999**, *38*, 251-254.

62. Souza, A.M.C.d.; Calvao, P.S.; Demarquette, N.R. Linear viscoelastic behavior of compatibilized PMMA/PP blends. *J Appl Polym Sci* **2013**, *129*, 1280-1289.
63. Genoyer, J.; Demarquette, N.R.; Soulestin, J. Effect of clay particles size and location on coalescence in PMMA/PS blends. *J Rheol* **2019**, *63*, 883-893.
64. Zare, Y.; Rhee, K.Y. A power model to predict the electrical conductivity of CNT reinforced nanocomposites by considering interphase, networks and tunneling condition. *Composites Part B: Engineering* **2018**, *155*, 11-18, doi:<https://doi.org/10.1016/j.compositesb.2018.08.028>.
65. Irin, F.; Das, S.; Atore, F.O.; Green, M.J. Ultralow percolation threshold in aerogel and cryogel templated composites. *Langmuir* **2013**, *29*, 11449-11456.
66. Murphy, R.; Nicolosi, V.; Hernandez, Y.; McCarthy, D.; Rickard, D.; Vrbancic, D.; Mrzel, A.; Mihailovic, D.; Blau, W.J.; Coleman, J.N. Observation of extremely low percolation threshold in MoS₂/5I4. 5 nanowire/polymer composites. *Scripta materialia* **2006**, *54*, 417-420.
67. Jouni, M.; Faure-Vincent, J.; Fedorko, P.; Djurado, D.; Boiteux, G.; Massardier, V. Charge carrier transport and low electrical percolation threshold in multiwalled carbon nanotube polymer nanocomposites. *Carbon* **2014**, *76*, 10-18.
68. Chen, Y.; Yang, Q.; Huang, Y.; Liao, X.; Niu, Y. Influence of phase coarsening and filler agglomeration on electrical and rheological properties of MWNTs-filled PP/PMMA composites under annealing. *Polymer* **2015**, *79*, 159-170.
69. Bruggeman, V.D. Berechnung verschiedener physikalischer Konstanten von heterogenen Substanzen. I. Dielektrizitätskonstanten und Leitfähigkeiten der Mischkörper aus isotropen Substanzen. *Annalen der physik* **1935**, *416*, 636-664.
70. Böttcher, C. The dielectric constant of crystalline powders. *Recueil des Travaux Chimiques des Pays-Bas* **1945**, *64*, 47-51.
71. Gödel, A.; Kasaliwal, G.R.; Pötschke, P.; Heinrich, G. The kinetics of CNT transfer between immiscible blend phases during melt mixing. *Polymer* **2012**, *53*, 411-421.
72. Bharati, A.; Cardinaels, R.; Seo, J.W.; Wübberhorst, M.; Moldenaers, P. Enhancing the conductivity of carbon nanotube filled blends by tuning their phase separated morphology with a copolymer. *Polymer* **2015**, *79*, 271-282.
73. Fang, D.; Zhou, C.; Liu, G.; Luo, G.; Gong, P.; Yang, Q.; Niu, Y.; Li, G. Effects of ionic liquids and thermal annealing on the rheological behavior and electrical properties of poly (methyl methacrylate)/carbon nanotubes composites. *Polymer* **2018**, *148*, 68-78.

74. Palza, H.; Garzón, C.; Arias, O. Modifying the electrical behaviour of polypropylene/carbon nanotube composites by adding a second nanoparticle and by annealing processes. *Express Polym. Lett* **2012**, *6*, 639-646.
75. Quan, H.; Zhang, S.-j.; Qiao, J.-l.; Zhang, L.-y. The electrical properties and crystallization of stereocomplex poly (lactic acid) filled with carbon nanotubes. *Polymer* **2012**, *53*, 4547-4552.
76. Li, J.; Peng, W.-J.; Tan, Y.-J.; Weng, Y.-X.; Wang, M. Adjusting Distribution of Multiwall Carbon Nanotubes in Poly (L-lactide)/Poly (oxymethylene) Blends via Constructing Stereocomplex Crystallites: Toward Conductive and Microwave Shielding Enhancement. *The Journal of Physical Chemistry C* **2019**, *123*, 27884-27895.
77. Liu, Z.; Ling, F.; Diao, X.; Fu, M.; Bai, H.; Zhang, Q.; Fu, Q. Stereocomplex-type polylactide with remarkably enhanced melt-processability and electrical performance via incorporating multifunctional carbon black. *Polymer* **2020**, *188*, 122136.
78. Zhang, D.; Lin, Y.; Wu, G. Polylactide-based nanocomposites with stereocomplex networks enhanced by GO-g-PDLA. *Compos Sci Technol* **2017**, *138*, 57-67.
79. Zhang, K.; Yu, H.-O.; Shi, Y.-D.; Chen, Y.-F.; Zeng, J.-B.; Guo, J.; Wang, B.; Guo, Z.; Wang, M. Morphological regulation improved electrical conductivity and electromagnetic interference shielding in poly (L-lactide)/poly (ϵ -caprolactone)/carbon nanotube nanocomposites via constructing stereocomplex crystallites. *J Mater Chem C* **2017**, *5*, 2807-2817.
80. Wang, J.; Kazemi, Y.; Wang, S.; Hamidinejad, M.; Mahmud, M.B.; Pötschke, P.; Park, C.B. Enhancing the electrical conductivity of PP/CNT nanocomposites through crystal-induced volume exclusion effect with a slow cooling rate. *Composites Part B: Engineering* **2020**, *183*, 107663.
81. Kazemi, Y.; Kakroodi, A.R.; Wang, S.; Ameli, A.; Filleter, T.; Pötschke, P.; Park, C.B. Conductive network formation and destruction in polypropylene/carbon nanotube composites via crystal control using supercritical carbon dioxide. *Polymer* **2017**, *129*, 179-188.
82. Huang, C.; Bai, H.; Xiu, H.; Zhang, Q.; Fu, Q. Matrix crystallization induced simultaneous enhancement of electrical conductivity and mechanical performance in poly (l-lactide)/multiwalled carbon nanotubes (PLLA/MWCNTs) nanocomposites. *Compos Sci Technol* **2014**, *102*, 20-27.

83. Harrats, C.; Thomas, S.; Groeninckx, G. *Micro- and nanostructured multiphase polymer blend systems : phase morphology and interfaces*; CRC/Taylor & Francis: Boca Raton, 2006; p. 442 p.
84. Miles, I.S.; Zurek, A. Preparation, structure, and properties of two-phase co-continuous polymer blends. *Polymer Engineering & Science* **1988**, *28*, 796-805.
85. Jordhamo, G.; Manson, J.; Sperling, L. Phase continuity and inversion in polymer blends and simultaneous interpenetrating networks. *Polymer Engineering & Science* **1986**, *26*, 517-524.
86. Wu, S. Calculation of interfacial tension in polymer systems. In Proceedings of the Journal of Polymer Science Part C: Polymer Symposia, 1971; pp. 19-30.
87. Wu, S. Interfacial and surface tensions of polymers. *Journal of Macromolecular Science—Reviews in Macromolecular Chemistry* **1974**, *10*, 1-73.
88. Charfeddine, I.; Majesté, J.; Carrot, C.; Lhost, O. A model for the prediction of the morphology of immiscible blends of polymers. *Polymer* **2020**, *193*, 122334.
89. Yu, W.; Zhou, W.; Zhou, C. Linear viscoelasticity of polymer blends with co-continuous morphology. *Polymer* **2010**, *51*, 2091-2098.
90. Sengers, W.; Sengupta, P.; Noordermeer, J.W.; Picken, S.; Gotsis, A. Linear viscoelastic properties of olefinic thermoplastic elastomer blends: melt state properties. *Polymer* **2004**, *45*, 8881-8891.
91. Vinckier, I.; Laun, H. Assessment of the Doi–Ohta theory for co-continuous blends under oscillatory flow. *J Rheol* **2001**, *45*, 1373-1385.
92. Coran, A.; Patel, R. Predicting elastic moduli of heterogeneous polymer compositions. *J Appl Polym Sci* **1976**, *20*, 3005-3016.
93. Huang, C.; Yu, W. Role of block copolymer on the coarsening of morphology in polymer blend: effect of micelles. *AIChE Journal* **2015**, *61*, 285-295.
94. Kou, Y.; Cote, A.T.; Liu, J.; Cheng, X.; Macosko, C.W. Robust networks of interfacial localized graphene in cocontinuous polymer blends. *J Rheol* **2021**, *65*, 1139-1153.
95. Veenstra, H.; Verkooijen, P.C.; van Lent, B.J.; van Dam, J.; de Boer, A.P.; Nijhof, A.P.H. On the mechanical properties of co-continuous polymer blends: experimental and modelling. *Polymer* **2000**, *41*, 1817-1826.

96. Filippone, G.; Romeo, G.; Acierno, D. Viscoelasticity and structure of polystyrene/fumed silica nanocomposites: filler network and hydrodynamic contributions. *Langmuir* **2010**, *26*, 2714-2720.
97. Filippone, G.; Salzano de Luna, M. A unifying approach for the linear viscoelasticity of polymer nanocomposites. *Macromolecules* **2012**, *45*, 8853-8860.
98. Genoyer, J.; Soulestin, J.; Demarquette, N.R. Influence of the molar masses on compatibilization mechanism induced by two block copolymers in PMMA/PS blends. *J Rheol* **2018**, *62*, 681-693.
99. Vermant, J.; Cioccolo, G.; Nair, K.G.; Moldenaers, P. Coalescence suppression in model immiscible polymer blends by nano-sized colloidal particles. *Rheol Acta* **2004**, *43*, 529-538.
100. Kong, M.; Huang, Y.; Lv, Y.; Wang, S.; Yang, Q.; Li, G. Flow-induced morphological instability in nanosilica-filled polyamide 6/polystyrene blends. *Polymer* **2014**, *55*, 4348-4357.
101. Zhang, Y.; Wu, D.; Zhang, M.; Zhou, W.; Xu, C. Effect of steady shear on the morphology of biodegradable poly (ϵ -caprolactone)/polylactide blend. *Polymer Engineering & Science* **2009**, *49*, 2293-2300.
102. Bose, S.; Ozdilek, C.; Leys, J.; Seo, J.W.; Wübberhorst, M.; Vermant, J.; Moldenaers, P. Phase separation as a tool to control dispersion of multiwall carbon nanotubes in polymeric blends. *Acs Appl Mater Inter* **2010**, *2*, 800-807.
103. Martin, J.D.; Velankar, S.S. Effects of compatibilizer on immiscible polymer blends near phase inversion. *J Rheol* **2007**, *51*, 669-692.
104. Nofar, M.; Heuzey, M.; Carreau, P.; Kamal, M.; Randall, J. Coalescence in PLA-PBAT blends under shear flow: Effects of blend preparation and PLA molecular weight. *J Rheol* **2016**, *60*, 637-648.
105. Thareja, P.; Moritz, K.; Velankar, S.S. Interfacially active particles in droplet/matrix blends of model immiscible homopolymers: Particles can increase or decrease drop size. *Rheol Acta* **2010**, *49*, 285-298.
106. Moghimi, E.; Goharpey, F.; Foudazi, R. Role of droplet bridging on the stability of particle-containing immiscible polymer blends. *Rheol Acta* **2014**, *53*, 165-180.
107. Zou, Z.-M.; Sun, Z.-Y.; An, L.-J. Effect of fumed silica nanoparticles on the morphology and rheology of immiscible polymer blends. *Rheol Acta* **2014**, *53*, 43-53.

108. Vandebriel, S.; Vermant, J.; Moldenaers, P. Efficiently suppressing coalescence in polymer blends using nanoparticles: role of interfacial rheology. *Soft Matter* **2010**, *6*, 3353-3362.
109. Taylor, G.I. The viscosity of a fluid containing small drops of another fluid. *Proceedings of the Royal Society of London. Series A, Containing Papers of a Mathematical and Physical Character* **1932**, *138*, 41-48.
110. Grace, H.P. Dispersion phenomena in high viscosity immiscible fluid systems and application of static mixers as dispersion devices in such systems. *Chemical Engineering Communications* **1982**, *14*, 225-277.
111. Tucker III, C.L.; Moldenaers, P. Microstructural evolution in polymer blends. *Annual Review of Fluid Mechanics* **2002**, *34*, 177.
112. Bousmina, M.; Ait-Kadi, A.; Faisant, J. Determination of shear rate and viscosity from batch mixer data. *J Rheol* **1999**, *43*, 415-433.
113. Kohlgrüber, K. *Co-Rotating Twin-Screw Extruders - Fundamentals, Technology, and Applications*; Carl Hanser Verlag GmbH & Co. KG: 2008; Volume Chapter 3: Rheological Properties of Polymer Melts, p. 367.
114. Perrin-Sarazin, F.; Ton-That, M.-T.; Bureau, M.; Denault, J. Micro-and nano-structure in polypropylene/clay nanocomposites. *Polymer* **2005**, *46*, 11624-11634.
115. Shi, X.; Wang, J.; Jiang, B.; Yang, Y. Influence of nanofiller dimensionality on the crystallization behavior of HDPE/carbon nanocomposites. *J Appl Polym Sci* **2013**, *128*, 3609-3618.
116. Sadeghi, S.; Arjmand, M.; Otero Navas, I.; Zehtab Yazdi, A.; Sundararaj, U. Effect of nanofiller geometry on network formation in polymeric nanocomposites: Comparison of rheological and electrical properties of multiwalled carbon nanotube and graphene nanoribbon. *Macromolecules* **2017**, *50*, 3954-3967.
117. Helal, E.; Amurin, L.; Carastan, D.; de Sousa Jr, R.; David, E.; Frechette, M.; Demarquette, N. Interfacial molecular dynamics of styrenic block copolymer-based nanocomposites with controlled spatial distribution. *Polymer* **2017**, *113*, 9-26.
118. Trifkovic, M.; Hedegaard, A.T.; Sheikhzadeh, M.; Huang, S.; Macosko, C.W. Stabilization of PE/PEO cocontinuous blends by interfacial nanoclays. *Macromolecules* **2015**, *48*, 4631-4644.
119. Kuester, S.; Barra, G.M.; Ferreira Jr, J.C.; Soares, B.G.; Demarquette, N.R. Electromagnetic interference shielding and electrical properties of nanocomposites based on

poly (styrene-*b*-ethylene-*r*-butylene-*b*-styrene) and carbon nanotubes. *Eur Polym J* **2016**, *77*, 43-53.

120. Strugova, D.; Ferreira Junior, J.C.; David, É.; Demarquette, N.R. Ultra-Low Percolation Threshold Induced by Thermal Treatments in Co-Continuous Blend-Based PP/PS/MWCNTs Nanocomposites. *Nanomaterials-Basel* **2021**, *11*, 1620.

121. Omonov, T.; Harrats, C.; Moldenaers, P.; Groeninckx, G. Phase continuity detection and phase inversion phenomena in immiscible polypropylene/polystyrene blends with different viscosity ratios. *Polymer* **2007**, *48*, 5917-5927.

122. Thareja, P.; Velankar, S. Rheology of immiscible blends with particle-induced drop clusters. *Rheol Acta* **2008**, *47*, 189-200.

123. Filippone, G.; Causa, A.; de Luna, M.S.; Sanguigno, L.; Acierno, D. Assembly of plate-like nanoparticles in immiscible polymer blends—effect of the presence of a preferred liquid–liquid interface. *Soft Matter* **2014**, *10*, 3183-3191.

124. Altobelli, R.; de Luna, M.S.; Filippone, G. Interfacial crowding of nanoplatelets in co-continuous polymer blends: Assembly, elasticity and structure of the interfacial nanoparticle network. *Soft Matter* **2017**, *13*, 6465-6473.

125. Bird, R.B.; Armstrong, R.C.; Hassager, O. Dynamics of polymeric liquids. Vol. 1: Fluid mechanics. **1987**.

126. Carreau, P.J.; De Kee, D.C.; Chhabra, R.P. *Rheology of polymeric systems: principles and applications*; Carl Hanser Verlag GmbH Co KG: 2021.

127. Macaubas, P.; Demarquette, N. Morphologies and interfacial tensions of immiscible polypropylene/polystyrene blends modified with triblock copolymers. *Polymer* **2001**, *42*, 2543-2554.

128. Galloway, J.A.; Montminy, M.D.; Macosko, C.W. Image analysis for interfacial area and cocontinuity detection in polymer blends. *Polymer* **2002**, *43*, 4715-4722.

129. Pawar, S.P.; Bose, S. Peculiar morphological transitions induced by nanoparticles in polymeric blends: retarded relaxation or altered interfacial tension? *Phys Chem Chem Phys* **2015**, *17*, 14470-14478.

130. Alig, I.; Skipa, T.; Lellinger, D.; Pötschke, P. Destruction and formation of a carbon nanotube network in polymer melts: Rheology and conductivity spectroscopy. *Polymer* **2008**, *49*, 3524-3532.

131. Alig, I.; Pötschke, P.; Lellinger, D.; Skipa, T.; Pegel, S.; Kasaliwal, G.R.; Villmow, T. Establishment, morphology and properties of carbon nanotube networks in polymer melts. *Polymer* **2012**, *53*, 4-28.
132. Fenouillot, F.; Cassagnau, P.; Majesté, J.-C. Uneven distribution of nanoparticles in immiscible fluids: Morphology development in polymer blends. *Polymer* **2009**, *50*, 1333-1350.
133. Strugova, D.; David, É.; Demarquette, N.R. Linear viscoelasticity of PP/PS/MWCNT composites with co-continuous morphology. *J Rheol* **2022**, *66*, 671-681.
134. Liu, X.-Q.; Wang, Q.-Y.; Bao, R.-Y.; Yang, W.; Xie, B.-H.; Yang, M.-B. Suppressing phase retraction and coalescence of co-continuous polymer blends: effect of nanoparticles and particle network. *Rsc Adv* **2014**, *4*, 49429-49441.
135. Zou, Z.-M.; Sun, Z.-Y.; An, L.-J. Effect of fumed silica nanoparticles on the morphology and rheology of immiscible polymer blends. *Rheol Acta* **2014**, *53*, 43-53.
136. Vinckier, I.; Moldenaers, P.; Terracciano, A.; Grizzuti, N. Droplet size evolution during coalescence in semiconcentrated model blends. *AIChE journal* **1998**, *44*, 951-958.
137. Skipa, T.; Lellinger, D.; Böhm, W.; Saphiannikova, M.; Alig, I. Influence of shear deformation on carbon nanotube networks in polycarbonate melts: Interplay between build-up and destruction of agglomerates. *Polymer* **2010**, *51*, 201-210.